

**University of Alberta**

Detection of Foodborne Pathogenic Bacteria using  
Bacteriophage Tail Spike Proteins

by

Somayyeh Poshtiban

A thesis submitted to the Faculty of Graduate Studies and Research  
in partial fulfillment of the requirements for the degree of

Doctor of Philosophy

in

Micro-Electromechanical Systems and Nanosystems

Department of Electrical and Computer Engineering

© Somayyeh Poshtiban

Spring 2014

Edmonton, Alberta

Permission is hereby granted to the University of Alberta Libraries to reproduce single copies of this thesis and to lend or sell such copies for private, scholarly or scientific research purposes only. Where the thesis is converted to, or otherwise made available in digital form, the University of Alberta will advise potential users of the thesis of these terms.

The author reserves all other publication and other rights in association with the copyright in the thesis and, except as herein before provided, neither the thesis nor any substantial portion thereof may be printed or otherwise reproduced in any material form whatsoever without the author's prior written permission.

*To love of my life, Reza  
my heroes, my parents, Akram and Behrouz  
and my little sunshine, Adrian.*

# Abstract

Foodborne infections are worldwide health problem with tremendous social and financial impacts. Efforts are focused on developing accurate and reliable technologies for detection of food contaminations in early stages preferably on-site. This thesis focuses on interfacing engineering and biology by combining phage receptor binding proteins (RBPs) with engineered platforms including microresonator-based biosensors, magnetic particles and polymerase chain reaction (PCR) to develop bacterial detection sensors.

We used phage RBPs as target specific bioreceptors to develop an enhanced microresonator array for bacterial detection. These resonator beams are optimized to feature a high natural frequency while offer large surface area for capture of bacteria. Theoretical analysis indicates a high mass sensitivity with a threshold for the detection of a single bacterial cell. We used phage RBPs as target specific bioreceptors, and successfully demonstrated the application of these phage RBB-immobilized arrays for specific detection of *C. jejuni* cells.

We also developed a RBP-derivatized magnetic pre-enrichment method as an upstream sample preparation method to improve sensitivity and specificity of PCR for detection of bacterial cells in various food samples. The combination of RBP-based magnetic separation and real-time PCR allowed the detection of small number of bacteria in artificially contaminated food samples without any need for time consuming pre-enrichment step through culturing. We also looked into integration of the RBP-based magnetic separation with PCR onto a single microfluidic lab-on-a-chip to reduce the overall turnaround time.

# Preface

The work contained in this dissertation was carried out under the supervision of Dr. Stephane Evoy between January 2010 and January 2014, except of the Chapter 9 which was carried out under supervision of Dr. Christopher Backhouse between January 2009 and January 2010.

Chapter 6. Tables 6.1 and 6.2 and Figures 6.1, 6.2, 6.3, 6.4 are used with permission from applicable sources. Portions of the text at sections 6.2.2 and 6.3.1 are used with permission from Afzal Javed *et al.* (2013) of which I am the second author. I was responsible for data collection and analysis for the materials provided in these sections. The rest of the text has been published as [S. Poshtiban, M. A. Javed, D. Arutyunov, A. Singh, G. Banting, C. M. Szymanski and S. Evoy, Phage receptor binding protein-based magnetic enrichment method as an aid for real time PCR detection of foodborne bacteria, *Analyst*, 2013, 138, 5619 - 5626] in which I was the lead investigator and responsible for all major areas of concept formation, data collection and analysis, as well as manuscript composition

Chapter 7. Majority of this chapter has been published as [S. Poshtiban, A. Singh, G. Fitzpatrick, S. Evoy, Bacteriophage tail-spike protein derivitized microresonator arrays for specific detection of pathogenic bacteria, *Sensors and Actuators: B. Chemical*, 2013, 181, 410 - 416]. I was the lead investigator, responsible for major areas of concept formation, data collection and analysis, as well as manuscript composition. Dr. Amit Singh was involved in the early stages of this project by providing trainings on designing surface functionalization experiments. Mr. Glen Fitzpatrick provided technical support on microresonator array devices. Dr. Stephane Evoy was the supervisory author on this project and was involved throughout this project in concept formation and manuscript edits.

Chapter 8. A version of this chapter has been published as [S. Poshtiban, M. A. Javed, D. Arutyunov, A. Singh, G. Banting, C. M. Szymanski and S. Evoy, Phage receptor binding protein-based magnetic enrichment method as an aid for real time PCR detection of foodborne bacteria, *Analyst*, 2013, 138, 5619 - 5626]. I was the lead investigator for the project located in Chapter 8 where I was responsible for all major areas of concept formation, data collection and analysis, as well as manuscript composition. I performed all of the molecular biology experiments at the Molecular Biology Service Unit at the Department of Biological Sciences at the University of Alberta. Dr. Amit Singh and Dr. Graham Banting were involved in the early stages of concept formation and contributed to manuscript edit. Dr. Muhammad Afzal Javad, Dr. Denis Arutunov and Dr. Christine Szymanski provided phage tail spike proteins and bacterial cells required for the entire experiments and contributed to manuscript edit. Dr. Stephane Evoy was the supervisory author no this project and was involved throughout this project in concept formation and manuscript edits.

Chapter 9. The work contained in this chapter was carried out under supervision of Dr. Christopher Backhouse between January 2009 and January 2010. The hardware design was done primarily at the Applied Miniaturization Laboratory at the University of Alberta in which I was involved in the testing of electronic units and thermal calibration of microfluidic devices. The system model provided at Section 9.2.2 was developed by Dr. Reza Banaei Khosroushahi and his contribution is cited where appropriate. The rest of the chapter presents my original work on development of a robust thermal controller for the PCR microfluidic device.

### **Refereed Journal Publications**

1. S. Poshtiban, M. A. Javed, D. Arutyunov, A. Singh, G. Banting, C. M. Szymanski and S. Evoy, Phage receptor binding protein-based magnetic enrichment method as an aid for real time PCR detection of foodborne bacteria, *Analyst*, 2013, 138, 5619 - 5626
2. S. Poshtiban, A. Singh, G. Fitzpatrick, S. Evoy, Bacteriophage tail-spike protein derivitized microresonator arrays for specific detection of pathogenic bacteria, *Sensors and Actuators: B. Chemical*, 2013, 181, 410 - 416

3. A. Singh, S. Poshtiban, S. Evoy, Recent advances in bacteriophage based biosensors for food-borne pathogen detection, *Sensors*, 2013, 13(2) 1763–1786
4. M. A. Javed, S. Poshtiban, D. Arutyunov, S. Evoy, C. M. Szymanski, Bacteriophage receptor binding protein based assays for the simultaneous detection of *Campylobacter jejuni* and *Campylobacter coli*, *PloS ONE*, 2013, 8(7): e69770
5. N. Fitzpatrick, C. Guthy, S. Poshtiban, E. Finley, K. Harris, B. Worfolk, S. Evoy, Atomic layer deposition of TiN for the fabrication of nanomechanical resonators, *Journal of Vacuum Science and Technology A*, 2013, 31(2), 021503-021503-7
6. A. Janzen, S. Poshtiban, A. Singh, S. Evoy, Fabrication of nanoresonator biosensing arrays using nanoimprint lithography, *Journal of Micro/Nanolith. MEMS, and MOEMS*, 2012, 11

### **Book Chapters**

1. A. Singh, S. Poshtiban, S. Evoy, (2013). Biosensors for food safety. In *Introduction to advanced food processing engineering*. (pp. 399-432) CRC Press

### **Refereed Conferences**

1. S. Poshtiban, S. Evoy, "Specific detection of pathogenic bacteria using tail spike proteins", poster presentation to Biosensors 2012, Cancun, Mexico, May 2012.
2. S. Poshtiban, A. Singh, D. Arutyunov, C. M. Szymanski, S. Evoy, "Enhanced microresonator arrays for the specific detection of pathogenic bacteria", 9th International Workshop on Nanomechanical Sensing, Mumbai, India, June 2012.
3. M. A. Javed, D. Arutyunov, A. Singh, S. Poshtiban, S. Evoy, C. M. Szymanski, "Phage receptor binding proteins as novel ligands for bacterial detection", 16th Workshop on *Campylobacter, Helicobacter* and Related Organisms, Vancouver, Canada, August 2011.

4. S. Poshtiban, S. Evoy, "Mechanical characterization and mass sensitivity analysis of a microresonator array", 2nd Faculty of Engineering Graduate Research Symposium, Edmonton, Alberta, June 2011.
5. S. Poshtiban , C. J. Backhouse, "Rapid temperature control of a polymerase chain reaction Lab- on-a-Chip devices", Faculty of Engineering Graduate Research Symposium (FERGS), University of Alberta, Edmonton, Canada, Jun. 2010
6. G. V. Kaigala, M. Behnam, V. J. Sieben, S. Poshtiban , A. C. E. Bidulock, A. Olanrewaju, C. H. Lim, C. Bergen, J. Booth, L. M. Pilarski and C. J. Backhouse "Molecular diagnostics: From clinical sample to answer Integration of sample prgenetic amplication and analysis/detection ", 12th Nanotech-Montreux, Switzerland, Nov. 17-19, 2008. Oral.
7. M. Behnam, G.V. Kaigala, V. J. Sieben, S. Poshtiban , A. C. E. Bidulock, C. Bergen, S. Choi, J. M. Quijada, S. Ho, A. Olanrewaju, J. Lauzon, R. W. Johnstone, D.G. Elliott and L. M. Pilarski, "Medical diagnostics in your hand (and on your desk) ", 12th Nanotech-Montreux, Switzerland, Nov. 17-19, 2008. Oral.

# Acknowledgements

First and foremost, I would like to thank my supervisor, Dr. Stephane Evoy for providing me the opportunity to work on this interesting project, opening my eyes to countless aspects of engineering and science. His support, advices and encouragement has given me the freedom to explore this research field and the opportunity to think independently in my research field. Dr. Evoy taught me how to identify the key scientific obstacle in a project, manage project and design experiments. Most importantly, he taught me how to cultivate a vision in a clear, precise reality. For this, I can not thank him enough.

I also thank my PhD committee members, Dr. Doug Barlage and Dr. Roger Zemp, for their valuable suggestions to improve the content and presentation of this thesis. My appreciation as well to Dr. Dan Sameoto and Dr. Robin Turner for their constructive suggestions and comments. I also thank all the past, present and fellow groupmates at NEMS Lab, other ECEGSA council members, departmental staff and faculty, and collaborators who have made my overall experience as a graduate student at University of Alberta fruitful and rewarding. In particular, my thanks to Dr. Amit Singh for his mentorship and calm and always astute guidance; to my cubicle mates and friends Dr. Nathan Nelson-Fitzpatrick, Dr. Upasana Singh for countless hours of fruitful discussions. I would also like to thank Mr. Glen Fitzpatrick for providing technical support on micro resonator arrays throughout the project. Additionally, our collaborators Dr. Christine Szymanski, Dr. Denis Arutunov, and Dr. Afzal Muhammad Javed have been of great support throughout this research. I also appreciate Dr. Graham Banting for his advices on PCR aspect of the work. I would also like to thank my former supervisor, Dr. Chris Backhouse, for his advices and insights on the work provided in Chapter 9.

This thesis would have not been possible without three people. My parents Akram Ashrafian and Behrouz Poshtiban have supported me all the way along. They are my mentors and two of my best friends. They taught me that I can learn all my life; they showed me that I can try, fail, learn something new, fail again, succeed, change again ... and that is all very exciting and rewarding. To my husband Reza Banaei: your love, support and encouragement made all this achievable.

Finally, I would like to express my gratitude to the funding agencies that supported me along the way. This work was made possible by financial support from National Institute for Nanotechnology (NINT) and Alberta Livestock and Meat Agency (ALMA).

Somayyeh Poshtiban  
Edmonton, AB  
January, 2014

# Contents

<b>1</b>	<b>Introduction</b>	<b>1</b>
1.1	Motivation for Early Detection . . . . .	1
1.2	Limitations of Available Technologies . . . . .	2
1.3	Project Description and Scope . . . . .	4
1.4	Overview of Remaining Chapters . . . . .	9
<b>2</b>	<b>Background on Pathogen Detection Methods</b>	<b>11</b>
2.1	Laboratory-based Methods . . . . .	11
2.1.1	Gram Staining . . . . .	11
2.1.2	Culture and Colony Counting . . . . .	12
2.1.3	Immunassays . . . . .	12
2.1.4	Polymerase Chain Reaction . . . . .	13
2.2	Biosensors . . . . .	16
2.2.1	Optical Biosensors . . . . .	16
2.2.2	Electrochemical Biosensors . . . . .	19
2.2.3	Micromechanical Biosensors . . . . .	21
2.3	Lab-on-a-Chip technology for Pathogen Detection . . . . .	23
2.4	Biomarkers . . . . .	26
2.4.1	Nucleic Acids . . . . .	26
2.4.2	Antibodies . . . . .	28
2.4.3	Bacteriophage . . . . .	29
2.5	Sample Preparation . . . . .	29
2.5.1	Chemical Methods . . . . .	30
2.5.2	Physical Methods . . . . .	31

2.5.3	Physico-chemical Methods . . . . .	32
2.5.4	Magnetic Separation . . . . .	32
<b>3</b>	<b>Introduction to Micro/Nano-Resonator Sensors</b>	<b>37</b>
3.1	Introduction . . . . .	37
3.2	Vibration Theory of Discrete Systems . . . . .	37
3.2.1	One Degree of Freedom Simple Harmonic . . . . .	37
3.2.2	Effective Mass and Stiffness . . . . .	38
3.2.3	Multiple Degree of Freedom . . . . .	39
3.2.4	System with Damping . . . . .	39
3.3	Vibration Theory of Continuous Systems . . . . .	40
3.3.1	The Euler-Bernoulli Equation . . . . .	40
3.3.2	Energy Methods . . . . .	42
3.4	Resonator Mass Sensors . . . . .	43
3.4.1	Principle of Detection . . . . .	43
3.4.2	Mass Sensitivity . . . . .	43
3.4.3	Stress Effects . . . . .	44
3.5	Conclusion . . . . .	46
<b>4</b>	<b>Introduction to Polymerase Chain Reaction</b>	<b>47</b>
4.1	Introduction . . . . .	47
4.2	Principles and Components of PCR . . . . .	47
4.3	Phases of PCR . . . . .	50
4.4	Methods of PCR . . . . .	50
4.4.1	Conventional PCR . . . . .	50
4.4.2	Quantitative PCR . . . . .	51
4.5	Real time qPCR Chemistry . . . . .	52
4.5.1	Fluorescent Intercalater Dye-based Chemistry . . . . .	52
4.5.2	Fluorogenic-labeled Probe-based Nuclease Chemistry . . . . .	54
4.6	Methods of Quantification . . . . .	55
4.7	Determination of LOQ and LOD . . . . .	57

<b>5</b>	<b>Introduction to Bacteriophage Technology</b>	<b>59</b>
5.1	Introduction . . . . .	59
5.2	Phage Structure and Anatomy . . . . .	60
5.3	Phage Infection Cycle . . . . .	61
5.4	Phage as Diagnostic Tools . . . . .	63
5.4.1	Wild-type Phages . . . . .	63
5.4.2	Engineered Phages . . . . .	65
5.4.3	Phage Receptor Binding Proteins (RBPs) . . . . .	67
<b>6</b>	<b>Surface Immobilization of Phage Receptor Binding Proteins (RBPs) for Specific Bacterial Capture</b>	<b>69</b>
6.1	Introduction . . . . .	69
6.2	Experimental Methods . . . . .	70
6.2.1	Expression and Purification of Phage Tail Spike Proteins . . . . .	70
6.2.2	Localization of Host Binding Domain in the GP48 . . . . .	71
6.2.3	Immobilization of GST-Gp48 and Derivatives onto Au Surfaces . . . . .	72
6.2.4	Magnetic Beads . . . . .	73
6.2.5	Immobilization of GST-GP48 Protein onto Magnetic Beads . . . . .	73
6.2.6	Capture and Separation of Bacterial Cells . . . . .	75
6.3	Results and Discussion . . . . .	75
6.3.1	Analysis of Bacterial Capture on Immobilized GST-GP48 and Derivatives . . . . .	75
6.3.2	Bacterial Capture on RBP-derivatized Magnetic Beads . . . . .	77
6.4	Conclusion . . . . .	80
<b>7</b>	<b>Phage RBP-based Microresonator Array for Detection of Bacteria</b>	<b>81</b>
7.1	Introduction . . . . .	81
7.2	Device Structure and Fabrication . . . . .	83
7.3	Finite Element Modeling . . . . .	84
7.3.1	Finite Element Model Verification . . . . .	84
7.3.2	Bacterial Detection Frequency Analysis . . . . .	89
7.4	Experimental Methods . . . . .	91
7.4.1	Resonator Frequency Measurements . . . . .	91

7.4.2	Phage RBP Immobilization onto Resonators . . . . .	92
7.5	Results and Discussion . . . . .	94
7.5.1	Characterization of Unloaded Resonators . . . . .	94
7.5.2	Effect of Funtionalization Layers on Frequency Response of Resonators . . . . .	95
7.5.3	Detection and Qauntification of <i>C. jejuni</i> Cells . . . . .	96
7.5.4	Capture Specificity . . . . .	97
7.5.5	Practical Limitations . . . . .	97
7.6	Conclusion . . . . .	98

**8 Phage RBP-derivatized Magnetic Pre-Enrichment Coupled with PCR 101**

8.1	Introduction . . . . .	101
8.2	Experimental Methods . . . . .	102
8.2.1	Primer and Probe Design . . . . .	102
8.2.2	Conventional PCR Assay . . . . .	103
8.2.3	TaqMan Real Time PCR Assay . . . . .	103
8.2.4	Primer and Probe Concentration Optimization . . . . .	103
8.2.5	DNA Extraction from Bacterial Cells . . . . .	104
8.2.6	Creating Standard Curve with Genomic DNA for PCR Sensitivity Analysis . . . . .	104
8.2.7	Preparation of Artificially Contaminated Food Samples . . . . .	105
8.2.8	Coupling RBP-based Magnetic Pre-enrichment with qPCR . . . . .	106
8.2.9	Calculation of Recovery Rate (RR) (%) and Statistical Analysis . . . . .	106
8.3	Results and Discussion . . . . .	107
8.3.1	Sensitivity and Linear Range of <i>C. jejuni</i> qPCR Assay . . . . .	107
8.3.2	DNA Extraction from Bacteria Captured on RBP-Derivarized Magnetic Beads . . . . .	108
8.3.3	Capture Efficiency and Recovery Rate of RBP-Derivatized Beads . . . . .	108
8.3.4	Analysis of Artificially Spiked Food Samples Using RBP-based Pre-enrichment Method and qPCR . . . . .	109
8.4	Conclusion . . . . .	111

<b>9</b>	<b>Thermal Management of a PCR Lab-on-a-Chip Device</b>	<b>115</b>
9.1	Introduction . . . . .	115
9.2	PCR Microchip . . . . .	117
9.2.1	Microfluidic Chip Structure . . . . .	117
9.2.2	Microfluidic Chip System Model . . . . .	118
9.2.3	Model Linearization . . . . .	120
9.3	Thermal Calibration of PCR Microfluidic Chip . . . . .	122
9.4	Controller Design . . . . .	123
9.4.1	Observability and Controllability . . . . .	123
9.4.2	Eigenvalue Selection . . . . .	124
9.4.3	State Feedback Controller on Linearized Model . . . . .	124
9.4.4	Feedforward Compensator . . . . .	127
9.4.5	Inverse Nonlinear Function for Nonlinear System . . . . .	127
9.4.6	Feedforward Trajectory Optimization . . . . .	128
9.5	Results and Discussion . . . . .	129
9.5.1	Performance of Controller . . . . .	129
9.5.2	Discretization and Implementation . . . . .	131
<b>10</b>	<b>Summary and Conclusions</b>	<b>136</b>
10.1	Thesis Contribution . . . . .	136
10.2	Future Directions . . . . .	138
10.2.1	Integration of RBP-based Magnetic Separation with PCR on a Lab-on-a-Chip Device . . . . .	138
10.2.2	Automated Sample Delivery System for Microresonator Array	139
<b>A</b>	<b>Protocol for Bacteria DNA Extraction</b>	<b>141</b>
A.1	Equipments and Reagents . . . . .	141
A.2	Notes and Precautions . . . . .	142
A.3	Protocol . . . . .	142
	<b>Bibliography</b>	<b>146</b>

# List of Tables

2.1	A list of foodborne pathogens detected using various biosensors highlighting the transduction platform used and limit of detection achieved.	36
6.1	List of plasmids used to study RBP binding domain localization [110]	71
6.2	List of primers used to study RBP binding domain localization [110]	72
6.3	Capture density for different protein derivatives . . . . .	77
7.1	Material properties . . . . .	85
7.2	Simulated frequency . . . . .	86
8.1	List of primers and probes; the TaqMan probe was labeled with a 6-FAM reported at the 5' end and a MGB quencher at 3' end . . . .	103
8.2	PCR reaction mix for primer optimization . . . . .	104
8.3	PCR reaction mix for probe optimization . . . . .	104
8.4	Mass of DNA (fg) and final concentration of DNA <i>vs</i> Copy # . . . .	105
8.5	Capture efficiency of RBP magnetic separation method . . . . .	109
9.1	System parameters at the operating point . . . . .	121

# List of Figures

1.1	The flowchart illustrates the processing steps involved and relative time taken in detecting a pathogen in a food sample. . . . .	5
3.1	A single degree of freedom mechanical system. . . . .	38
3.2	A mechanical system with damping. . . . .	39
4.1	PCR reaction diagram. . . . .	49
4.2	PCR amplification plot . . . . .	50
4.3	The endpoint qPCR reaction variation for runs with 96 identical reactions [231]. . . . .	51
4.4	Principle of realtime qPCR. Ct value is inversely proportional to the initial copy number[231]. . . . .	53
4.5	The mechanism of SYBR Green I dye chemistry. The dye bind to dsDNA in the reaction. . . . .	54
4.6	TaqMan PCR assay. [231]. . . . .	58
5.1	Tailed bacteriophage . . . . .	60
6.1	Diagram of steps involved in surface immobilization of GST-Gp48 proteins on magnetic beads . . . . .	74
6.2	Scanning electron microscopy images of <i>C. jejuni</i> cells captured by the immobilized Gp48 and its derivatives . . . . .	76
6.3	Scanning electron microscopy images of different bacteria captured by the immobilized GST-Gp48 . . . . .	77
6.4	Bacterial capture on TSP derivatized Tosylactivated beads . . . . .	78
6.5	Bacterial capture on TSP derivatized Epoxy beads . . . . .	79

7.1	Microresonator array chip . . . . .	84
7.2	Unloaded resonator model . . . . .	85
7.3	SEM of a resonator element fabricated by imprint lithography . . . . .	87
7.4	FEA of resonance response versus initial stress . . . . .	88
7.5	FEA of frequency shift versus accrued mass . . . . .	89
7.6	The effect of mass and stiffness of bacteria on resonance response . . . . .	90
7.7	Resonance response to random capture of bacteria . . . . .	92
7.8	Schematic of resonance measurement interferometric setup [168]. . . . .	93
7.9	resonance spectrum . . . . .	93
7.10	Device characterization . . . . .	94
7.11	Pressure dependency analyses . . . . .	95
7.12	Resonant frequency measurements . . . . .	97
7.13	Bacterial capture on a microresonator array . . . . .	98
7.14	SEM of bacterial capture artifacts on a microresonator array . . . . .	99
8.1	Dynamic range and sensitivity of <i>C. jejuni</i> real-time PCR assay . . . . .	107
8.2	Capture efficiency of GST-Gp48 magnetic beads . . . . .	112
8.3	Standard curve of <i>C. jejuni</i> PCR assay . . . . .	113
8.4	PCR on artificially contaminated food samples with/without RBP magnetic enrichment . . . . .	114
9.1	PCR microfluidic chip [21]. . . . .	117
9.2	PCR microchip architecture [96]. . . . .	118
9.3	System level model of PCR lab-on-a-chip device. . . . .	118
9.4	Heater subsystem . . . . .	119
9.5	State-space representation of heater subsystem. . . . .	120
9.6	Model of chamber subsystem. . . . .	120
9.7	Linearized model of heater subsystem. . . . .	122
9.8	Block diagram of controller design on linearized model. . . . .	125
9.9	Block Diagram of controller design with feedforward compensator on linearized model. . . . .	127
9.10	Block Diagram of controller design with nonlinear inverse function. . . . .	128
9.11	Controller performance on linearized model . . . . .	130

9.12 Performance of controller with feedforward compensator on heater model with the nonlinearity . . . . .	132
9.13 Performance of controller with feedforward compensator on the linearized model . . . . .	133
9.14 Performance of controller with nonlinear inverse function and feedforward compensator on heater model with the nonlinearity . . . . .	134
9.15 Performance of controller . . . . .	135
A.1 Spin column procedure for DNA extraction [193]. . . . .	145

# List of Acronyms

Abs	Antibodies
AK	Adenylate kinase
AML	Applied miniaturization laboratory
CFU	Colony forming unit
CGE	Capillary gel electrophoresis
CV	Crystal violet
DEP	Dielectrophoretic
DNA	Deoxyribonucleic acid
dsDNA	Double-stranded DNA
ELISA	Enzyme-linked Immunosorbent Assay
FEA	Finite element analysis
FEM	Finite element modelling
FRET	Fluorescence resonance energy transfer
HOT	High order terms
IMS	Immunomagnetic separation
LAMP	Loop-mediated isothermal amplification
LOC	Lab-on-a-chip
LOD	Limit of detection
LOQ	Limit of quantification
NAH	Nucleic acid hybridization
NASBA	Nucleic acid sequence-based amplification
PCR	Polymerase chain reaction
QCM	Quartz crystal microbalance
QD	Quantum dots

RBP	Receptor Binding Proteins
SDA	Strand displacement amplification
SPR	Surface plasmon resonance
TLC	Thermochromic liquid crystal
TSP	Taikspike Proteins
VBNC	Viable but non-culturable

# Chapter 1

## Introduction

### 1.1 Motivation for Early Detection

Bacteria are omnipresent and thus their existence in food is natural. While the majority of bacterial strains are harmless or even beneficial to humans, several others, being pathogenic in nature, can cause severe threats to health and safety and consequently inflict tremendous burden on our socio-economic balance and health care systems. The Center for Disease Control and Prevention (CDC) estimates around 76 million cases of foodborne illnesses, resulting in 325,000 hospitalization and 5000 deaths annually in USA [7]. The cooking process successfully kills any potential bacteria that are present in food, however, food styles have changed significantly in recent years, and more processed and ready-to-eat packaged foods are available, which increases the chance of exposure to pathogenic contamination. In addition to direct bacterial contaminations, enterotoxins can cause foodborne diseases even when the causative bacteria have been killed. Processed meat, poultry, vegetables and milk products are among the most probable carriers of potent foodborne pathogens, including *E. coli*, *Salmonella*, *Listeria* and *Campylobacter jejuni* and there have been numerous incidents of product recalls across United States in past years. *E. coli* O157:H7 was considered a rare serotype when first reported in 1983, but is now one of the major causes of foodborne diseases in developed countries [199, 253]. Food producers also experience dramatic financial losses in an incidence of foodborne outbreak. For example, XL Food Inc. received a lawsuit of \$17-million in damage for financial and emotional loss after Canada's largest beef recall in 2012

[44]. Monitoring food has therefore been argued as the most important priority towards national and international health and safety with global emphasis on rapid and early detection of pathogen contamination in food and water.

## 1.2 Limitations of Available Technologies

Conventional culture methods largely rely on microbiological and biochemical analysis which involve the isolation and enumeration of bacteria through several enrichment and culturing steps followed by analysis of results morphologically or biochemically. Culture based methods have been the most reliable and accurate technique for foodborne pathogen detection; and have been used for detection of wide variety of pathogens including *L. monocytogenes*, *S. aureus*, *Salmonella*, *E. coli*, *C. jejuni* [57, 16, 18, 209], The main drawback of culture-based detection methods is their slow process time (usually 2-3 days for initial results and more than a week for confirmation), as they rely on the ability of bacteria to grow to visible colonies [57, 16]. In addition, some bacteria may enter viable but non-culturable (VBNC) phase resulting in failure to isolate bacteria from a contaminated sample or underestimation of number of bacteria [240, 188, 263]. Detection of *Campylobacter* takes 4-9 days to obtain a negative result and between 14 to 16 days to confirm positive result [36]. Therefore, despite being highly accurate, these microbiological methods are overly time consuming, cost-ineffective and non-amenable to integration for on-site diagnosis in industrial applications. Besides, successful execution of pathogen identification and detection by conventional methods require extensive training and experience.

Alternative rapid but accurate methods for pathogen detection have therefore been sought to overcome these limitations. Advances in immunological methods such as enzyme-linked immunosorbent assay (ELISA) have paved the way towards development of easier and quicker pathogen detection methods, relying on the recognition specificity of antibodies (Abs). Immunology-based methods have been used for detection of various pathogens such as *E. coli* [11, 13], *Salmonella* [11, 47, 154], and *Campylobacter* [35, 46, 223]. Immunological methods however suffer from cross-reactivity of polyclonal Abs, high production cost of monoclonal Abs, and need for

sample pre-processing and pre-enrichment due to low processing sample volume and lower limit of detection [2].

Recently, more sophisticated traditional analytical methods such as liquid/gas chromatography coupled with mass spectrophotometry have been used for more accurate analysis of pathogen. Although these methods have enjoyed tremendous popularity, their feasibility towards point-of-care onsite pathogen monitoring tools is hard to realize. Development of alternative tools for fast, accurate and sensitive detection of pathogens has therefore been an area of continued interest to researchers across the globe.

Nucleic acid based detection methods have found great interests in recent years due to several features. First, any living organisms poses its own unique nucleic acids in terms of sequence and quantity. Nucleic acids are also easy to extract, purify, label and sequence and therefore are daily adaptable to clinical applications for sensitive and rapid detection. However, nucleic acids extracted from microorganisms are relatively small, and thus there is need for DNA amplification prior to detection. Polymerase chain reaction (PCR) is a well established DNA amplification technique that offers major advantages in terms of speed, specificity, and sensitivity [240]. PCR amplifies a small quantity of DNA to detectable levels within relatively short assay times. Conventional PCR methods are coupled with DNA size separation methods such as gel electrophoresis to qualitatively detect the amplified DNA at the end point of reaction. Quantitative real-time PCR is a newer technology that labels DNA with fluorescent tag and can quantify the DNA concentration by measuring the intensity of fluorescent signal.

Despite these superior features, direct identification of pathogenic microorganisms in food samples is problematic. The major impediment to the realtime or near realtime detection of foodborne pathogens is the low infectious dose ( 10- 1000 bacterial cells) of pathogenic bacteria [211]. Besides, the residual food components and competitor microorganisms interfere with detection mechanism and reduce the test sensitivity and specificity. Therefore, a pre-detection sample preparation step is necessary for separation, purification and subsequently concentration of the target bacteria from a complex food sample.

Biosensors are relatively new technologies that have been looked upon as poten-

tial alternatives for bacterial detection. Biosensors are analytical devices that are composed of three parts, a target-specific bioreceptors, a transducer, and a signal processing unit, to translate a specific bio-recognition event into a measurable signal. They have the potential for rapid and sensitive analysis with minimal sample preparation at low cost. They also have the promise to be miniaturized to realize portable devices for in situ real-time monitoring, thus to reduce overall turnaround time from sample to result. Despite much progress, biosensors are still in their early developmental stages, and there is an ongoing research to improve their sensitivity, stability and reliability.

The conventional clinical methods for sample preparation involves lengthy pre-enrichment steps which may take several days. Figure 1.1 outlines the steps involved in analysis of a food sample by various popular detection methods and time involved to reach a conclusive pathogen identity. Clearly, these lengthy sample preparation steps are the main Achilles' heels for rapid and real-time analysis of food samples regardless of the detection technology.

### 1.3 Project Description and Scope

This dissertation aims to harness natural advantages of phage receptor binding proteins (RBPs) to develop new technologies to overcome the key technological barriers that presently limit realtime detection of bacterial contaminations in food. In order to achieve the above objective, we first developed methods to effectively immobilize the phage RBPs onto solid surfaces. Various derivatives of phage RBPs have been identified and tested to study the capture efficiency and specificity. We next used the proposed surface immobilization method to overcome major limitations associated with two detection platforms: microresonator-based biosensor and polymerase chain reaction.

Microresonator-based biosensors are extremely sensitive, scalable and conducive to integration into large arrays, and therefore are proposed as promising platforms for high-throughput and label-free diagnosis. The mass sensitivities down to the single cell have been reported for cantilever-based resonators [107]. However, this platform lacks the specificity for recognition of target cell. Any particle landing on

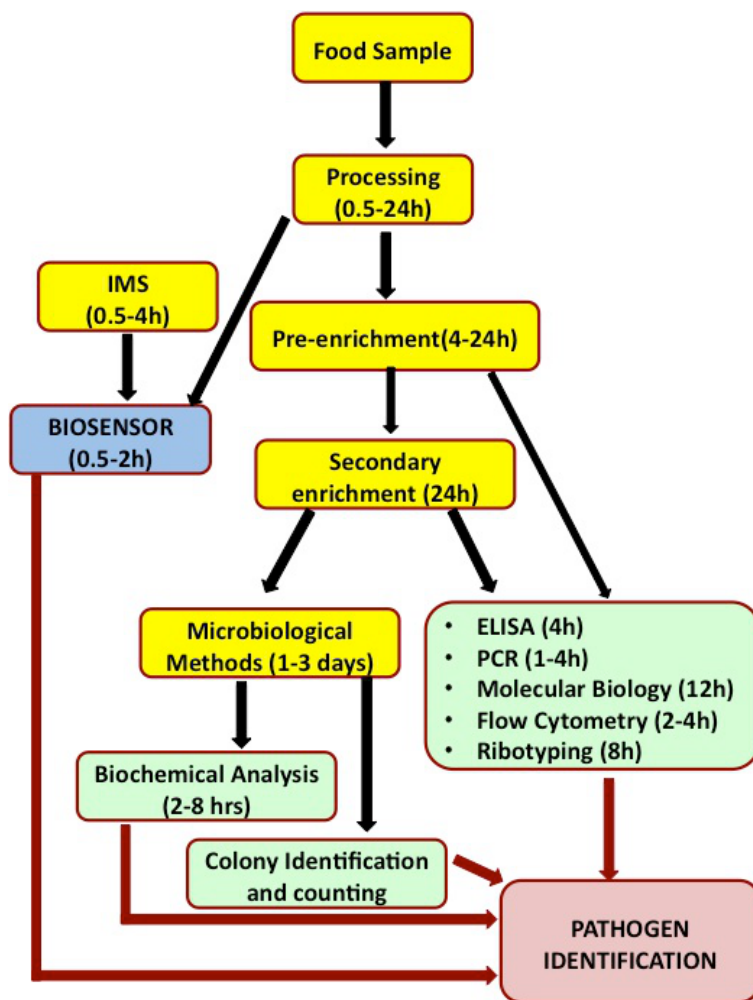


Figure 1.1: The flowchart illustrates the processing steps involved and relative time taken in detecting a pathogen in a food sample.

the surface will result in changes in sensor response. The specificity of recognition is usually provided by means of target-specific bioreceptors. Frequently, antibodies have been used as recognition probes which offer some degree of selectivity and specificity for the detection of bacteria antigens. However, they are expensive and suffer from instabilities against environmental factors.

Bacteriophages (or phages) have been proposed as an alternative approach for the detection of bacteria. They are viruses that attach to their host bacteria using their tail-spike proteins to initiate infection. This recognition is highly specific, and thus makes bacteriophages good candidates for the development of pathogen detection sensors. Whole phages have been exploited for the development of various detection platforms [19, 61, 166, 179, 221, 17]. However, immobilization based on

whole phages has two main drawbacks. First, the capture efficiency is severely impaired after drying surface-immobilized whole-phages. Secondly, overexposure to the surface-immobilized phages leads to bacterial lysis and eventual destruction of the captured target pathogen. Alternatively, phage TSPs have been looked upon, and have shown to circumvent the limitations associated with whole phage probes [218, 220]. Phage TSPs show relatively higher capture efficiency due to the smaller size of molecules. Moreover, their affinity and binding properties can be improved by genetically expressing desired tags on TSPs. These properties in addition to their high level of stability make TSPs advantageous over antibodies as well as whole-phage probes.

We leverage phage RBPs to develop an enhanced microresonator array for bacterial detection. This biosensing platform features a large surface area for the capture of bacteria with high mass sensitivity with a threshold for the detection of single bacterium. The application of these devices for bacterial detection is studied using finite element analysis and experimental methods. We have successfully demonstrated the specific detection of *Campylobacter jejuni* cells on this RBP immobilized microresonator array. This platform, however, is not readily suitable for realtime applications mainly due to the challenges associated with the transportation of cells onto the surface. Although the current "dip and dry" format is good for quick proof of concept studies, it is not efficient for high throughput clinical analysis as it is lengthy, laborious and requires large amount of analytes. Besides, there is no control over the landing position of cells which may result in cells landing on places other than beams surface.

PCR, on the other hand, is a well established technique for nucleic acid amplification in clinical applications, which is a rapid, sensitive and specific. PCR is theoretically capable of amplifying a single copy of DNA million times. An ideal set of primers can be designed to efficiently hybridize to the target sequence with negligible binding to other related sequences present in the sample. Therefore, PCR-based assays in combination with DNA measurement tools provides a sensitive and selective way of detecting small number of bacteria in samples, and thus has had a high impact in the field of diagnostic microbiology. Despite these advantages, the application of PCR assays for on-site food analysis is still problematic due to several

factors.

One major impediment to the application of PCR for direct realtime analysis of food samples is the need for sample preparation preceding the PCR assay. Food samples are usually complex, and contain PCR inhibitory substances. For example, the presence of Ca ions and fat in milk is known to degrade the enzyme activity and reduce PCR sensitivity. Pre-PCR sample preparation is a complex procedure as it needs to isolate bacteria from food sample, purify it from refractory elements, and pre-concentrate it to very small volumes used in PCR reactions (1  $\mu$ l to 10  $\mu$ l). Due to the importance of sample preparation step, a large variety of methods have been developed [72, 131]. However, most of these methods are laborious, time-consuming and expensive, or they do not provide the desired template quality.

Immunomagnetic separation (IMS) is shown to be an effective method for isolation of bacteria from food [224]. Immunomagnetic separation method is frequently combined with PCR for the detection of foodborne bacteria in various food samples [255, 268, 249, 118]. IMS is ideally applied to samples in an effort to eliminate lengthy cultural enrichment steps; nonetheless, a cultural enrichment step prior to IMS is still necessary to provide sufficient target bacteria for low limit of detection of pathogens in foods [101, 45]. Reports also have shown that the recovery rate of IMS methods highly depends on the target pathogen and its antigenic expression, the binding affinity of the pathogen antigen to the available antibody, and physiochemical properties of the sample matrix [59]. The specificity of capture and recovery by IMS varies with the choice of antibody. Monoclonal antibodies are designed to provide high degree of selectivity towards a single target epitope, but their production is expensive. Polyclonal antibodies are cheap to produce but they suffer from cross-reactivity with related targets. Therefore, there is a tradeoff between choosing polyclonal versus monoclonal antibodies with respect to balancing the likelihood of false positives versus the cost of assay when designing IMS assays [251]. Moreover, antibodies relatively have a short shelf time. Various physical or chemical properties of sample medium affect the expression of the target epitope(s) on a bacterial cell. The binding affinity of antibodies towards bacterial cells may also be compromised by the metabolic state of the bacterial cell itself [71, 84, 229].

We use phage RBPs to develop a novel phage RBP-based magnetic separation

and pre-enrichment method as an alternative to IMS by replacing antibodies with the bacteriophage receptor binding proteins (RBPs). To achieve these objectives, we first identified the phage receptor binding proteins specific to the target pathogen in collaboration with Dr. Szymanski's group. Next, we investigated strategies to efficiently immobilize these phage RBPs onto gold surfaces and magnetic beads. The capture of *Campylobacter jejuni* cells were studied and specificity of capture was confirmed using other pathogens as negative control. Next, we coupled the proposed RBP-derivatized magnetic pre-enrichment method with real-time PCR. The combination of RBP-based magnetic separation and real-time PCR improved PCR sensitivity and allowed rapid detection of *C. jejuni* cells in milk and chicken broth samples without a time consuming culture-based pre-enrichment.

Another obstacle for application of PCR for food analysis in industrial field is the long turnaround time of the assay from sample in to answer out considering the time required for pre-PCR sample preparation and post-PCR DNA analysis steps. Besides, commercial PCR devices are bulky, relatively expensive, and quite slow (1-2h run time for a single PCR) . More than 90% of total PCR assay time is spent on temperature cycling due to large thermal mass as not only the PCR mixture but also the whole reaction chamber needs to heat up and cool down. In the past decade, microPCR lab-on-a-chip (LOC) devices have been extensively looked upon with a goal of miniaturization of PCR modules and integration of pre-PCR and post-PCR functionalities onto a single chip to realize a rapid and portable device for point-of-care diagnosis. Miniaturization of reaction volumes typically reduces reagent consumption, shortens analysis time and minimizes the risk of sample contamination, and overall enhances PCR efficiency.

We looked into integration of our proposed RBP-based magnetic separation method with PCR on a single microfluidic chip. We selected a microchip with the potential for performing magnetic separation, PCR and capillary electrophoresis for our study. This microchip was designed and fabricated by researchers at Applied Miniaturization Laboratory at the University of Alberta [113, 114]. But, a critical aspect for adapting PCR technique to LOC devices is the precise and localized temperature control for an efficient amplification. The high amplification efficiency requires a  $\pm 1$  °C temperature precision at each temperature stage, minimized over-

shoot and undershoot in transitions and fast transition during temperature changes [275]. The fundamental challenge for design of such an accurate temperature controller for a microPCR LOC device is the temperature measurement without perturbation. Direct sensor in the micro scale reaction chamber affects heat transfer dynamics, and increases the risk of sample contamination. Therefore, it is desirable to estimate the temperature inside the reaction chamber based on the measured temperature outside the chamber.

We investigated temperature control problem of a PCR microfluidic chip with the goal to minimize the transition times in the PCR thermal cycling process and maintain tight fluctuation limits in each of the temperature stages. We designed a robust observer-based state feedback controller to rapidly and accurately track the PCR profile trajectory. The total analysis time was improved 30- 50 % using this controller. We used thermochromic liquid crystal (TLC) to verify the accuracy of temperature setting at each stage of PCR thermal cycling.

## 1.4 Overview of Remaining Chapters

Chapter 2 - 5 presents background information on materials in relation to this dissertation, and also summarizes key aspects of previous works. This is followed by a breakdown of the core project into component parts. Chapter 6 describes our method for immobilization of phage receptor binding proteins onto solid surfaces. Chapter 7 presents an enhanced RBP-based microresonator array for detection of pathogenic bacteria. Chapter 8 presents a novel phage RBP-derivatized magnetic pre-enrichment method as an upstream sample preparation step. This sample preparation method is coupled with PCR to detect bacterial contaminations in food samples. We present our work progress for integration of our proposed sample preparation with PCR on a single LOC microchip in Chapter 9. Finally, Chapter 10 presents a set of concluding remarks, a look at future directions, and a summary of main contributions of this work.

In summary, this dissertation presents the development of phage RBP-based methods for detection of pathogenic bacteria. Coupling this technology with microresonator array biosensors and PCR enables detection of bacteria with high level

of specificity. The proposed RBP-derivatized microresonator array offers large surface area for capture of bacteria, and is theoretically capable of detection of a single bacterial cell on entire array. However, the transportation of cells onto the resonator surface is still a practical challenge. Moreover, the resonance quality is compromised when these devices are operated in liquid resulting in less than optimal sensitivity. Therefore, they are still in early developmental stages with lots of methodological hurdles for field applications. The proposed PCR assay in conjunction with RBP-based pre-enrichment methods, on the other hand, is sensitive, specific, and reliable for detection of bacterial cells in food samples. The proposed RBP-based magnetic separation technique successfully removes the PCR-inhibitory elements from food samples and pre-concentrate target cells for PCR assays.

## Chapter 2

# Background on Pathogen Detection Methods

### 2.1 Laboratory-based Methods

#### 2.1.1 Gram Staining

Gram staining is a basic bacteriological laboratory method for classification of bacterial species into two groups, gram-positive and gram-negative based on the physical properties of their cell walls. Gram stain procedures involves four steps: (1) staining the heat fixed smear of bacterial culture with primary stain (crystal violet (CV)), (2) addition of gram iodine, which reacts with crystal violet and adhere it to the cell wall, (3) decolorization with alcohol or acetone, and (4) counterstaining with safranin. Gram-positive bacteria have a thick cell wall that is rich in teichoic acid, while gram-negative bacteria have a thin cell wall rich in lipid. The decolorizer penetrates throughout the thin cell wall of the gram-negative bacteria and washes away the crystal violet, resulting in pink or red colour of gram-negative bacteria. Gram-positive bacteria appears purple as decolorizer can not penetrate the cell wall. Gram stain test is used to identify presence of bacteria in direct smears made from swabs, aspirates, secretions. It can also be used to identify colonies isolated from cultures. Although gram staining is an effective diagnostic tool in clinical as well as research applications, it is generally not as specific or informative as other techniques, and thus all positive gram stain results need to be confirmed by culture

counting or molecular methods.

### **2.1.2 Culture and Colony Counting**

Culture and colony counting is the oldest microbiological method for bacteria detection, and it is considered the gold standard for bacterial detection due to its high reliability and accuracy. These methods rely on growing live bacterial cells on specific media under controlled laboratory conditions, and then enumerating the number of bacteria by using optical methods, mainly by ocular inspection. These methods are very sensitive and relatively inexpensive. However, the entire process is extremely time consuming and laborious. For example in the case of campylobacter, it takes 4-9 days to obtain negative results and 14-16 days for the confirmation of positive results.

### **2.1.3 Immunassays**

Immunology based methods works based on antigen-antibody interaction and has been widely used for identification of foodborne pathogens. They work based on the principle that each bacteria have various antigens on their cell wall. Some of these antigens are specific to certain strains of bacteria. Antibodies specific to that certain antigens can be used to specifically recognize that specific strain of bacteria.

The most common examples of immunological based techniques are enzyme immunoassay (EIA) and enzyme linked immunosorbent assay (ELISA). ELISA is a bioassay that determines the concentration of target substance through several steps as follows:

- The primary antibodies, called recognition antibodies, are immobilized onto the wells of a microtiter plate. These antibodies binds specifically to the target antigen.
- The buffered solution of the sample is next introduced to each well of a microtiter plate. The target antigens (on the cell wall of bacteria) will bind to the recognition antibodies on the wells.
- The wells are washed with a blocking agent such as bovine serum albumine to prevent unspecific binding.

- Secondary antibodies, called detection antibodies, are added to each well. This secondary antibodies, usually modified with an enzyme, bind to the target antigens upon recognition.
- The substrate for this enzyme is then introduced to the wells. The colour of the substrate changes upon reaction with the enzyme which can be measured with a plate reader.

Immunological methods are faster compared to conventional culture techniques. However, they require two different antibodies specific to the target bacteria. They also suffer from cross-reactivity of monoclonal antibodies, high production cost of polyclonal antibodies, and need for sample pre-processing and pre-enrichment due to small sample volume and lower limit of detection.

#### 2.1.4 Polymerase Chain Reaction

Polymerase chain reaction (PCR) is an in vitro laboratory procedure for amplification of specific sequence of DNA from tiny amounts by a factor of 1,000,000. This method is promising as it amplifies the target organism rather than the signal. PCR can detect a single copy of target DNA with high specificity, therefore, PCR offers potential for detection of a single pathogenic bacterium. PCR shortens the analysis time compared to conventional techniques and offer comparable or even better sensitivity for detection of pathogenic microorganisms. PCR is also preferable to immunoassays for detection of microbial pathogens because it can obtain detailed genetic information about a particular pathogen virulence, resistance against antibiotics and epidemiology [25]. Conventional PCR assays in conjunction with gel electrophoresis DNA analysis have been widely used for detection of wide range of foodborne pathogens such as *L. monocytogenes* [49, 119, 163, 202], *Salmonella* [119, 186], *C. jejuni* [64, 267], *E. coli* [182, 119], *S. aureus* [244, 119].

In field applications, realtime PCR is more applicable as it does not require time consuming post-PCR DNA measurement analysis with gel or capillary electrophoresis. Realtime PCR stains the dsDNA with fluorescent dye and monitors the increase in fluorescent signal with the amplification of DNA during PCR. In simpler qPCR assay formats, a DNA intercalating dye such as SYBR Green dye was used that binds

to minor grooves of dsDNA and fluoresces several times brighter at bound state. There are several reports on detection of foodborne pathogens using SYBR Green qPCR [68, 112, 165, 66]. The main drawback of SYBR Green qPCR is that it binds to any dsDNA nonspecifically, therefore lacks the desired specificity of recognition. This can be accounted for by running a melt curve analysis. The unspecific amplification will generate a melting curve peaks at different temperatures compared to target amplicon. Alternatively, probe-based qPCR assays are developed to provide the desired level of specificity and sensitivity for detection of target pathogens [40]. The TaqMan assay is the most commonly used probe-based assay. TaqMan probes has a reporter dye at 5' end and a quencher molecule at other end (i.e. 3' end). The TaqMan probe works based on fluorescence resonance energy transfer (FRET) process in which the reporter dye's emission is absorb by the quencher molecule when they are in close proximity. During PCR amplification, the *Taq* polymerase cleaves off the annealed probe through an 5' - 3' exonuclease activity, resulting in increased fluorescence. TaqMan probe assay is highly specific, but costly to design and use [140, 122]. There have been various reports on the use of TaqMan real time PCR for specific detection of *Salmonella* [111, 155, 27], *Campylobacter* [207, 201, 30, 128], *E. coli* [99, 175], *L. monocytogenes* [91].

Commercial PCR devices however have several features with respect to size, weight, power usage and speed that make them less suitable for on-site analysis. Ideally, PCR process can be shorten to 2.5 min ( 5s/cycle: 1s for denaturation, 1s for annealing, and 3s for extension) [257] providing precise temperature control. However, the ramping rate in conventional devices is very slow (1 - 2 °C/s due to large thermal masses, since not only the PCR mixture but also the entire reaction chamber needs to heat up and cool down. This lead to very lengthy PCR reactions typically in the order of 1-2 h. In addition, PCR reactions in conventional setup requires significant amount of reagents. Microfluidic PCR devices are proposed to miniaturize the reaction chambers and integrate other functionalities (e.g. pre-PCR sample preparation and post-PCR analysis) onto a single chip. Microfluidic PCR devices can achieve faster heat transfer due to a smaller thermal mass of reaction chambers and a large surface to volume ratio.

Although PCR offers major advantages in terms of speed, specificity, and sensi-

tivity, the widespread application of this technology for detecting bacteria in food and environmental samples has been limited due to several methodological hurdles. The major challenge is the possibility of generation of false negatives due to issues associated with (1) the low infectious dose of foodborne pathogens [211], (2) assay detection limit (theoretical limit of detection of 1 cell per reaction is usually translated into  $10^3$ - $10^4$  cells per gram or per ml of food samples due to the small reaction volumes (10-50  $\mu$ L)), (3) the complexity of food sample matrix, and (4) presence of matrix-related interfering components that may degrade or inhibit PCR enzyme activity [203, 132, 191]. These issues decrease the limit of detection of PCR assay to  $10^3$ - $10^4$ , while the detection threshold for foodborne pathogens is one cell per 25g of sample based on international standards derived from traditional detection methods [156]. An efficient upstream sample preparation method is necessary to isolate, purify and pre-concentrate target pathogen for downstream PCR detection.

Culture-based pre-enrichment steps are successful in improving PCR sensitivity, however they are lengthy and laborious [155, 90, 207, 178]. Target-specific approaches have been developed as pre-PCR sample preparation methods that rely on natural biological interactions between bioaffinity ligands and bacterial cell surface receptors such as magnetic separation methods and flow cytometry. Antibodies, nucleic acid aptamers, lectins, bacteriophage, and phage receptor binding proteins are the widely used bioaffinity ligands that specifically recognize and bind to specific cell surface receptors, and have the advantage of high specificity and affinity. There are reports on successful application of each of these ligands for isolation, purification and pre-concentration of foodborne bacteria to improve the sensitivity of PCR assays [31, 14, 26]. However, as will be discussed later, each of these methods suffers from a practical hurdle that limits their application [59]. Therefore, there is still great interest in developing better alternatives to overcome these limitations.

Immunomagnetic separation in conjunction with PCR has been tested for detection of many foodborne pathogens such as *S. enterica* in milk (1 cfu/ml), ground beef (25 cfu/25g), and alfalfa sprouts (1.5 cfu/25g) within 13h [31], *E. coli* in ground beef ( $1.3 \times 10^4$  cells/g) [67], and *L. monocytogenes* in milk [14]. Overall, the capture and recovery efficiency of IMS methods highly depends on the sample matrix, target pathogen and its antigenic expression, and the affinity of antibody to its antigen.

The short shelf time of antibodies as a result of changes in environmental condition is another major challenge for the application of IMS. Phage or phage receptor binding protein mediated magnetic separation methods have been recently looked upon with the promise to overcome the challenges associated with the available methods [63, 28, 124].

## **2.2 Biosensors**

Rapid monitoring of food products with high levels of reliability, sensitivity and selectivity is critical for inspection of food products in industrial firms considering the short shelf time of products and low infection dose of foodborne pathogens. Biosensors have found great interests; and efforts have been focused on optimizing the biosensor transducers to improve the detection sensitivity. Bioprobes have been combined with various analytical methods to provide the specificity of recognition. We will review the biosensor transduction platforms that have been successfully employed for specific detection of foodborne pathogens. Table 2.1 summarizes various organisms that have been detected with these detection platforms.

### **2.2.1 Optical Biosensors**

Optical biosensors are rapid, sensitive, and adaptable to a wide variety of assay conditions, and have been widely investigated for bacterial pathogen detection. Optical techniques are divided into two main subcategories based on their working principles, labeled and label-free, The most commonly employed techniques for bacterial detection are surface Plasmon resonance (SPR), fluorescence/phosphorescence spectrometry and bio/chemiluminescence. In the following section, we will focus on optical biosensors that are employed for detection of foodborne pathogens.

#### **Surface Plasmon Resonance Sensors**

Surface Plasmon Resonance is the oscillation phenomenon that occurs at the interface between two media with oppositely charged dielectric constants. SPR sensors monitor events happening at surfaces and interfaces by excitation of plasmons by light in thin metal films, which generates evanescent electromagnetic wave. These

evanescent waves propagate along the interface between metal film and the ambient medium [208]. SPR sensors measure the refractive index near the sensor surface that changes as a result of interaction of target analyte in solution with receptors on transducer surface. SPR has been widely used for real-time monitoring of biochemical interactions of small analyte such as DNA hybridization, cell-ligand, protein-peptide, and protein-lipid. SPR systems have also been modified to enable the direct label-free detection of larger biomarkers such as bacterial pathogens. Successful detection of pathogenic bacteria has been reported on antibody-immobilized SPR sensors [236, 177]. Bacteriophages-based probes have also been immobilized on SPR sensors and successful detection of *S. aureus*[19] , *E. coli* K12 [17], *E. coli* O157:H7 and methicillin-resistant *Staphylococcus aureus* (MRSA) [235] has been reported. The limit of detection was typically in the range of  $10^2$  to  $10^3$  cfu ml<sup>-1</sup>. Bacteriophage receptor binding proteins have also been used as biorecognition probes on SPR. For example, Singh *et al.* immobilized genetically engineered tailspike proteins (TSP) from P22 bacteriophag *S. aureus* e and *Campylobacter* bacteriophage NCTC 12673 onto the gold-coated SPR plates, and demonstrated a selective real-time detection of *Salmonella* and *Campylobacter jejuni* bacteria with the LOD of  $10^3$  cfu ml<sup>-1</sup> and  $10^2$  cfu ml<sup>-1</sup> of bacteria, respectively [220, 219]. Recently, some efforts have been focused to simplify the bacterial detection with SPR to protein-protein interaction by combining a subtractive inhibition assay with a SPR immunosensor, and successful detection of *E. coli* O157:H7 cells [274] and *Listeria monocytogenes* [138] have been reported. In this method the target bacteria are incubated in antibodies for short amount of time, and then the cells bound to antibodies are separated from unbound antibodies by stepwise centrifugation. The remaining free antibodies are exposed to the surface of antibody immobilized SPR sensor chip and the general response is inversely proportional to the bacterial cell concentration. The lowest limit of detection reported is  $3 \times 10^4$  cfu ml<sup>-1</sup>.

### **Bioluminescence Sensors**

Bioluminescence assays quantitatively detects bacteria by measuring the level of light emission from interacellular components. This assay involves two major steps of bacterial cell lysis for release of interacellular components, followed by measuring the

content level using a bioluminescent reaction with luciferase. The major drawback of this technique is the lack of specificity. Using lytic phage specific to target bacteria as a recognition probe overcomes this limitation. Blasco *et al.* demonstrated successful detection of *E. coli* and *Salmonella newport* combining an ATP bioluminescence assay with lytic phage as bioprobe and lysis agent [32]. Ten- to 100-fold better sensitivity was reported when adenylate kinase (AK) was used as an alternative cell marker, and fewer than  $10^4$  cfu ml<sup>-1</sup> *E. coli* could be detected in less than 1 h [32]. A similar assay for *Salmonella* was slower and took up to 2 h [32]. Wu *et al.* showed that various factors such as the bacterial type, the growth stage, the phage type, and the infection time influence the amount of released AK from bacterial cells [260]. The use of lytic phage as biorecognition probe provides sensitivity and eliminates the need for lengthy conventional microbiological methods and selective media.

### **Fluorescent Bioassay**

Fluorescent bioassay is a sensitive and selective detection method that involves staining bacteria with fluorescence labels. For example, the fluorescently stained bacteriophages are used to recognize and bind to their host bacteria. The flow cytometry or epifluorescent filter techniques are then used to detect the complex of phage-bacteria with the average sensitivity of around  $10^2$  -  $10^3$  cfu ml<sup>-1</sup> for epifluorescent microscopy and is  $10^4$  cfu ml<sup>-1</sup> for flow cytometric detection [136, 92, 93]. This technique is further combined with immunomagnetic separation method, and improved the detection limit to  $10$  -  $10^2$  cfu ml<sup>-1</sup> *E. coli* O157:H7 in artificially contaminated milk after 10 h enrichment [79] and  $10^4$  cfu ml<sup>-1</sup> concentration of *E. coli* O157:H7 in broth [78].

Edgar *et al.* [61] and Yim *et al.* [273] further improved the sensitivity of this approach by tagging bacteriophage with fluorescent quantum dots (QD). QD improves the sensitivity of detection platforms such as flow cytometry and epifluorescence microscopy by boosting the intensity and stability of fluorescent signal. The streptavidin coated QDs were bound to the head of bacteriophage modified with biotin binding peptide. This method enabled detection of as low as 20 *E. coli* cells in 1 ml water sample in 1 h [61]. The fluorescent assays have also been used for detection of bacterial toxins. Goldman *et al.* applied phage display to select a 12-

mer peptide that could bind to *Staphylococcal enterotoxin B (SEB)*, which causes food poisoning [76]. They could detect as low as 1.4 ng of SEB per sample well in a fluorescence-based immunoassay using a fluorescently labeled SEB-binding phages. Array biosensors were also developed based on a similar principle to simultaneously detect *Bacillus globigii*, MS2 phage and SEB [204].

## 2.2.2 Electrochemical Biosensors

### Amperometric Biosensors

Amperometric biosensors usually rely on enzyme-based system that converts the analyte to a electrochemically active product that can be reduced or oxidized at a working electrode. They are usually composed of a pair of reference and working electrodes. They apply a bias voltage between two electrodes to generate a current through analyte that directly depends on the rate of electron transfer, which changes with variation in ionic concentration of analyte. Various amperometric biosensors are developed for detection of foodborne pathogens including phage-based, microbial metabolism-based, and antibody-based biosensors. Phage-based amperometric sensors work based on the principle that the overexposure of phages to bacterial cells results in bacteria lysis leading to release of bacteria cell content, such as enzyme, into the surrounding medium. This enzymatic activity can be measured and quantified using specific substrate. The product of the reaction between substrate and enzyme is oxidized at the carbon anode at the reference electrode, producing a current. Neufeld *et al.* combined amperometric technique with phage typing for specific detection of *E. coli* K12, *Mycobacterium smegmatis*, and *Bacillus cereus* bacteria [169]. They could achieve limit of detection of 1 cfu ml<sup>-1</sup> within 68 h using this technique in combination with filtration and pre-incubation before infecting bacteria with phage.

Amperometric biosensors are also employed to detect bacteria by monitoring a specific metabolic process. Ruan *et al.* developed a new in situ method for monitoring of *Salmonella typhimurium* in selective media by measuring the oxygen reduction peak on a gold electrode surface using electrochemical cyclic voltammetry during proliferation of bacteria [205]. The growth of *S. typhimurium* in selective

media consumes oxygen dissolved in medium causing a sharp decrease in the oxygen peak current at a time, termed the detection time (threshold value), during the growth of bacteria. They could successfully detect  $1-2 \times 10^0$  and  $1-2 \times 10^6$  cells per mL of viable *Salmonella* in 10 and 2.1 h, respectively [205]. Antibody-based amperometric sensors immobilize antibodies specific to bacteria directly on an electrode surface. Croci *et al.* [54] used 3, 3', 5, 5'-tetramethyl-benzidine as a substrate to measure the activity of horseradish peroxidase as label enzyme for detection of *Salmonella* in artificially contaminated pork, chicken and beef. Abu-rabeah *et al.* reported a double layered amperometric immunosensor for detection of E.coli, consisting of a polypyrrole-NH<sub>2</sub>-anti-E.coli antibody (PAE) inner layer followed by an alginate-polypyrrole (Alg-Pply) outer packing layer. Presence of bacterial enzyme, p-aminophenyl  $\beta$ -D-galactopyranoside (PAPG),  $\beta$ -D-galactosidase produces the p-aminophenol (PAP) product resulting in an amperometric signal. The low limit of detection of 10 cfu/ml is reported with this technique [12]. A disposable amperometric magnetoimmunosensor was developed for detection of Staphylococcal protein A and *Staphylococcus aureus* (*S. aureus*) with very low limit of detection (1 cfu/ml of raw milk sample). This assay involved immobilization of anti-protein A antibody onto protein A-functionalized magnetic beads, followed by a competitive immunoassay involving protein A labeled with HRP. The modified magnetic beads were captured on the surface of tetrahiafulvalene-modified Au/ SPEs and the amperometric response was obtained with respect to the silver pseudo-reference electrode of the Au/SPE after the addition of H<sub>2</sub>O<sub>2</sub> [56].

### **Impedimetric Biosensors**

Electrochemical impedance spectroscopy (EIS) biosensors monitor biomolecular interactions by measuring the resulting changes in impedance over a range of frequencies. For example, EIS bacterial biosensors monitors the changes in the solution-electrode interface due to the capture of microorganisms on the sensor surface. The capture of target analyte such as bacteria on sensor increases the insulation resulting in increase in the impedance. Shabani *et al.* [214] and Mejri *et al.* [158] developed a EIS bacterial detection platform by immobilizing T4 phage onto the functionalized screen-printed carbon electrode, and showed specific detection of *E.*

*coli* bacteria with limit of detection of approximately  $10^4$  cfu ml<sup>-1</sup>. Although EIS offers label-free detection of pathogens compared to amperometry technique, its application for pathogen detection is limited due to its lower detection limit compared to other techniques.

### Potentiometric Biosensors

Potentiometry is the simplest, most widespread and most field portable method among electrochemical techniques. It allows the determination of various ions in the wide range of concentrations and requires inexpensive equipments. Potentiometric solid-state electrodes have been used for bioanalysis in liquid samples. Carbon nanotube and aptamer-based potentiometric biosensors have been used for detection of 1cfu *Salmonella* Typhi in 5mL of buffered sample in less than 1 min [278] or 12 cfu of *E. coli* in 2 mL of milk in a couple of minutes [280], and  $8 \times 10^2$  cfu/mL of *S. aureus* in a couple of minutes [279]. Recently, chemically modified graphene-based aptasensor was reported for detection of a single cfu/mL of *S. aureus* in near realtime [94]. The application of these aptasensors in real samples with complex matrices however requires filtration prior to analysis to remove undesired electroactive species within the original matrix [94]. Otherwise, the results may not be accurate.

### 2.2.3 Micromechanical Biosensors

#### Quartz Crystal Microbalance Biosensors

Quartz crystal microbalance (QCM) sensors are very sensitive with capability for detection of nanogram changes in mass. A QCM sensor is composed of two metallic electrodes coated on two sides of a thin piezoelectric plate. Applying an electrical field across the quartz crystal excites the mechanical resonance. The fundamental wavelength ( $\lambda$ ) and resonance wavelength ( $\lambda = 2d/n$ ) are determined based on the plate thickness  $d$ , and thus the corresponding resonant frequency:

$$f_n = n.f_0 = \frac{n.\nu}{2d} \quad (2.1)$$

where  $\nu$  is the sound velocity, and  $f_0$ ,  $f_n$  are the fundamental and the  $n$ th overtone resonant frequency, respectively. The resonance frequency shifts to lower

frequencies after adsorption of mass onto the electrode surface. The rate of frequency change is proportional to the adsorbed mass with uniform distribution according to the Sauerbrey Equation:

$$\Delta f = \frac{-2f_0^2 \Delta m}{A(\mu\rho)^{\frac{1}{2}}} \quad (2.2)$$

in which  $\mu$  is the shear modulus of quartz ( $2.947 \times 10^{11} \text{ gcm}^{-1}\text{s}^{-2}$ ), A is the piezoelectrically active crystal area, and  $\rho$  is the density of the quartz ( $2.648 \text{ gcm}^{-3}$ ). QCM sensors are used to measure the mass of various target analytes by immobilizing specific probes on a sensor surface. Bacteriophage probes are immobilized onto QCM sensors for specific detection of bacteria. Olsen *et al.* developed a sensitive platform for rapid detection of *Salmonella typhimurium* by physical adsorption of  $3 \times 10^{10} \text{ phagescm}^{-2}$  on piezoelectric transducer surface. This phage-immobilized QCM sensor had a low detection limit of  $10^2 \text{ cells ml}^{-1}$  with a wide linear range of  $10 - 10^7 \text{ cells ml}^{-1}$  and a rapid response time of less than 180 s [179].

### Magnetoelastic Sensors

Magnetoelastic sensors are mechanical oscillators that are excited with an AC magnetic field. The sensor resonates when the applied field frequency equals the natural frequency of sensors. The fundamental resonant frequency of longitudinal oscillations is given by:

$$f = \sqrt{\frac{E}{\rho(1-\nu^2)}} \frac{1}{2L} \quad (2.3)$$

where E is the Youngs modulus of elasticity,  $\rho$  the density of the sensor material,  $\nu$  the Poissons ratio, and L is the long dimension of the sensor. The mechanical oscillation is damped when non-magnetoelastic material are added to the sensor surface resulting in frequency shift:

$$\Delta f = -\frac{f}{2} \frac{\Delta m}{M} \quad (2.4)$$

where f is the initial resonance frequency, M the initial mass,  $\Delta m$  (smaller than M) the mass change and  $\Delta f$  is the shift in the resonant frequency of the sensor. The

response of the magnetoelastic sensors can be measured wireless, making the real-time and in vivo bio-detection feasible. Filamentous bacteriophages are immobilized on magnetoelastic sensors for the detection of various bacteria including *Salmonella typhimurium* and *Bacillus anthracis* spores in different food matrixes such as fat free milk, and fresh tomato [129, 129, 130]. The limit of detection was typically in the range of  $10^3$  cfu ml<sup>-1</sup>.

### **Cantilever-based Sensors**

Cantilever sensors are a class of micro mechanical sensors which hold promises as label-free, sensitive, portable, inexpensive sensors with potential for integration into large arrays for parallel, high throughput analysis of samples. Cantilevers are used in two modes: the static mode and the dynamic mode. The static mode cantilevers measures the changes in the cantilever deflection caused by differential surface stress upon adsorption of target analyses. The resonant mode (i.e. dynamic mode) cantilevers rely on the shifts in resonant frequency caused by mass changes. Cantilever sensors have been used to measure mass of various cells and biomolecules [38, 264, 157, 281, 82, 42, 172, 74, 142] with mass sensitivities down to the single cell level [107].

The resonant mode cantilevers measure the binding induced changes in mass directly, however the interference from the sensing medium (e.g. effects such as viscous damping) can strongly effect the sensors response. The static mode cantilevers are usually not influenced by surrounding medium as long as the cantilever deflection can be measured accurately. The theory behind resonant mode cantilever will be discussed in detail in chapter 3

## **2.3 Lab-on-a-Chip technology for Pathogen Detection**

In the past decade, developments in microfluidic technology led to introduction of lab-on-a-chip (LOC) devices which miniaturize and integrate several chemical and biological assays on a single chip. Integrated LOC devices offer major advantages such as rapid analysis, lower cost, smaller reagent consumption, and lower turnaround time. These features make them favourable for point-of-care (POC)

applications. Various laboratory-based methods for pathogen detection are miniaturized into microfluidic LOC devices. Microfluidic PCR devices were introduced in the early 1990s [171]. Integrating PCR onto microfluidic devices reduces the size of amplification reaction chamber to micro/nano scale and increases the surface to volume ratio, thus yields lower thermal capacities and a higher heat transfer rates leading to faster amplification ( 5-10 minutes) compared to the conventional PCR systems (30 min - 2h). Initially, silicon microstructures were proposed with rapid ramp rates in the order of  $\approx 4$  °C/s for cooling and  $\approx 6$  °C/s for heating, and rapid thermal cycling in the order of 30 s/cycle [217, 170, 237] and even 17 s/cycle [25] were achieved. In such devices, the dwell times of denaturation and annealing steps were reduced to 1 - 5 s and realtime TaqMan PCR assay was performed in 7 min [25]. Glass microchips with non-contact infrared-mediated thermal cycling was also reported with fast heating and cooling rates of 10 °C/s and 20 °C/s [176] and even faster of 67 °C/s and 53 °C/s [225]. Droplet-based microfluidics have also been looked upon for development of microbial detection platforms. Heyries *et al.* presented a microfluidic "megapixel" digital PCR device that employs surface tension-based sample partitioning and dehydration control to enable high-fidelity single DNA molecule amplification in 1,000,000 reactors of pico litre volume with densities up to 440,000 reactors  $\text{cm}^{-2}$ [95]. They reported a dynamic range of  $10^7$ , single-nuceotide-variant detection below one copy per 100,000 wild type sequence. Their devices could also achieve the discrimination of a 1% difference in chromosome copy number [95]. The droplet-based microfluidic devices hold promise for the development of universal and programmable microfluidic devices. Leung *et al.* presented a versatile microfluidic device that enables the execution of different experiments as well as independent recovery of reaction products, through simple reprogramming of device operation [139].

Detection methods are also miniaturized and integrated onto microfluidic PCR devices. Capillary gel electrophoresis [114, 148, 60, 100, 117, 276] and fluorescence detection [170, 51, 115, 134, 145, 144] are the most common techniques for measurement of amplified DNA products that have been integrated within microfluidic PCR systems. The capillary electrophoresis (CGE) is an alternative technique for conventional slab gel electrophoresis. This technique is suitable for integration with

PCR microchips for practical DNA/PCR product analysis. CGE offers excellent performance due to fast separation and detection, reduced risk of contamination due to minimum manual sample handling and transportation, and high sensitivity and capability for quantification of results. Fluorescence detection has also been implemented in microfluidic devices to realize realtime PCR using two common methods. The first one uses fluorescent dye to intercalate with dsDNA and to emit fluorescence. The intensity of fluorescent signal is in direct relationship with the amount of dsDNA (e.g. amplified DNA/ PCR product). The second fluorescence measurement method is based on using a spectrometer with continuous spectral dispersion and a linear charge-coupled-device (CCD) array detector during thermal cycling in a realtime PCR machine.

Further efforts have been expanded so far as to integration of sample preparation modules along with detection methods on a single LOC device. The common approaches for separation of cells, bacteria, viruses from clinical samples are hydrodynamic forces [102, 206, 261, 265, 270, 271], microfiltration [52, 213, 243, 256, 259, 266], acoustic forces [133, 262], dielectrophoretic (DEP) forces [23, 24, 70, 86, 147], and magnetic separators [69, 141, 258, 200]. Cell lysis is also a very critical step for extraction of nucleic acids for variety of applications. Various microfluidic devices are also developed to perform cell lysis including chemical, thermal, laser, ultrasonic, mechanical, electrical and electrochemical approaches. DNA/RNA extraction is another important step in molecular biology which has been integrated in microfluidic devices based on DEP forces or magnetic beads. The sample pre-treatment is crucial for successful DNA based detection as it increases the limit of detection of the sensing system. White *et al.* presented a fully-integrated microfluidic device capable of performing high-precision RT-qPCR measurements of gene expression from hundreds of single cells per run. Their proposed device performs all steps of single-cell processing including cell capture, cell lysis, reverse transcription, and quantitative PCR on a single chip [254]. Miniaturization of these processes significantly reduces the required sample volume and processing time.

Microfluidic systems have been used for identification of various pathogens such as *Listeria monocytogenes*. Shu *et al.* developed an integrated microfluidic platform for detection of low level of *Listeria monocytogenes* (around 0.2 copies/ $\mu\text{L}$

of genomic DNA) with a single phase continuous-flow nested PCR strategy [216]. An integrated microfluidic device capable of monoazide pre-treatment and PCR was developed for rapid detection of live methicillin-resistant *Staphylococcus aureus* (MRSA) [150]. Chen *et al.* reported a complex polycarbonate microfluidic system for saliva-based bacterial detection. The microfluidic chip contains a fluidic network for cell lysis, DNA extraction, PCR, and labelling of PCR product with phosphor particles for detection on the lateral flow strip [50]. Simultaneous detection of *Salmonella enterica*, *Escherichia coli* O157:H7, *Listeria monocytogenes* was reported using an oscillatory-flow multiplex PCR microfluidic device [248]. These reports shows that microfluidic systems are promising for detection of bacteria, however, the detection is mainly limited to clean samples using purified genomic DNA.

## 2.4 Biomarkers

Biomarkers are vital for specific identification of biological species. Ideal attributes of any recognition element would be high stability, ease of immobilization on sensor platform and recognition specificity towards host with minimum cross-reactivity from interfering pathogens. The popular bio-probes that have been employed for pathogen detection are nucleic acids, antibodies, whole phages, phage-display peptides (PDPs) and most recently phages receptor binding proteins (RBPs).

### 2.4.1 Nucleic Acids

The fundamental principle behind nucleic acid based detection lies in the sequence complementarity. The careful choice of probe is essential to maintain specificity of detection. Deoxyribonucleic acid (DNA), ribonucleic acid (RNA), peptide nucleic acids (PNAs) and locked nucleic acids (LNA) are the molecular probes that have been explored for such applications. The major advantage of using DNA-based probes is the ability to amplify a desired target DNA sequence from the host pathogen using PCR and consequently augment the signal generated by the biosensor in the event of hybridization on the detection platform. RNA could similarly be amplified by reverse transcription PCR (RT-PCR) using RNA polymerase enzymes to similar effect. Alternatively, PNAs are pseudopeptide DNA mimics that

show high binding affinity to DNA or RNA by sequence-specific complementary base pairing. LNA s are modified RNA nucleotides with an extra bridge connecting the 2' oxygen and 4' carbon. LNAs have better hybridization properties since the locked ribose conformation enhances base staking and backbone pre-organization. They are therefore looked upon as attractive substitutes for DNA- or RNA-based probes due to their improved binding characteristics and better stability against physical, chemical and biological degradation. The use of PNAs as biological probes for pathogen detection is a relatively new but rapidly growing area of investigation but their application is limited due to the high cost involved in the synthesis of these probes. DNA and RNA based detection approach therefore is simple, stable, versatile, rapid and cost-effective. Besides, the development of microarray technology [277] and multiplex-PCR [234] provides opportunities for detection of several pathogens simultaneously in complex food matrices. In addition, nucleic acid-based probes (especially DNA) are highly stable in a variety of solvents [33] and buffers, which facilitates their application in a wider range of food samples. The advancement in the nucleic acid-based probe technology has led to several commercialized products for pathogen detection mostly for clinically relevant samples.

Though nucleic acid hybridization-based detection systems are tremendously popular for pathogen identification, they have several drawbacks that limit their application. PCR-based amplification methods rely heavily on the purity of the template nucleic acid and are therefore prone to contaminations that would amplify and result in false positives. Similarly, degradation of the template nucleic acid could also result in a false negative result. One such product, LCx (Abbott Laboratories, Abbott Park, IL, USA), a ligase chain reaction based system for Chlamydia detection was pulled from the market in 2003 due to problems with reproducibility of results [80]. Nucleic Acid Hybridization (NAH) detection systems are also incapable of predicting the viability of the bacteria and thus the true bacterial load in a sample. Besides, these systems cannot be used to detect toxins produced by certain bacteria in a food sample. Despite these limitations, NAH-based systems have enjoyed considerable success and have been extensively studied. A details account of nucleic acid based detection system has been reviewed [161] and is recommended to the readers.

### 2.4.2 Antibodies

Antibodies have been extensively explored as bio-probes for pathogen detection and monitoring due to the ease of their immobilization on biosensor surface and high level of specificity ( $kd \ 10^7 10^{11}$ ) towards their target. Polyclonal and monoclonal Abs, Abs fragments, recombinant Abs and llama bodies have been successfully employed for detection of pathogens, their spores as well as toxins. They have also been simultaneously used for immune-magnetic separation of pathogens during sample processing for pre-enrichment and pre-concentration [81]. Enzyme-linked immunosorbent assay (ELISA) is the most commonly used method for Ab-based detection, though they have been successfully integrated on other biosensor platforms as well. The PCR-based target amplification and ELISA-based detection specificity have also been combined as PCR-ELISA to attain improved detection limits. Perelle *et al.* demonstrated that PCR-ELISA could be successfully employed to detect five Salmonella cells in milk or meat samples of 25 g size [185]. Abs have similarly been integrated into optical [97], electrochemical [180], mass-based [232], magnetic [162], surface-acoustic wave (SAW) [29] and cantilevers [42] based platform for detection of pathogen mostly in clinical samples though there is a dearth of commercialized systems for analysis of food samples. Abs as bio-probes however suffer from several drawbacks that limit their application. They are highly prone to physical (temperature, pH), chemical and enzymatic damage. They have to be stored in a controlled refrigerated environment and even then the shelf life is low, limiting their application in in situ conditions outside the lab. Polyclonal Abs have several recognition epitopes and thus show cross-reactivity, while monoclonal antibodies, though specific to a single epitope, involve high production costs. Production of the Abs also involves immunization of animals, which poses ethical issues with their application. Stability of the Abs at higher temperature has been addressed to some extent by production of llama bodies, which are truncated Abs with single heavy chain (VH) with small antigen binding site and lack light chain (VL) [85]. These llama bodies have been found to be stable up to 90 °C and their engineered clones have been successfully applied in pathogen detection [75, 241]. Phage display Abs is yet another approach that overcomes several shortcomings of conventional Abs, which will be

discussed in detailed in the next section. Byrne *et al.* have recently reviewed the principles, problems and potential applications of Ab-based sensors for detection of pathogens and toxins [4]. Table 2 provides a list of some commercially available kits for the detection of foodborne pathogens along with the method of detection, company name, product name and limit of detection if available.

### 2.4.3 Bacteriophage

Phages are obligate parasites that lack their own metabolic machinery. They use their bacterial hosts for multiplication and propagation of mature virions. Most phages recognize their host very specifically to the strain level of bacteria, with few exceptions, such as Listeria phage A511 that identifies, binds and kills within an entire genus [282] while some phages show inter-species binding capability. Phages bind to their host bacteria, inject their DNA and take over the host machinery to propagate new virions that lyse the bacteria to infect new host (lytic phages) or integrate their genome into the host DNA, remain dormant until stimulated for replication and propagation (lysogenic phage). With an estimated pool of  $10^{31}$  phages existing in the environment, this provides a unique class of recognition elements that can be exploited not only for bacterial identification and binding on biosensor surface but also as therapeutic biocontrol agents. Structure and anatomy of bacteriophage as well as phage-based recognition elements that have been employed as bio-probe on sensor platforms for pathogen detection will be described in details in 5.4.3.

## 2.5 Sample Preparation

The application of many detection methods for analysis of food samples is usually problematic due to the complexity of food samples and presence of various interfering components. In addition, the contaminating dose of pathogenic bacteria in food products is usually very low (10-1000 cells) and barely reaches the limit of detection of rapid technologies. These issues reduces test specificity and sensitivity and leads to less than optimal detection results. Traditionally, lengthy cultural enrichment steps are included to overcome these limitations. However, the ultimate objective of new detection technologies is to shorten the analysis time which is not possible

with such lengthy pre-enrichment processes. Efforts have been focused on developing better sample preparation techniques. An efficient sample preparation process addresses several important issues: (1) it separates target pathogens from a complex food sample, (2) removes matrix-associated inhibitory factors, (3) ideally recovers all of the pathogens without any cell disruption, and (4) pre-concentrate the recovered pathogens to the concentrations suitable with downstream assays. Various sample preparation methods are investigated with the goal to achieve high recovery of target bacteria and removal of interfering components. Some of the common techniques are chemical methods based on adsorption and desorption of bacterial cell walls to solid surfaces such as biofilms, lectins, and ion exchange resins, physical separation methods such as centrifugation, filtration and dilution, or the combination of two methods called physico-chemical methods using metal hydroxide. Magnetic separation methods are yet another approach that immobilizes biomarkers on magnetic particles for recognition and separation of bacteria from crude samples.

### 2.5.1 Chemical Methods

Bacterial cells are adsorbed to food particulates by cell wall constituents including proteins and carbohydrate. Chemical methods disrupts the attractive force between the bacterial cells and the food components to separate bacteria from food samples. Most microorganisms have a net negative charge and therefore they can be absorbed to positively charged compounds. Solid surfaces such as ion exchange resins and lectins are used to separate target microorganisms. In the next step, the absorbed substances are eluted from the solid surface by a reversible physicochemical interaction between pathogen surface and the solid matrix such as pH manipulation. Chemical methods are rapid and inexpensive, but sample pre-treatments are necessary to remove debris. In addition, they are generally not specific to the target microorganism and the pH manipulations needed for elution of adsorbed destroys cell viability. Jacobsen *et al.* used ion exchange resins in combination with differential centrifugation to recover *Pseudomonas cepacia* from soil and reported 35 % recovery rate [108].

### 2.5.2 Physical Methods

Centrifugation is the most common physical separation method that uses the centrifugal force to drive particles suspended in liquid medium to sediment. The sedimentation rate depends on variety of physical factors including particle diameter, particle density, solution entity, volume, angle, and speed of rotation. The sedimentation rate also depends on the solution viscosity and gravitational force. Various centrifugation methods are developed by manipulating solution density, particle size, and rotational speed. High speed centrifugation ( $9000 \times g$ ) was used to isolate *E. coli*, *Listeria*, *Salmonella* from seafood and soft cheese [250]. Differential centrifugation (i.e. low speed centrifugation ( $\leq 1,000 \times g$ ) followed by high speed centrifugation ( $\geq 8,000 \times g$ ) was also used to separate *Listeria* from meat homogenate [167] and *E. coli* from soft cheese [159]. Separation by means of centrifugation is rapid, simple and inexpensive, however, this method is not specific, and in most cases not efficient as bacteria adhere to and sediment with the matrix component. In addition, bacterial cells are usually damaged during centrifugation due shear force [230].

Filtration is another physical method that separate bacteria and inhibitors based on either solubility of molecular weight. Iso-Grid (Neogen Corporation, Lansing, MI) is a commercial method that uses dual filtration procedure for separation and quantification of microorganisms. First, a  $5 \mu\text{m}$ , pre-filter is used to remove gross food particulates. The sample is then passed through  $0.45 \mu\text{m}$  hydrophobic, grid filter which is designed to minimize the spread of colonies and is divided into sections of a known area to facilitate counting after incubation on the surface of agar plate [183]. Iso-Grid methods are available for *E. coli*, *Salmonella*, *Listeria*, etc. Electropositively charged filters are also used for bacterial separation. Although bacteria adsorbs to these filters quite efficiently since bacteria have a net negative charge, adsorption rates are relatively poor. Thomas *et al.* used this method for recovery of yeast and lactic acid bacteria from wine and beverages [238]. Overall, filtration has not been a successful method for bacterial concentration from food samples because large particles tend to clog the filters. In addition, some components of food matrix also tend to concentrate with the bacteria that are inhibitory for downstream applications such as PCR. More importantly, some number of bacteria may attach

to the upper surface of the filter or may trap in filter pores, and the recovery of the microorganisms from filter is almost always incomplete which may result in underestimate of bacterial load. Moreover, the filtration process usually impairs the ability of microorganisms to grow on solid media.

### 2.5.3 Physico-chemical Methods

One of the efficient techniques for separation and concentration of bacteria combines physical and chemical principles using metal hydroxides. This method adds high molecular weight charged material to bridge oppositely charged particles to produce a loose aggregate. This aggregate is simply removed by physical methods such as low speed centrifugation. Kennedy *et al.* first proposed the use of titanous and zirconium hydroxide to immobilize bacterial cells to eliminate tedious enzyme purification procedures for use in enzymatic assays [116]. Ibrahim *et al.* later reported the use of titanous hydroxide to immobilize and recover various gram-negative and gram-positive organisms with recovery rates varying from 90-98% [104]. Later, they employed a similar immobilization platform for solid-phase ELISA detection of *Salmonella*, and demonstrated 100- to 160- fold improvement in limit of detection when applied to food enrichment broth [105]. Overall, bacterial immobilization and isolation using metal hydroxide is easy, rapid, and inexpensive. Recovered bacteria usually reserve their viability. Since the introduction of the method, it has been coupled with various detection methods such as culture and colony counting and RT-PCR after RNA extraction [153]. Cullison *et al.* coupled magnetized carbonyl iron to zirconium hydroxide suspension to facilitate magnetic separation of hydroxide-bacteria complexes without the need for any centrifugation steps [55].

### 2.5.4 Magnetic Separation

Magnetic separation of cells offers several advantages over other sample preparation techniques. Throughout magnetic separation, the target cells are isolated directly from crude samples such as food, water, stool, blood, etc in relatively fast and simple process. This method allows selective separation of desired bacteria due to the large difference between the permeability of magnetic particles and non-magnetic com-

ponents. In addition, magnetic separation technique is generally a gentle process, and does not disrupt delicate bacterial cells during sample preparation, and the recovered cells by magnetic separation are usually unchanged, pure, and viable. This technique does not require too much handling, costly equipments, or expensive consumables, and therefore can be easily integrated into automated or semiautomated platforms for high throughput preparation of multiple samples.

The particles used magnetic separation of bacteria are usually on the order of a cell diameter (1 - 5  $\mu\text{m}$ ). These particles are typically superparamagnetic, meaning that they only show magnetic properties in presence of an external magnetic field. Therefore, these particles can be suspended in homogeneous mixture without attracting to each other in the absence of an external magnetic field. The fine grains of iron oxides are dispersed inside a polymer shell to eliminate direct exposure of cells to iron. The polymer surface chemistry is usually modified to provide linking agents.

The typical magnetic separation process for isolation of target cells consists of three fundamental steps:

- The magnetic particles are coated with target-specific biorecognition probes. Antibodies are the most commonly used agents for this purpose. However, they suffer from several limitations as will be discussed later. Therefore, there is need to find better bioreceptors alternatives for immobilization of magnetic particles for purification of cells from various matrixes.
- The functionalized magnetic particles are incubated in the suspension containing the cells of interest usually for 30- 60 min to allow interaction between cells and bioreceptors. The cell-magnetic particle clusters are then separated using an appropriate magnetic separator and the supernatant is discarded.
- The cell-magnetic particle complex are then washed in buffered solutions to remove unwanted contaminant or loosely bound cells. The cell-bead clusters are resuspended in a small volume of buffer for later analysis.

Immunomagnetic separation (IMS) is the most widely studied sample preparation method that uses antibody coated magnetic beads for isolation of bacterial

cells from different samples. IMS has been combined with PCR for the detection of various pathogens such as *Salmonella* [198, 31], *L. monocytogenes* [242, 268, 65], and *E. coli* [135, 67] in different food samples such as dairy [65, 268, 242, 31], egg products [198], and meat samples [101, 31]. Combination of IMS with PCR has also shown promise for simultaneous detection of pathogens unambiguously [249, 98]. Although antibodies as bio-probe provide some level of specificity, they suffer from several drawbacks. They are highly prone to physical (temperature, pH), chemical and enzymatic damage, and therefore they have a short shelf time even when stored in a controlled refrigerated environment. Polyclonal Abs are inexpensive but they show cross-reactivity. Alternatively, monoclonal antibodies are specific to a single epitope, but they involve high production cost. Therefore, there is need to develop better recognition and linking agents.

Quite recently, bacteriophage based probes were immobilized on magnetic particles for separation and concentration of *Salmonella* from food samples [63][28]. The bacteriophages offer several advantages over antibodies such as ease of production, high specificity of recognition, natural affinity of phage to bacterial cells, and stability against environmental factors. Bacteriophage based probes however are relatively large, and therefore uniform functionalization of such large entities on microsize particles are challenging. In addition, immobilized phages may wrap themselves around the magnetic particles, and consequently loose the availability of their tail fibers for the capture of bacteria. Moreover, phages may undergo a lytic activity, resulting in lysis of captured cells, consequently leading to the inefficient detection. Recently, Kretzer *et al.* demonstrated that the cell wall-binding domains of bacteriophage endolysins are suitable for the capture and separation of bacteria when immobilized on paramagnetic beads [124]. Recently, we developed phage RBP-derivatized magnetic separation method as an upstream sample preparation method for PCR and demonstrated their efficiency in improving the sensitivity of PCR assays for detection of pathogenic bacteria in food samples [189]

With recent developments in MEMS technology, magnetic separation modules are integrated in with biosensors and microfluidic devices [146, 226, 121, 149, 194]. Varshney *et al.* integrated magnetic nano particle-antibody conjugates (MNAC) within a microfluidic flow cell with embedded gold interdigitated array micro elec-

trode (IDAM) and demonstrated detection of pathogenic bacteria in ground beef [245]. Self-assembled magnetic bead biosensors are also developed for measuring bacterial growth and antimicrobial susceptibility testing [121]. Despite significant developments in magnetic manipulation on microfluidic systems, the integration of the magnetic separation methods with PCR on chip and its in field application is still topic of ongoing researches.

Table 2.1: A list of foodborne pathogens detected using various biosensors highlighting the transduction platform used and limit of detection achieved.

Transducer	Organism	Bioreceptor	Limit of Detection	Ref
SPR	<i>E. coli</i> K12	T4 Phage	$7 \times 10^2$ cfu.ml <sup>-1</sup>	[17]
SPR	<i>E. coli</i> O157:H7	T4 Phage	$1 \times 10^3$ cfu.ml <sup>-1</sup>	[235]
SPR	MRSA	BP14 Phage	$1 \times 10^3$ cfu.ml <sup>-1</sup>	[235]
SPR	<i>Salmonella</i>	P22 Phage TSP	$1 \times 10^3$ cfu.ml <sup>-1</sup>	[220]
SPR	<i>C. jejuni</i>	Phage NCTC 12673 TSP	$1 \times 10^2$ cfu.ml <sup>-1</sup>	[219]
SPR	<i>S. aureus</i>	Lytic Phage (Phage 12600)	$1 \times 10^4$ cfu.ml <sup>-1</sup>	[19]
SPR/subtractive inhibition assay	<i>E. coli</i> O157:H7	Goat polyclonal antibodies	$3 \times 10^4$ cfu.ml <sup>-1</sup>	[274]
SPR /subtractive inhibition assay	<i>Listeria monocytogenes</i>	Antibodies	$1 \times 10^5$ cfu.ml <sup>-1</sup>	[138]
Bioluminescence	<i>E. coli</i>	E.coli phage	$1 \times 10^3$ cfu.ml <sup>-1</sup>	[32]
Bioluminescence	<i>Salmonella newport</i>	Felix phage	$1 \times 10^3$ cfu.ml <sup>-1</sup>	[32]
Bioluminescence	<i>Salmonella enteritidis</i>	Phage SJ2	$1 \times 10^3$ cfu.ml <sup>-1</sup>	[260]
Bioluminescence	<i>E. coli</i> G2-2	AT20	$1 \times 10^3$ cfu.ml <sup>-1</sup>	[260]
Fluorescent	<i>Staphylococcal enterotoxin B (SEB)</i>	Phage-diplayed peptides	1.4 ng	[76]
Fluorescent	<i>E.coli</i>	QD-labeled lambda phage	N/A	[273]
Fluorescent	<i>E.coli</i>	T7 phage	20 cell.ml <sup>-1</sup>	[61]
QCM	<i>Salmonella typhimurium</i>	Filamentous phage	$1 \times 10^2$ cell.ml <sup>-1</sup>	[179]
Magnetoelastic	<i>Salmonella</i>	Filamentous E2 phage	$5 \times 10^2$ cell.ml <sup>-1</sup>	[130, 143]
Magnetoelastic	<i>Bacillus anthracis</i> spores	Filamentous phage clone JRB7	N/A	[215]
Amperometric combined with pre-filtration	<i>E. coli</i> K12	Phage Lambda	$1 \times 10^2$ cfu.ml <sup>-1</sup>	[169]
Amperometric	<i>Salmonella</i>	N/A	$1-2 \times 10^0$ cfu.ml <sup>-1</sup>	[205]
Amperometric immunosensor	<i>E. coli</i>	Polypyrrole-NH2-anti-E. coli antibody	10 cfu.ml <sup>-1</sup>	[12]
Amperometric magnetoimmunosensor	<i>Staphylococcus aureus</i>	Anti- Prot A antibody	1 cfu.ml <sup>-1</sup>	[56]
Impedimetric	<i>E. coli</i>	T4 Phage	$10^4$ cfu.ml <sup>-1</sup>	[136, 214]

## Chapter 3

# Introduction to Micro/Nano-Resonator Sensors

### 3.1 Introduction

Microresonator based biosensors have attracted attention in recent years due to their potential as a sensitive and high-throughput platform. A basic understanding about the vibration mechanics of micromechanical resonators is important for developing sensors with optimized sensitivity and structural design. This chapter overviews the mechanical vibration of microresonator-based sensors and includes some of the associated fundamental materials. Reader can read ref [197] for more theory.

### 3.2 Vibration Theory of Discrete Systems

#### 3.2.1 One Degree of Freedom Simple Harmonic

Any mechanical system is literally susceptible to vibrations. A basic mechanical system can be modelled with a mass ( $M$ ) attached to a spring ( $K$ ). The equation of motion of this systems without any external excitation is determined using Equation (3.1)

$$M\ddot{x} + Kx = 0. \tag{3.1}$$

The solution of this equation is:

$$x(t) = A_1 \sin(\sqrt{\frac{K}{M}}t) + A_2 \cos(\sqrt{\frac{K}{M}}t), \quad (3.2)$$

leading to the natural frequency:

$$f = \frac{1}{2\pi} \sqrt{\frac{K}{M}}. \quad (3.3)$$

The natural frequency of the system is the frequency at which the system oscillates without any external excitation. The maximum vibration amplitude occurs when the external force is applied at the natural frequency.

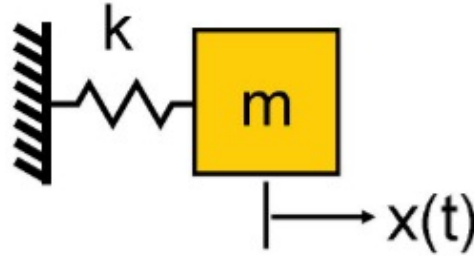


Figure 3.1: A single degree of freedom mechanical system.

### 3.2.2 Effective Mass and Stiffness

Mechanical systems with more than one mass and stiffness components can be mathematically described with a similar equation with slight modifications:

$$M_{eff}\ddot{x} + K_{eff}x = 0. \quad (3.4)$$

in which,  $M_{eff}$  and  $K_{eff}$  are effective mass and spring constant, respectively. The effective mass and stiffness is determined by writing the velocities of all components with respect to one reference point using the energy methods. The effective mass is calculated based on the total maximum kinetic energy ( $E_k$ ) of a point mass with velocity  $v_r$  at the reference point using following equation:

$$E_k = \frac{1}{2}M_{eff}v_r^2, \quad (3.5)$$

The effective stiffness is calculated considering the potential energy ( $E_p$ ) and the displacement of the reference point ( $x_r$ ) as follows:

$$E_p = \frac{1}{2}K_{eff}x_r^2. \quad (3.6)$$

### 3.2.3 Multiple Degree of Freedom

More complicated systems have more degree of freedom. In such cases, the equation of motion becomes:

$$[M_{eff}]\ddot{x} + [K_{eff}]x = 0. \quad (3.7)$$

where  $x$  is a vector of the reference position and  $[M_{eff}]$  and  $[K_{eff}]$  are effective mass and stiffness matrices, respectively. A system with  $n$  degree of freedom has  $n$  different mode of vibration. Each mode adds another solution to Equation (3.7), which corresponds to a movement trajectory and a natural frequency.

### 3.2.4 System with Damping

Different dissipation mechanisms influence a mechanical system with a kinetic energy and cause the loss of kinetic energy. Dissipation mechanisms are either intrinsic process (e.g. phonon-phonon interaction, phonon-electron interaction, thermoelastic damping, and clamping point damping) or extrinsic due to interaction with the surrounding media. A basic mechanical system with damping can be represented as following:

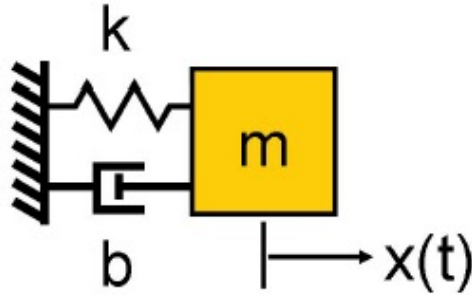


Figure 3.2: A mechanical system with damping.

$$M_{eff}\ddot{x} + b\dot{x} + K_{eff}x = 0. \quad (3.8)$$

where  $b$  is the damping coefficient. The presence of damping will cause the vibrations to eventually stop. The natural frequency is also affected by the presence of damping as given in Equation (3.9):

$$f_r = \frac{1}{2\pi} \sqrt{\frac{K_{eff}}{M_{eff}}} \sqrt{1 - \zeta^2} \quad (3.9)$$

where  $\zeta$  is the damping ratio and is given by:

$$\zeta = \frac{b}{2\sqrt{M_{eff}K_{eff}}} \quad (3.10)$$

Equation (3.9) is only valid for the values of  $\zeta$  less than one. The amplitude of vibration is theoretically unbound for undamped systems. However, most systems practically experience some damping which limits the amplitude of motion to a finite value. Damping ratio determines the bandwidth in the frequency response of the system, which is measured by the quality factor ( $Q$ ) of the device. The quality factor is defined as the ratio between stored vibrational energy  $W_0$  to the total energy lost per cycle  $\Delta W$ :

$$Q = \frac{1}{2\zeta} = \frac{f_r}{f_{BW}} = 2\pi \frac{W_0}{\Delta W}. \quad (3.11)$$

where  $f_{BW}$  is the one-half peak power bandwidth.

### 3.3 Vibration Theory of Continuous Systems

#### 3.3.1 The Euler-Bernoulli Equation

Mechanical systems with infinite number of degree of freedom acts like a continuum in which the stiffness, inertial and damping properties are distributed throughout the structure. The motion of a continuous system is determined with partial differential equations as opposed to ordinary differential equations. This complicates the problem mathematically. However, the resonant frequency of a beam-based microresonator, a simple mechanical structure, is derived by using Euler Bernoulli differential equation:

$$\hat{E}I_x \frac{\delta^4 U(x,t)}{\delta x^4} + (\rho A) \frac{\delta^2 U(x,t)}{\delta t^2} + \zeta \frac{\delta U(x,t)}{\delta t} = q(x,t), \quad (3.12)$$

where  $U(x,t)$ ,  $\hat{E}$  and  $I$  are the beam deflection in x-direction, the Young's modulus and the moment of inertia, respectively.  $\rho$  is the mass density of beam material,

and  $A$  is the cross sectional area.  $\zeta$  is the damping coefficient per unit length per unit velocity, and  $q(x, t)$  denotes the driving load in  $Nm^{-1}$ . In these calculations, we neglect the effect of rotary inertia and shear deformation, and nonlinear effects due to large deformations. The  $\hat{E}$  is equal to the Young's modulus of the beam material for a thin beam with a width smaller than its length. Otherwise, the Young's modulus needs to be replaced with  $\hat{E} = \frac{E}{1-\nu^2}$ , where  $\nu$  is Poisson's ratio, to account for the contraction in the transverse direction. The moment of inertia for a rectangular beam,  $I$  can be calculated as:

$$I = \int_A z^2 dA = \int_0^b \int_{-h/2}^{h/2} z^2 dz dy = \frac{1}{12} bh^3. \quad (3.13)$$

Assuming a harmonic solution, we separate the solution into two terms: time-dependent term and position-dependent term,  $U(x, t) = U(x)T(t)$ . In case of free vibration, we can rewrite equation (3.12) as following:

$$\frac{\hat{E}I \frac{\partial^4 U(x)}{\partial x^4}}{(\rho A)U(x)} = -\frac{\zeta \frac{\partial T(t)}{\partial t}}{(\rho A)T(t)} - \frac{\partial^2 T(t)}{T(t)} = \omega_0^2 = \text{const}. \quad (3.14)$$

The time-dependent term can be written as:

$$\frac{d^2 T(t)}{dt^2} + \frac{\zeta}{\rho A} \frac{dT(t)}{dt} + \omega_0^2 T(t) = 0. \quad (3.15)$$

The solution is equal to the model of the 1D harmonic oscillator with  $T(t) = Be^{-\alpha t} \sin(\omega_0 t + \phi)$ . The position-dependent term can be written as:

$$\frac{\delta^4 U(x, t)}{\delta x^4} = \alpha^4 U(x, t), \quad (3.16)$$

where

$$\alpha^4 = \frac{\omega^2 \rho A}{\hat{E}I}. \quad (3.17)$$

The solution of this simplified differential function is :

$$U_n(x) = A_n(\cos \alpha_n x - \cosh \alpha_n x) + B_n(\sin \alpha_n x - \sinh \alpha_n x). \quad (3.18)$$

The constants are determined from the boundary conditions. For a singly clamped beam (i.e. cantilever), the frequency equation becomes:

$$1 + \cos(\alpha_n L) \cosh(\alpha_n L) = 0, \lambda_n = \alpha_n L = (2n - 1)\pi/2. \quad (3.19)$$

For a doubly-clamped beam (bridge), the frequency equation is

$$1 - \cos(\alpha_n L) \cosh(\alpha_n L) = 0, \lambda_n = \alpha_n L = (2n + 1)\pi/2. \quad (3.20)$$

The resonance frequency of a clamped beam with rectangular cross section is calculated as below by substituting these values in (3.17):

$$\omega_n = \frac{\lambda_n^2}{L^2} \sqrt{\frac{\hat{E}I_z}{\rho A}}. \quad (3.21)$$

We mentioned earlier that a beam based resonator can be modeled with a harmonic oscillator with effective mass of  $M_{eff}$ , and effective spring constant of  $K_{eff}$ :

$$M_{eff}\ddot{x} + K_{eff}x = f(\omega t). \quad (3.22)$$

The solution of this equation is:

$$x(t) = A_1 \sin\left(\sqrt{\frac{K_{eff}}{M_{eff}}}t\right) + A_2 \cos\left(\sqrt{\frac{K_{eff}}{M_{eff}}}t\right), \quad (3.23)$$

leading to the resonance frequency:

$$f = \frac{1}{2\pi} \sqrt{\frac{K_{eff}}{M_{eff}}}. \quad (3.24)$$

### 3.3.2 Energy Methods

The mathematics of motion is more complicated for more complex systems. The energy approach is generally used to predict the natural frequency of such systems. The maximum kinetic energy is expressed as:

$$E_{k,max} = 2\pi^2 f_n^2 \int_0^L \rho A(x) (U(x))^2 dx. \quad (3.25)$$

Similarly, the maximum elastic potential energy stored in the beam is expressed as:

$$E_{p,max} = \frac{1}{2} \int_0^L (EI(x) \frac{\delta^2 U(x)}{\delta x^2})^2 dx. \quad (3.26)$$

This is a conservative system assuming that damping is negligible, thus the maximum kinetic energy equals the maximum potential energy. Therefore, the natural frequency is given by the following equation:

$$f_n^2 = \frac{1}{4\pi^2} \frac{\int_0^L (EI(x) \frac{\delta^2 U(x)}{\delta x^2})^2 dx}{\int_0^L \rho A(x) (U(x))^2 dx}. \quad (3.27)$$

Equation (3.27) is called Raleigh's quotient.  $U(x)$  is usually unknown for more complicated systems. In these cases, the natural frequency is estimated using Rayleigh's quotient choosing an arbitrary function such that it follows the boundary conditions.

## 3.4 Resonator Mass Sensors

### 3.4.1 Principle of Detection

Resonant micro mechanical mass sensors work based on the principle that their resonant frequency depends on their mass. Thus, a small change in their mass results in changes in their resonant frequency. The effective mass depends on the mass of beam with a geometrical factor  $n$ , leading to  $M_{eff} = nM_{osc}$ . The additional mass with uniform distribution changes the resonance frequency to:

$$f_L = \frac{1}{2\pi} \sqrt{\frac{K_{eff}}{M_{eff} + n\delta M}} = f_0 \sqrt{\frac{1}{1 + \frac{n\delta M}{M_{eff}}}}. \quad (3.28)$$

Therefore, the added mass can be calculated as:

$$\delta M = -\frac{K_{eff}}{4\pi^2 n} \left( \frac{1}{f_0^2} - \frac{1}{f_L^2} \right). \quad (3.29)$$

Assuming that the added mass  $\delta M$  is small compared to the effective mass  $M_{eff}$  of resonator, we can write first-order Taylor series approximation:

$$f_L \approx f_0 \left( 1 - \frac{1}{2} \frac{\delta M}{M} \right) \Rightarrow \frac{\delta f}{f_0} \approx -\frac{1}{2} \frac{n\delta M}{M_{eff}}. \quad (3.30)$$

Therefore, the small added mass is calculated with this linearized expression:

$$\delta M \approx -2 \frac{M_{eff}}{f_0} \delta f_0. \quad (3.31)$$

### 3.4.2 Mass Sensitivity

Several factors affect the minimum detectable mass of a resonant mechanical sensors. The minimum detectable mass critically depends on the minimum measurable

frequency shift and the inverse mass responsivity  $S^{-1} = -2\frac{M_{eff}}{f_0}$ , which mainly depends on the structural design of resonator. The minimum measurable frequency depends on the measurement bandwidth of system  $\Delta f$ , the dynamic range  $DR$  and, the quality factor  $Q$  of microresonator. The mass sensitivity  $\delta m$  of a mechanical resonator is given by [62]:

$$\delta m \approx 2M_{eff} \sqrt{\frac{\Delta f}{Q\omega_0}} 10^{-DR/20}. \quad (3.32)$$

This equation indicates that there are several essential considerations for optimizing inertial mass sensors. First, the microresonator should be optimized to possess low mass with high resonance frequency. Second, the full range of measurement bandwidth should be employed. Third, the dynamic range for the measurement should be optimized through minimizing the noise level in measurement system.

### 3.4.3 Stress Effects

The vibration of a beam is also affected by stress. The resonant behaviour of a doubly clamped beam is influenced by both tensile and compressive stress. A thin doubly clamped beam with stress exhibits a similar resonant behaviour as a taut string under tension with the one dimensional wave equation. The natural frequency of a string ( $f_s$ ) depends on its tension ( $T_s$ ), its mass per unit length ( $\mu$ ), its length ( $L$ ) and the mode number ( $n$ ) as follows:

$$f_s = \frac{n}{2\pi L} \sqrt{\frac{T_s}{\mu}} \quad (3.33)$$

The natural frequency will have a  $L^{-1}$  (like a string) dependence instead of a  $L^{-2}$  (like a beam) if stress is the dominating factor.

Surface stress can also affect the vibration of a mechanical resonator by changing its spring constant. The Equation (3.24) for resonant frequency can be modified as follows:

$$f_{ss} = \frac{1}{2\pi} \sqrt{\frac{K_{eff} + \delta K}{M_{eff}}} \quad (3.34)$$

The surface stress also generates a radial force:

$$F_r = \int_0^L \int_{-t/2}^{t/2} [s_1 \delta(z + \frac{t}{2}) + s_2 \delta(z - \frac{t}{2})] dt dl = (s_1 + s_2)L. \quad (3.35)$$

where  $s_1$  and  $s_2$  are the surface stress at the top and bottom of resonator. This force causes contraction or expansion depending on the sign of  $(s_1 + s_2)$ . A thin beam can be modelled with a taut string. The equation of transverse free vibration is given by:

$$\frac{\partial^2 z}{\partial y^2} = \frac{m_1}{F_r} \frac{\partial^2 z}{\partial t_2} \quad (3.36)$$

where  $m_1$  is a uniform linear density (mass of unit length),  $F_r$  is the tension. The propagation speed of the transverse wave ( $C = \nu\lambda$ ) equals  $(F_r/m_r)^{1/2}$ . The fundamental resonance frequency due to surface stress is given by Equation (3.37):

$$f = \frac{1}{\lambda} \sqrt{\frac{F_r}{n_1 m_1}} = \frac{1}{4} \sqrt{\frac{s_1 + s_2}{n_1 m_b}} \quad (3.37)$$

The geometrical factor  $n_1$  is used to adjust for the difference between a mechanical resonator and a string. By comparing Equation (3.24) to (3.37), the spring constant can be expressed as:

$$K_s = \frac{\pi^2 n}{4n_1} (s_1 + s_2) \quad (3.38)$$

and changes in spring constant due to surface adsorption is given by:

$$\delta K = \frac{\pi^2 n}{4n_1} (\delta s_1 + \delta s_2) \quad (3.39)$$

where  $\delta s_1$  and  $\delta s_2$  are the changes of the surface stress on the top and bottom surface of the beam due to adsorption.

In most cases, the addition of mass on resonator sensors changes both the mass and spring constant of resonator. Therefore, the changes in resonance frequency is approximated by Equation (3.40) given than  $\delta M \ll M_{eff}$  and  $\delta K \ll K_{eff}$ :

$$df = \frac{1}{2} \left( \frac{\delta K}{K_{eff}} - \frac{\delta M}{M_{eff}} \right) \quad (3.40)$$

### **3.5 Conclusion**

This chapter reviewed the theory behind resonator mass sensors. The principle of operation for detection of added mass and mass sensitivity was discussed. The effect of surface stress on resonant behaviour of resonators were also reviewed.

## Chapter 4

# Introduction to Polymerase Chain Reaction

### 4.1 Introduction

The polymerase chain reaction is a molecular biology method that amplifies a single or a few copies of DNA to generate thousands to millions of copies of a particular sequence of target DNA. PCR was first introduced by Kary Mullis in 1983, and has been used for variety of applications such as DNA cloning for sequencing, functional analysis of genes, diagnosis of heredity disorders, detection and diagnosis of infectious diseases.

### 4.2 Principles and Components of PCR

PCR is based on a thermal cycling process consisting repeated heating and cooling steps to melt DNA, to hybridize primers containing target-complementary sequences along with a DNA polymerase, and to generate double-stranded DNA. Ideally, the amount of DNA doubles at each cycle. In almost all PCR applications, a heat-stable DNA polymerase, known as Taq polymerase, is used to enzymatically assemble a new DNA strand from nucleotides (i.e. DNA building blocks) on the single strand template DNA using primers.

The PCR is commonly carried out in a machine called thermal cycler in a reaction volume of 10 - 200  $\mu\text{l}$  in small reaction tubes with thin walls which permits

favourable thermal conductivity. PCR reaction usually require several components and reagents:

- Template, DNA sequence of interest to be amplified
- DNA polymerase, an enzyme for DNA synthesis
- two primers (i.e. forward and reverse), short DNA fragments (primers) complementary to target DNA sequence
- dNTPs (deoxynucleoside triphosphates), building blocks for synthesis of DNA
- Buffer solution, to provide a suitable chemical environment for optimal enzymatic activity.
- Cations such as magnesium, manganese, potassium ions

PCR process consists of 30-40 temperature cycles, each consisting of three temperature steps:

- *Denaturation step*: This is the first cycling step in which the reaction is heated to 94-98 °C to melt a double stranded DNA (dsDNA) into two single stranded ones (ssDNA). The complete denaturation is the key for successful amplification as the incomplete one will result in inefficient use of template in the first cycle, and consequently yielding poor amplification efficiency.
- *Annealing step*: The reaction temperature is reduced to around 50-65 °C to allow the primers to anneal to the single stranded DNA. The primers are carefully designed to match the DNA template sequence. The polymerase enzyme known as Taq polymerase is attached to the primer-template hybrid and begins to form dsDNA throughout the next step (i.e. extension step). The optimal annealing temperature is critical to ensure specificity of amplification.
- *Extension/elongation step*: The reaction temperature is raised to 70-80 °C to allow the enzymatic activity of polymerase. Polymerase is like biological glue that attaches the deoxynucleoside triphosphates (dNTPs) to the freshly denatured ssDNA to synthesize a new DNA strand complementary to the DNA template strand. Theoretically, the amount of DNA is doubled at this step resulting in the exponential amplification of the specific DNA fragment.

Figure 4.1 shows the schematic of PCR reaction, during which the amplification leads to the exponential growth of DNA.

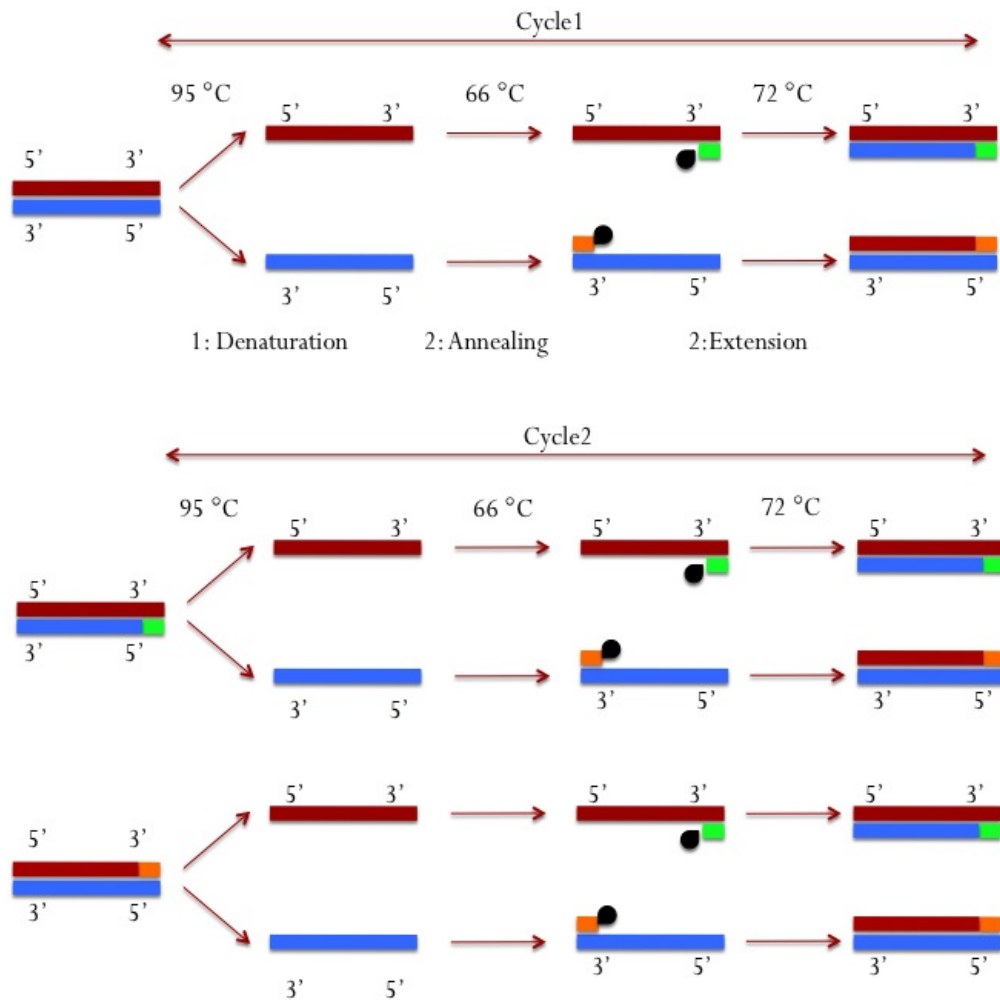


Figure 4.1: PCR reaction diagram.

PCR assays are extremely sensitive, thus prevention of contaminations is critical to obtain successful amplification and achieve reliable results. Therefore, certain precautions are necessary; Pre-PCR processing (i.e. DNA extraction), PCR reaction mixing, and post processing (i.e. gel-based detection) need to be performed in separate areas.

## 4.3 Phases of PCR

Figure 4.2 shows the amplification plot in a PCR reaction, which can be divided into three phases. In the exponential amplification phase, the amount of product is doubled at every cycle. At later cycles, the PCR reaction enters the linear phase in which the reaction slows down as enzyme starts to degrade and the other reagents such as dNTPs and primers are consumed. Finally, the amplification reaches the plateau phase as all reagents and enzyme are used up, and no more product accumulates.

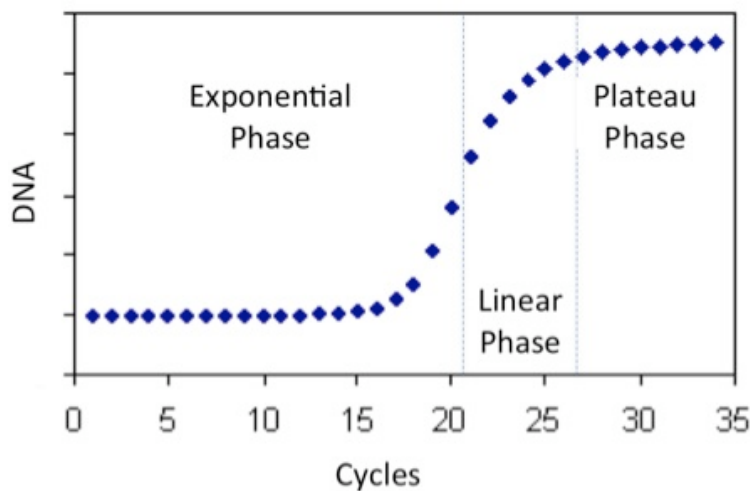


Figure 4.2: PCR amplification plot

## 4.4 Methods of PCR

### 4.4.1 Conventional PCR

Conventional PCR uses Agarose gel electrophoresis for size separation of PCR product at the end point of reaction (i.e. plateau phase). The size of PCR product is compared with a DNA molecular weight marker called DNA ladder, and positive results are confirmed if the size of product is within the expected range. End point detection however does not provide any quantitative information about the amount of PCR products. It also suffers few other limitations such as poor precision, low sensitivity, short dynamic range, low resolution, and long assay time.

#### 4.4.2 Quantitative PCR

Quantitative PCR is developed to quantify DNA along with the amplification of the target sequence. The amount of DNA usually doubles during each amplification cycle for an optimized reaction. In quantitative PCR (qPCR), the amplified product is tagged with a fluorescent reporter molecule, therefore, the amount of amplified product is linked to the intensity of fluorescent signal. The fluorescent signal is either measured at the end of reaction (endpoint qPCR) or during the amplification process (realtime qPCR).

In endpoint qPCR, fluorescence signal is measured after the amplification is complete. This signal is used to calculate the initial amount of template. However, this method is not very consistent for quantification of PCR product, because the efficiency of PCR reaction may decrease at the last cycles of PCR due to consumption of reagents and accumulation of inhibitors. These effects are not predictable, thus the final fluorescence signal value may not be related to the starting template concentrations. Figure 4.3 shows that the data collected at the endpoint of reaction may vary from run to run for an identical sample.

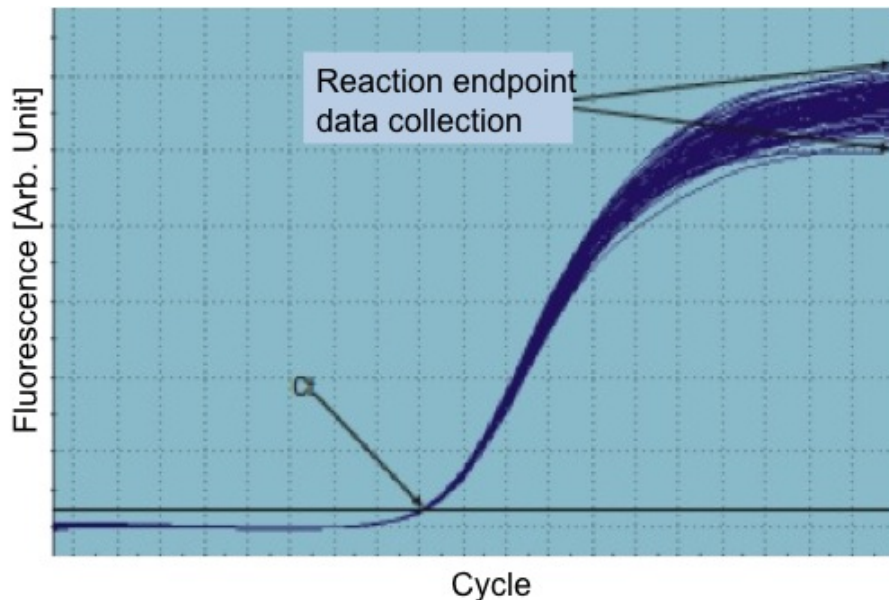


Figure 4.3: The endpoint qPCR reaction variation for runs with 96 identical reactions [231].

Realtime qPCR is a more sensitive and reproducible method which measures the fluorescent signal during the early cycles of the exponential phase of amplification,

before the efficiency of reaction is affected due to limiting reagents, accumulation of inhibitors, or inactivation of polymerase. The product DNA is labeled with a fluorescent reporter molecule, thus the fluorescent intensity increases proportional to the amplification cycle in response to the increased amplicon concentration. A level of fluorescent intensity- automatically set by the instrument software or manually set- is used to determine the threshold cycle value (Ct). This level is set to be above the baseline and sufficiently low to be within the exponential growth region of the amplification curve. The baseline is defined as an initial cycles of PCR in which there is little change in fluorescent signal [5]. The first cycle at which the fluorescent intensity is above the background signal is called the threshold cycle value (Ct), which is inversely proportional to the starting template concentration. The higher the starting concentration of template, the smaller is the Ct value (Figure 4.4). The threshold cycle value (Ct) above 8 and below 35 is desirable. A Ct value less than 8 means that there is too much template in the reaction. And a Ct value above 35 indicates a low amount of target in the reaction [6]. A standard curve of the dilution series is run on the same plate as the unknown samples to correlate the Ct values to the starting concentration of each unknown sample.

## 4.5 Real time qPCR Chemistry

Two types of chemistries have been developed to detect the PCR products on real-time qPCR:

- fluorescent intercalater dye-based chemistry
- Fluorogenic-labeled probe-based nuclease chemistry

### 4.5.1 Fluorescent Intercalater Dye-based Chemistry

Fluorescent intercalater dyes are small molecules that bind to any double-stranded DNA (dsDNA) formed during PCR, which results in increase in fluorescence intensity. SYBR Green I dye is a common intercalater dye used for real-time qPCR, which is excited using a blue light ( $\lambda_{max} = 488 \text{ nm}$ ) and emits a green light ( $\lambda_{max} = 522 \text{ nm}$ ). The intensity of fluorescent signal is 1000 fold higher in bound state compared to unbound dye. Figure 4.5 shows the SYBR Green I detection mechanism.

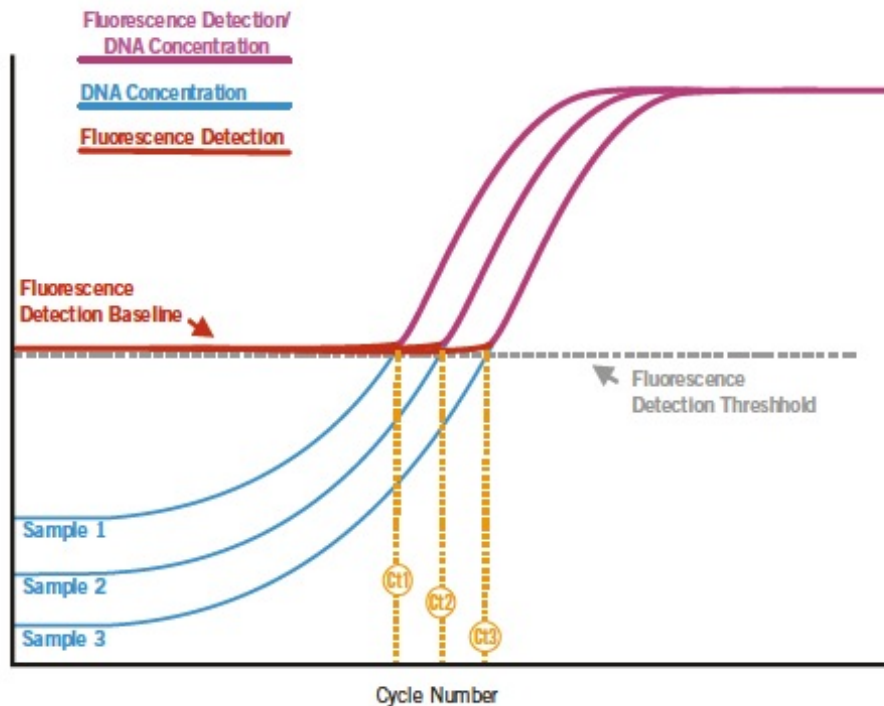


Figure 4.4: Principle of realtime qPCR. Ct value is inversely proportional to the initial copy number[231].

The qPCR assay based on SYBR Green I dye is usually used for initial assessments as it is relatively easy to design and inexpensive. However, this process is inherently non-specific as SYBR Green I dye binds to any dsDNA. Therefore, the specificity of the reaction is solely determined by primers. Any non-specific binding (e.g. primer-dimer formation) may result in increase in the measured fluorescence, yielding inaccurate determination of the initial template concentration. Although non-specific amplification is not always avoidable, its presence can be easily detected by performing a melt curve analysis after the completion of PCR reaction.

During melt curve analysis, the PCR product is heated and the fluorescence versus temperature curve is analyzed. The DNA molecule of the PCR product melts at a certain temperature (melting temperature  $T_m$ ), which depends on the length of DNA molecule. Therefore, a single thermal transition is detected in an optimized amplification with high specificity. The presence of non-specific PCR product will result in multiple thermal transitions in the fluorescence intensity.

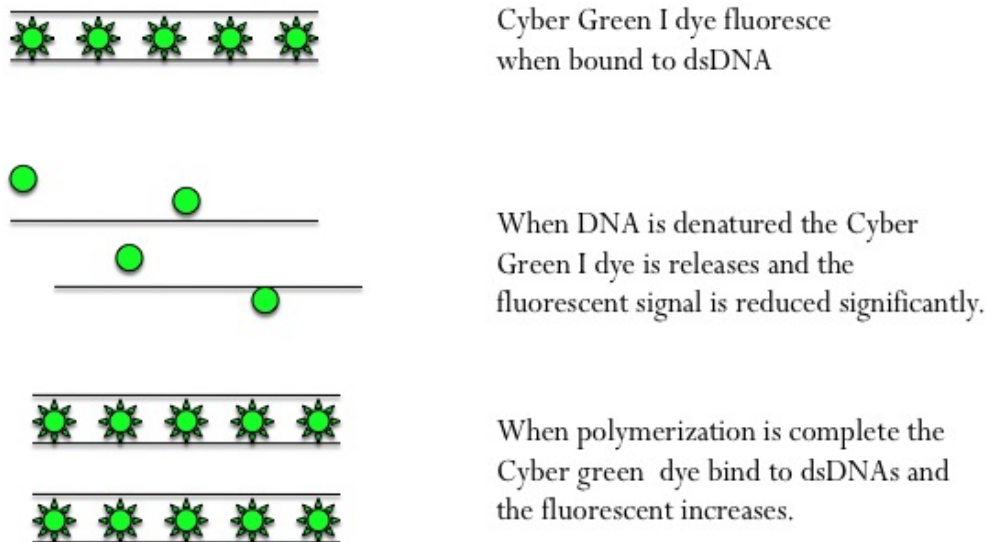


Figure 4.5: The mechanism of SYBR Green I dye chemistry. The dye bind to dsDNA in the reaction.

#### 4.5.2 Fluorogenic-labeled Probe-based Nuclease Chemistry

Probe-based chemistries provide higher level of detection specificity by using a sequence-specific fluorogenic-labeled probe along with primers in PCR reaction. Fluorogenic-labeled probes (hydrolysis or TaqMan probes) have a fluorescent dye, typically FAM, at the 5' end and a quencher, historically TAMRA, at 3' end. Linear probes uses a FRET (Fluorescence Resonance Energy Transfer) quenching mechanism where quenching will occur as long as the quencher is on the same oligonucleotide. The probe is hybridized to its complementary part on one strand of target sequence during annealing step of PCR amplification. During extension step, the 5' to 3' exonuclease activity of the Taq polymerase breaks the reporter-quencher proximity probe allowing the emission of fluorescence which is detectable after excitation with laser. It is important to optimize the thermal profile to ensure proper annealing and hybridization of both primers and probe and subsequent cleavage of probe. To fulfil these requirements, a two-step thermal profile is used with a denaturing step at around 95 °C and a combined annealing/extension at around 60 °C. Figure 4.6 shows the probe-based realtime PCR assay.

## 4.6 Methods of Quantification

There are two basic methods for calculating the results of real-time qPCR: absolute and relative quantification.

**Absolute Quantification** In this method, a standard curve is prepared from a dilution series of control template with known concentration. The value for unknown sample is extrapolated after comparing to the standard curve. The absolute quantification is used when the objective is to measure the exact level of template in the sample.

The standard curve can be prepared using plasmid containing a cloned gene of interest (GOI), genomic DNA, cDNA, or synthetic oligos. The choice of template for standard curve depends on the application. Nonetheless, It is critical to design primers to work efficiently with both standards and the sample under test. The standard curve is created by plotting the log of initial copy number against the Ct value for each dilution.

A standard curve consists of multiple points (at least 4 points) ranging several orders of magnitude. Each data point must be run at least in duplicate. Ideally, the standard curve must be linear over the whole range (i.e. the correlation coefficient  $R^2$  must be very close to 1) to ensure the efficiency of amplification is consistent at varying template concentrations. A nonlinear standard curve at low template concentration denote the limit of detection of the assay. The efficiency (E) of a realtime PCR assay is calculated with  $E = (10^{-1/slope} - 1) \times 100$  Ideally, the efficiency of reaction falls between 90 and 110%. The 100% efficiency corresponds to perfect doubling of amplicon at each cycle. Lower efficiency implies that the reaction is slowing down due to either presence of inhibitors in reaction, or less optimal primer sets or reaction condition. Poor serial dilution preparation as well as extreme ranges of concentrations also causes low efficiency. Higher efficiencies (i.e. significantly higher than 100% indicate error (e. g. nonspecific amplification, pipetting error, PCR inhibitors, probe degradation, primer-dimer formation). Primer-dimer formation is a major concern with SYBR Green I dye where any dsDNA is detected.

**Relative Quantification** Various scientific researches aim to study changes in gene expression in a given sample relative to another sample such as an untreated control sample or a zero time point in a time-course experiment. Relative quantification uses one of the following methods for calculations:

- **Standard curve method:** the standard curve is prepared to express the target gene quantity relative to some control sample (called a calibrator, e.g. untreated sample). In this approach, the target quantity is determined from the standard curve and divided by the target quantity of the calibrator. Therefore, the calibrator is the  $1\times$  sample, and all other quantities are determined as an n-fold difference relative to the calibrator. This method is advantageous as it requires the least amount of optimization and validation. For this method to be applicable, it is important to dilute DNA very accurately. However, the units of this dilution is irrelevant. For example, if the standard curve is prepared with two-fold dilutions, the units could be the dilution values 1, 0.5, 0.25, and so on.
- **Comparative Ct method:** In this method, the reactive expression levels are compared with a calibrator (i.e a control sample such as non-treated sample), and the amount of target is calculated using  $2^{-\Delta\Delta C_T}$ , where  $\Delta\Delta C_T = \Delta C_T(\text{sample}) - \Delta C_T(\text{calibrator})$ , in which  $\Delta C_T = C_T(\text{housekeepinggene}) - C_T(\text{targetgene})$ . Therefore, the equation compares the normalized expression of target gene in the unknown sample to the normalized expression of the calibrator sample. This methods offers several advantages including higher throughput and better accuracy, as it eliminates the need for a standard curve and related errors. However, the validity of the  $\Delta\Delta C_T$  method relies on the efficiency of PCR amplification which needs to be approximately equal for the target gene and the housekeeping gene. Otherwise, this method is not applicable and other quantification methods, such as standard curve method must be considered.

## 4.7 Determination of LOQ and LOD

Although real-time PCR is a valid technique for the quantification of pathogen in samples, there is not a generic method for the determination of limit of quantification (LOQ) and limit of detection (LOD) in qPCR. Nutz *et al.* suggest a method for determining the LOQ and LOD [174]. The LOQ is defined as the amount of target DNA that leads to a maximum of summation of sensitivity and specificity[174]. The LOD is defined as the lowest amount of DNA that was amplified while the false-negative rate is below a given threshold [174].

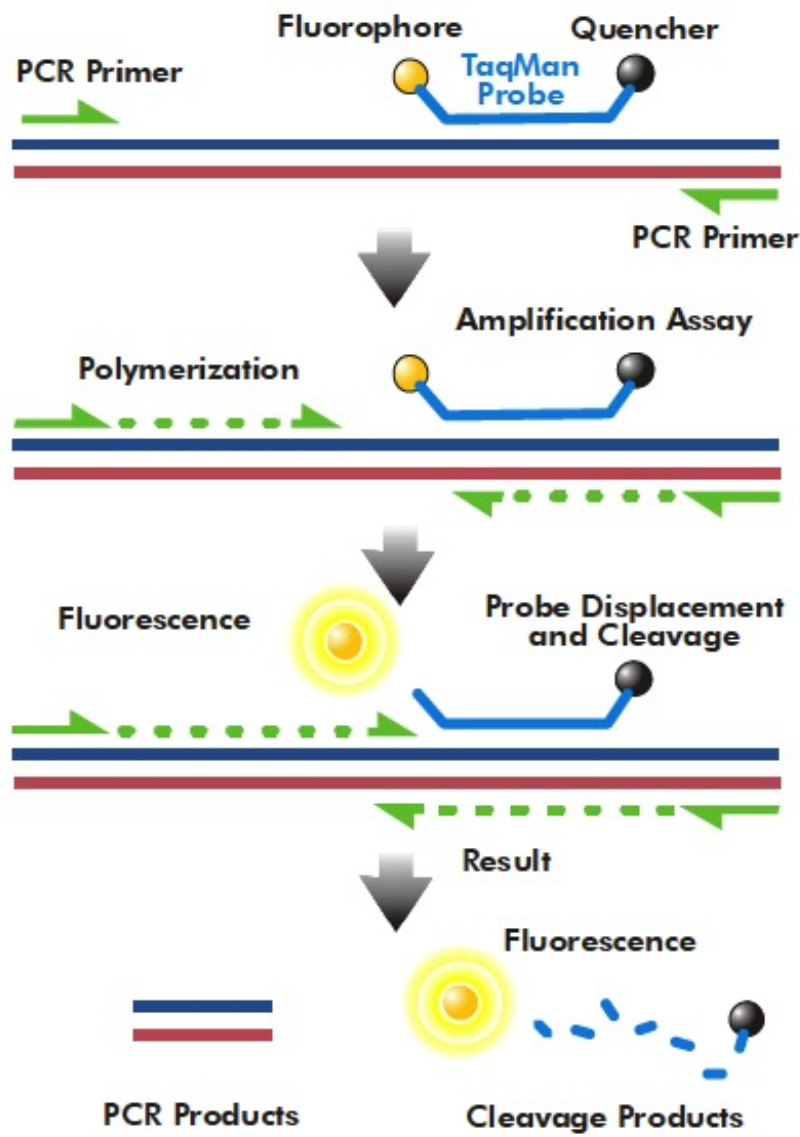


Figure 4.6: TaqMan PCR assay. [231].

## Chapter 5

# Introduction to Bacteriophage Technology

### 5.1 Introduction

Bacteriophages (also known as phages) are the most abundant micro-organisms with the estimate range from  $10^{30}$  to  $10^{32}$  in total [127], and can found in the sea, soil, drinking water, and food. Phages play a critical role in microbial balance of their surrounding ecosystem. Phages are viruses that recognize and bind specifically to their host bacteria, and thus are benign to other species. Phages have evolved with their bacteria counterpart, and therefore they are available in various types. Some phages are very specific to a certain strain level of bacteria while others can infect a larger range of bacteria [127].

Phages were independently observed by Fredrik Twort and Felix d'Herelle in 1915 and 1917, respectively. However, the nature of bacteriophages were under debate for long time until the advent of electron microscopy. Initial investigations on biological nature of phages raised interest in their potential for therapeutic applications for infectious diseases [187, 187]. Recently, phages have found great attention as recognition probes due to some inherent properties such as diversity, biological and environmental stability, ease of amplification, and unique selectivity and specificity for recognition of bacteria. They have been coupled with various biosensors for detection of bacteria [222].

## 5.2 Phage Structure and Anatomy

Phages are classified into two major groups: tailed phages and filamentous phages. Tailed phages are the largest and most widespread group of phages. The vast majority have dsDNA, but small group of phages contain ssDNA, ssRNA, and dsRNA. Most bacteriophages have complex structure. An example of a tailed bacteriophage with double-stranded DNA is shown in Figure 5.1. Tailed phages are composed of several structural components including the phage head, tail, sheath, base plate and tail fibers. The genetic material of a phage is highly condensed within the phage head. The size of phage head varies between 45 nm and 100 nm depending on the genome size they contain. The protein connecting head to tail is an important structural part. These proteins control the entry of DNA and assembly of the tail to the immature head during morphogenesis of new particles. During infection, the conformation of these proteins change to allow the DNA to exit the virions towards the bacterial cell. The tail support the bacteria binding site and they serve as conduit for genome insertion. The morphology of tails are different from phage to phage. For example, phage T4 has long, rigid, and contractile tails; Lambda phage has long, flexible, and non-contractile tails, and some other phages such as P22 has short tail.

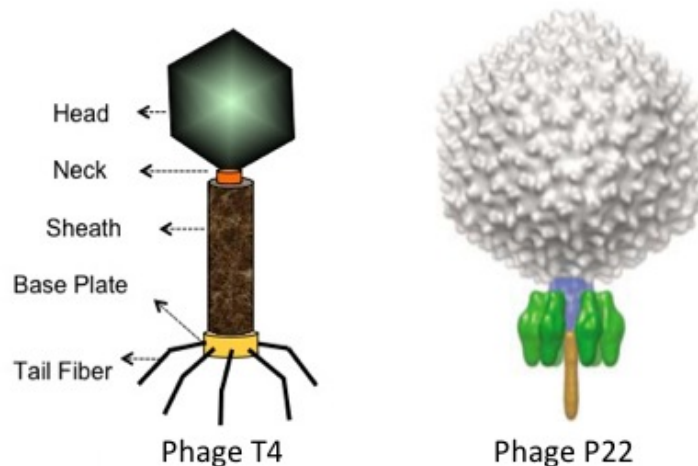


Figure 5.1: Tailed bacteriophage

Filamentous phages have completely different structure compared to tail phages. They are composed of a long tabular body with two ends, one infective end and one non-infective end. The tabular body is consisted of many repeating proteins which

also represent most of the phage's mass. The genetic material of phage is inside the tabular body structure.

### 5.3 Phage Infection Cycle

In essence, phage needs to induce a living bacteria to synthesize all the essential components to produce more phage progeny. Phage infection cycle can be divided into five steps as follows:

1. Attachment (adsorption) of the bacteriophage to the host bacteria
2. Penetration of the phage or its nucleic acids into the cell
3. Synthesis of phage nucleic acid and protein by bacterial cell metabolism as directed by bacteriophage
4. Maturation involving assembly of phage and packaging of viral genome into new progenies.
5. Release of mature virions from the cell.

The specificity of the recognition of bacteria by phage depends upon attachment. The phage has special proteins on the outside that interact with the specific surface components on their target bacteria called receptors. These receptors are normal surface components of bacteria such as proteins, polysaccharides, carbohydrates, glycoproteins, lipids, lipoproteins, or complex of these. The bacteriophage can not attach and therefore can not infect bacteria in the absence of the specific receptors. In the case that receptor site is altered e.g. due to mutation, the host becomes resistant to virus infection. Thus, the host range of phage is determined by the availability of a suitable receptor that can phage recognize.

Upon attachment of viruses to their host bacteria, the virus and cell surface changes to facilitate penetration of phage and its nucleic acid into the bacteria. Bacteriophages have the most complex penetration mechanism among all viruses. The bacteriophage T4 which infects *E. coli* is a good example. The proteins on the tail fibers recognizes the polysaccharides on the outer layers of the cell envelope and attaches phage to the bacteria. The tail fibers then retract and the core of the tail

makes contact with the cell wall of the bacteria. The tail sheath then contracts and the viral DNA passes into the cytoplasm. Most of the coat protein remains outside the cell.

After the successful transport of the phages DNA into the cytoplasm of the bacteria, the synthesis of host nucleic acids stops and transcription of specific phage genes starts. Bacteriophages are classified into two categories based on their viral life cycles: virulent and temperate. Virulent bacteriophages kill their host bacteria after infection through over expression of viral genome. This allows phage assembly to take place. On the other hand, temperate phages are able to undergo a lysogenic life cycle resulting in a stable genetic relationship with their host. In this state, the virus genes are not expressed, rather the virus genome called prophage is replicated synchronous with the host chromosome.

T-even phages are examples of virulent bacteriophages. And, T4 bacteriophage is the most extensively studied one. The time course of events during T4 phage infection is very short which takes less than 25 min. Following injection of phage DNA, the early and middle mRNA is produced that are translated into phage DNA. Late mRNA codes for structural proteins of phage resulting in assembly of head and tail independently. The phage DNA is actively pumped into the head until it reaches a certain pressure level. The tail subsequently attaches to the head followed by addition of smaller components such as tail fibers. Phage remains inside bacteria while the other virions are generated concurrently. The phage encodes an enzyme, T4 lysozyme which is eventually activated causing the lysis of the host bacteria. The newly developed phages are released in the environment causing infection of other bacteria.

Temperate phages have the ability to coexist with their host in a non virulent way. Lambda and P1 are the best characterized temperate phages. The temperate phage does not exist as a virus inside a bacterial cell during lysogeny. Instead, the virus genome is exist in the cytoplasm in plasmid form such as bacteriophage P1, or it is integrated into the bacterial chromosome (e.g. Lambda phage). In either case, it replicates with the host cell until the genes which activate its lytic pathway is expressed. Phages may enter lytic cycle under stress conditions such as UV light exposure or prolonged starvation. This will often cause massive assembly of phage

particles followed by the lysis of the lysogen cell.

## 5.4 Phage as Diagnostic Tools

### 5.4.1 Wild-type Phages

The inherent ability of the phages to bind to their target pathogen has been exploited to design biosensor surfaces using physical and chemical functionalization. The physical functionalization is achieved by surface adsorption, which is simple and straightforward, but gives inconsistent and unstable immobilization density. Physical adsorption nonetheless has been used for detection of *Staphylococcus aureus* using lytic phages (detection limit  $10^4$  cfu ml<sup>-1</sup>) by surface plasmon resonance (SPR) [19] and *Salmonella* using magnetoelastic sensor in suspension [129] and fat free milk (detection limit  $10^3$  cfu ml<sup>-1</sup>) [130]. Similarly, physical adsorption of the phages on sugar and amino acid modified gold surfaces [221] as well as surface modified silica particles [39] for pathogen capture have also been reported in the literature. The ELISA-based binding strength study of phages versus monoclonal antibody against  $\beta$ -galactosidase in *E. coli* reveals that phages (Kd = 21 172 nM) bind to their target with similar or better affinity compared to monoclonal antibody (Kd = 26 172 nM) [166]. Despite these successful functionalization reports, strong chemical immobilization of phages on a sensor platform is preferred due to several advantages.

The anchoring of phages by chemical bonds on a biosensor detection platform is pertinent to development of a consistent and stable detection system. The advantage of surface modification and chemically anchored immobilization approach was revealed by a methodical study that demonstrates a 7-fold and 37-fold improvement in the phage density respectively, on cysteamine-modified and glutaraldehyde activated gold substrate compared to that by physical adsorption on bare gold substrate [221]. This two-step method was further improved by application of dithio-bis(succinimidyl propionate) (DTSP) self-assembled monolayer (SAM) where the thiol group binds to the gold surface while the free succinimidyl interacts with the surface amine groups on the phages [17]. Silane chemistry has similarly been applied for silicon based substrates to facilitate P22 phage immobilization for *Salmonella*

capture [87] as well as study of phage receptor-host ligand binding strength using atomic force microscopy [88]. In yet another example, electrochemical oxidation was used to generate carboxyl group on carbon surface followed by amide coupling of T4 phages for subsequent *E. coli* capture [214].

Purity of the phage suspension is an important criterion to consider for chemical functionalization. Phages are amplified in their host bacterial culture to achieve high titers; and despite repeated centrifugation, the contamination of bacterial protein, lipids and carbohydrates could severely affect the efficiency of immobilization and binding ability of the phages. Phage lysate have therefore been purified by a host of methods such as ultra-high speed centrifugation [221], ultra-filtration [34], poly(ethylene glycol) precipitation-gradient centrifugation[103], chromatofocusing [37] and size exclusion chromatography [164]. An interesting study demonstrates that purified phage lysate can be essentially used to systematically study the binding kinetics of the phages on to an activated surface for chemical immobilization. Studies with T4, P22 and NCTC 12673 phages model systems revealed that the phage binding kinetics does not follow the idealized and homogenous Langmuir adsorption isotherm but is governed by heterogenous adsorption closely related to Brouers-Sotolongo isotherm [164]. Such rigorous surface binding studies are extremely important for understanding of phage immobilization on a surface and cannot be realized in the presence of contaminations in the lysate. Wild-type phages have been extensively explored for functionalization of biosensor platforms and subsequent pathogen detection.

Wild-type intact phages however suffer from certain drawbacks that limit their application on biosensor platforms. Intact phages are biologically active and thus result into the lysis of the host bacterium upon infection that would lead to loss of signal on a biosensor platform [220]. Besides, some phages show enzymatic activity towards their host bacterial surface receptor. For example, P22 phage shows endorhaminidase activity towards the O-antigen on the surface of *Salmonella enterica*, which results in binding and subsequent detachment of the bacterium. Such enzymatic activity would lead to inconsistent signals on a biosensor platform, leading to changes in detection efficiency. Results also suggest that intact phages bound on sensor platform lose their bacterial binding capability upon drying. This could

be explained due to the fact that intact phages collapse on the sensor surface upon drying, and consequently their tail fibers are unavailable to bind to the bacterial host [220]. In addition, intact phages have relatively large sizes, which limits their application as bioreceptors on particular sensor platforms such as in the surface plasmon resonance based sensor where detection signal is distance dependent.

#### 5.4.2 Engineered Phages

**Phage Display Peptides** Phages have a unique ability to display peptides or proteins on their surface, a technology that was first described in 1985 [227]. This technology enables the screening of proteins or peptide that would have affinity to a variety of target such as carbohydrates, proteins, small molecules or an entire cell. The underlying principal of this method is to fuse the gene encoding for the peptide or protein of interest to the phage surface protein encoding gene(s) resulting in the expression of the hybrid protein on phage surface [181]. Lambda, M13, f1, fd, T4 and T7 phages have most widely been used for the phage display technology. The phage libraries, thus developed can be screened against an immobilized target of interest, the unbound phages are washed away and the tightly bound phages are eluted, propagated and are used as probes against that target. A comprehensive review by Smith and Petrenko summarizes the central paradigm and technical details of the phage display technology [228].

Phage display not only enables peptide- and protein-based acquired recognition specificity towards a pathogen, but is also exploited to facilitate oriented immobilization of these bio-probes onto a biosensor platform. Gervais *et al.* demonstrated an oriented immobilization of T4 phages using the popular biotin-streptavidin recognition. T4 phages expressing biotin on the head region were immobilized on streptavidin coated gold substrates facilitating exposed tails for specific capture of *E. coli* [73]. In yet another study, biotin carboxyl carrier protein gene (bccp) and cellulose binding module gene (cbm) were expressed with the small outer capsid protein (soc) of T4 phages and the expressed surface ligand was leveraged for the phage immobilization on streptavidin coated magnetic particles and cellulose-based material [239]. Oriented immobilization of phages can also be achieved by a careful study of differences in physical properties in their head region compared to the tail region. Studies

with mutant phages reveal that the phage head carry a net negative charge while the tail region has a net positive charge [212]. This charge difference has been used to immobilize *Listeria* and *E. coli* infecting phages on a positively charged cellulose membrane by electrostatic interaction [15]. Such subtle differences in phage properties could be of tremendous importance for successful functionalization of sensor platforms.

**Reporter Phages** Reporter phages are genetically modified phages used as a reporting gene carrier, introducing a gene of interest into the host bacteria upon infection. The reporter gene of interest incorporates into the host chromosomes, expressed and codes for a fluorescent or substrate dependent colorimetric marker for subsequent pathogen identification. Bacteriophages, being host dependent for any physiological function, are incapable of expressing the reporter gene by themselves until host infection, thereby confirming the presence of the host bacterium upon gene expression. Prokaryotic and eukaryotic luciferase expressing gene (*lux* and *luc*), *E. coli*  $\beta$ -galactosidase (*lacZ*) gene, bacterial ice nucleation (*inaW*) gene and green fluorescent protein (*gfp*) expressing gene have been most commonly used for such applications. Reporter phage-based technology has been successfully leveraged for identification of several pathogens, including *E. coli* [246], *Mycobacterium* [184, 210], *Salmonella* [126], *Staphylococcus aureus* [192] and *Listeria monocytogenes* [151]. Loessner *et al.* successfully employed A511::luxAB recombinant phage for detection of one *Listeria* bacterium per gram of sample of artificially spiked ricotta cheese, chocolate pudding and cabbage [152]. Similarly, on more microbiologically complex food samples such as minced meat or soft cheese, 10 bacteria per gram of could be detected using the same system. The sample processing time and pre-enrichment steps were performed in 20 h and the total detection time was estimated to be 24 h compared to four days by conventional microbiological methods [152]. The ability to distinguish between live and dead bacteria is the biggest advantage of reporter phages since the phages will be unable to infect and express the reporter gene in dead bacteria. Reporter phages however suffer from limitations such as phage multiplication inhibition due to prophage presence [89], DNA restriction-modification system [120], presence of specific phage inhibition genes [53]

and antiviral bacterial immunity system.

### 5.4.3 Phage Receptor Binding Proteins (RBPs)

Some very recent research efforts have led to the evolution of bacteriophage RBPs as novel probes for pathogen detection. The unique host-specific recognition of the tailed phages comes from the RBPs located on the tail fibers and it is the binding of these proteins that trigger the translocation of the phage genetic material into the host [137, 43]. The phages RBPs generally recognize unique proteins or carbohydrate (polysaccharide) sequences on the surface of the host bacterium [77]. The recent advancement in genome information, cloning and molecular biology methods has led to the capability of specifically recognizing the genome of interest, cloning, transfecting and over-expressing the protein of interest. These advancements have greatly benefitted the phage-technology and strategies are devised to identify the phage RBPs and their subsequent application in therapy [252] and pathogen detection [218]. Genetically engineered RBPs offer several advantages over the antibody or intact phage-based technology for pathogen detection. Their agglutination ability towards bacterial cells is found to be similar to the monoclonal antibodies against the bacterial lipopolysaccharides [252]. The RBPs also offer better stability against environment factors such as pH and temperature and resistance against gastrointestinal proteases [252]. Their high level of stability in harsh environment is due to their compact structure that make them resistant to proteases, detergents and protein denaturing agents. For example, TSPs from bacteriophages Sf6, P22, and HK620 are rod-like homotrimers with comparable  $\beta$ -selenoid folds and similarly high kinetic stability in spite of different amino acid sequences [22]. Their binding affinity can be easily tailored to the requirement and multi-valency can be imparted if desired. Most importantly, suitable tags can be added to the RBPs sequence at appropriate position without altering their binding affinity and such tags can be exploited for oriented surface functionalization of the RBPs on the biosensor platforms.

Singh *et al.* demonstrated the use of cysteine-tagged P22 phage RBPs on gold surface for capture and detection of *Salmonella enterica* serovar Typhimurium [220]. Their results demonstrate that N-terminus Cys tagged proteins capture bacteria efficiently compared to the C-terminus Cys tagged protein due to preferential orienta-

tions. Besides, the endorhamnosidase mutant protein shows a 6-fold improvement in bacterial capture compared to the intact P22 phage as well as phage RBPs with endorhamnosidase activity. In yet another report, the *Campylobacter jejuni* binding RBPs (Gp48) from the phage NCTC 12673 were cloned and overexpressed as glutathione-S-transferase fusion protein (GST-Gp48) [125]. These GST-Gp48 proteins could be successfully functionalized on glutathione derivitized gold surface for specific detection of the *C. jejuni* host bacteria by surface plasmon resonance. The versatility of functionalization of the RBPs was further demonstrated by their immobilization on tosylactivated Dynabeads M-80 for specific capture of the host bacteria in buffered samples [219]. In an unpublished result, similar application has been validated for capture of *S. flexnari* using wtRBPs as well as endorhamnosidase mutant D399N RBPs. The results clearly indicated that wtRBPs show a low bacterial capture density of  $5.71 \pm 0.24$  bacteria/ $100\mu^2$  compared to mutant RBPs (capture density  $11.07 \pm 0.62$  bacteria/ $100\mu^2$ ) [218]. Although the initial experimental results show great promises for phage RBPs as potential probing element for pathogen detection, much work is still needed to achieve a commercial level biosensor.

## Chapter 6

# Surface Immobilization of Phage Receptor Binding Proteins (RBPs) for Specific Bacterial Capture

### 6.1 Introduction

This chapter focuses on strategies taken to enhance the attachment of bacteriophage receptor binding proteins to solid surfaces for bacterial capture. *Campylobacter jejuni* was chosen as the model bacteria, which is the common bacterial cause of food borne illnesses. Rapid and specific detection of this pathogen is critical for effective control and quick treatment of infection. Available diagnostics for this pathogen are laborious and time consuming and require equipped laboratories and expert personnel. Recently, Kropinski *et al.* sequenced the genome of phage NCTC12673 and identified its putative receptor binding protein, GP48, that recognize its host bacteria, *C. jejuni* [125]. Singh *et al.* reported the use of these RBPs for specific detection of *C. jejuni* cells using RBP-derivatized gold surfaces [219]. We developed new protocols for immobilization of GP48 RBPs onto magnetic beads. To that end,

---

<sup>1</sup>All work in this chapter was performed by S. Poshtiban except the expression and purification of proteins and their shorter derivatives . M. Afzal Javed expressed and purified phage tail spike proteins and their shorter derivatives [110].

we characterized magnetic beads to ensure they are suitable for protein immobilization. We assessed the efficiency and specificity of bacterial capture using fluorescent microscope. As will be discussed in next chapter, we will use the RBP-derivatized magnetic beads to develop an efficient sample pre-enrichment method for isolation, purification and concentration of bacterial cells from food samples. We also identified that the receptor binding domain is localized to the C-terminal quarter of GP48. GP48 is the largest protein encoded in the genome of NCTC12673 (152 KDa). Its large size poses a challenge for expressing an active form of the protein in high yields. The localization of the binding domain allowed us to generate a shorter derivatives that is one-quarter the size of the original protein, yet is capable of detection of *C. jejuni* cells.

## 6.2 Experimental Methods

### 6.2.1 Expression and Purification of Phage Tail Spike Proteins

The production of the tail spike proteins (TSPs) starts with amplifying gene 48 of bacteriophage NCTC 12673 (GeneBank ID:GU296433) using PCR. The appropriate PCR product is ligated into a properly cut pGEX 6P-2 plasmid (GE Healthcare), used as a cloning vector. This plasmid encodes the N-terminal glutathione-S-transferase (GST) tag and was used to produce a GST-Gp48 fusion protein. The insert is sequenced to confirm the correct orientation and product integrity. GST-Gp48 protein was expressed in *E. coli* BL21 cells transformed with the pGEX 6P-2 plasmid containing gene 48. Bacteria cells are incubated and grown at 30 °C overnight. *E. coli* cells are harvested and resuspended in PBS followed by disruption by sanitation in the presence of 5 mM EDTA and ProteoBlock protease inhibitor cocktail. The solution is centrifuged at 27000 g for 30 min to remove cell debris. The soluble fraction is filtered through the 0.22  $\mu$ m filter (Millipore). The proteins are purified as 170 KDa soluble glutathione S-transferase (GST) fusion protein using glutathione-agarose affinity chromatography and ion-exchange chromatography. The absorbance of protein solution was measured at 260 and 280 nm to determine protein concentration [125].

## 6.2.2 Localization of Host Binding Domain in the GP48

GP48 is relatively a large protein and thus it is challenging to achieve high expression yields with the intact proteins. Localization of binding domain and expression of shorter derivatives of GP48 will overcome this challenge. In addition, the surface coverage improves for the smaller size of proteins resulting in better bacterial capture efficiency. To localize the host binding domains, truncated versions of Gp48 were expressed as GST-fused protein using pGEX 6P-2 plasmid vector and *E. coli* BL21 cells. The list of plasmids and primers used in this study are given in Table 6.1 and 6.2, respectively.

Table 6.1: List of plasmids used to study RBP binding domain localization [110]

Plasmid	Description	Source or reference
pGEX 6P-2	Glutathione-S-transferase (GST) fused protein expression vector, ampicillin resistance marker, tac promoter	GE Healthcare
pGEX_ <i>gp48</i>	<i>gp48</i> in frame cloned into multiple cloning site of pGEX 6P-2 for expression of GST-fused Gp48	[125]
pGEX_ <i>ntgp48</i>	Expression construct of GST-fused N-Gp48 in pGEX 6P-2	This study
pGEX_ <i>ctgp48</i>	Expression construct of GST-fused C-Gp48 in pGEX 6P-2	This study
pGEX_ <i>ncgp48</i>	Expression construct of GST-fused NC-Gp48 in pGEX 6P-2	This study
pGEX_ <i>ccgp48</i>	Expression construct of GST-fused CC-Gp48 in pGEX 6P-2	This study
pGEX_ <i>3cgp48</i>	Expression construct of GST-fused 3C-Gp48 in pGEX 6P-2	This study
pGEX_ <i>4cgp48</i>	Expression construct of GST-fused 4C-Gp48 in pGEX 6P-2	This study
pET28_ <i>ccgp48</i>	Expression construct of 6xHis -fused CC-Gp48 in pET28a	This study
pET28_ <i>3cgp48</i>	Expression construct of 6xHis-fused CC-Gp48 in pET28a	This study
pET28_ <i>4cgp48</i>	Protein expression vector, 6xHis tag, kanamycin resistance marker, T7 promoter	Invitrogen

Initially, Gp48 DNA fragments encoding for the N- and C-terminal parts of Gp48 are amplified from pGEX\_*gp48* using primer pairs CS710/CS711 and CS712/CS713, respectively. Each amplicon is digested with *EcoRI* and *XhoI* and ligated with the *EcoRI/XhoI* double digested pGEX 6P-2 vector. The resulting vectors pGEX\_*ntg48* and pGEX\_*ctg48* are transformed into *E. coli* DH5  $\alpha$  and then BL21; colonies are

Table 6.2: List of primers used to study RBP binding domain localization [110]

Primers	Tm (°C)	Nucleotide sequence (5' - 3')
CS710	64.2	GCCCCCTGGGATCCCCAGGAATTCC
CS711	56.7	AAGGCTCGAGTTATAGAACTGCAATAACTTTAGTTCCACTAG
CS712	59.7	AAGGAATTCCCGCAGTTCTAACTTCTGATAACAGTAAAAACAAATG
CS713	59.1	CAGATCGTCAGTCAGTCACGATGC
CS716	53.4	AAGGAATTCCTCCAAACAAGTTGATAATATATCTTTTCA
CS717	56.2	AAGGCTCGAGGGAGCTATTTATATCAACTTGGTAATAAGG
CS725	52.3	AAGGCTCGAGTCCTATTTTAAACACCGCTCATACA
CS726	54.4	AAGGAATTCCCGGATTTGATAACGGATATGCTTCT
CS1005	54.9	ATATTAGCCATATGGTGAGCAAGGGCGAGGAG
CS1006	56.3	ATATGGATCCCTTGTACAGCTCGTCCATGCC

selected on LB agar supplemented with ampicillin. The in-frame cloning of the DNA fragments is confirmed by restriction analysis and nucleotide sequencing performed at the Molecular Biology Service Unit, Biological Sciences Department, University of Alberta.

The C-terminal half of Gp48 is further truncated into NC-Gp48 and CC-Gp48; their encoding DNA fragments were amplified using primer pairs CS710/CS717 and CS716/CS713, respectively. The amplicons encoding for NC-Gp48 and CC-Gp48 were double digested with *EcoRI* and *XhoI* and cloned into pGEX 6P-2 as described above. The resulting vectors pGEX\_ncpy48 and pGEX\_ccgp48 were confirmed by restriction analysis and nucleotide sequencing.

Further derivatives of CC-terminal were also produced into 3C-GP48 and 4C-Gp48. DNA fragments encoding for 3C-Gp48 and 4C-Gp48 were amplified from pGEX\_ccgp48 using primer pairs CS710/CS725 and CS726/CS713, respectively. PCR products were digested with *EcoRI* and *XhoI* and were cloned into pGEX 6P-2 as described above. The resulting vectors pGEX\_3cgp48 and pGEX\_4cgp48 were analyzed by restriction analysis and nucleotide sequencing.

### 6.2.3 Immobilization of GST-Gp48 and Derivatives onto Au Surfaces

The gold substrates are sonicated sequentially in acetone, isopropyl alcohol, ethanol and water for 5 min each to clean the surface prior to immobilization. The clean substrates are incubated in a 2 mg/ml solution of Glutathione in PBS for 1 h on an

orbital shaker at 1000 rpm to form a self assembled monolayer (SAM) of glutathione. The GSH SAM chips are washed twice in PBS for 5 min each to remove excess reagents from the surface. The clean GSH SAM substrates are incubated in 5  $\mu\text{g}/\text{ml}$  solution of GST-GP48 proteins in PBS for 1 h on an orbital shaker at 1000 rpm to ensure homogenous mixing. The TSP coated substrates are washed in 0.05% Tween-20 PBS solution for 5 min followed by two washes in PBS. The TSP functionalized substrates are incubated in 1mg/ml BSA for 30 min to block any free surface area, and thus prevent unspecific binding. The BSA blocked chips are washed in 0.05% Tween-20 PBS solution for 5 min followed by two washes in PBS. Then, the TSP immobilized substrates are used for bacterial capture. All the immobilization steps are carried out at room temperature.

#### **6.2.4 Magnetic Beads**

Dynabeads M-280 Tosylactivated and Lyophilized Dynabeads M-270 Epoxy were purchased from Life Technologies, Inc. These beads are 2.8  $\mu\text{m}$  in diameter and are pre-functionalized to actively bind to protein/peptide containing amino or sulfhydryl groups [9, 8]. Both types of beads are uniform, superparamagnetic, polystyrene beads coated with a polyurethane layer. The Dynabeads M-280 Tosylactivated beads are further activated by *p*-toluensulphonyl chloride. The amino groups on proteins react covalently with the resulting sulphonyl ester group on the functionalized beads [9]. Dynabeads M-270 Epoxy are functionalized with a hydrophilic layer of glycidyl ether (epoxy) groups which allow for covalent binding of proteins through amine group [8].

#### **6.2.5 Immobilization of GST-GP48 Protein onto Magnetic Beads**

Initially, 5 mg of Lyophilized Dynabeads M-270 Epoxy or 165  $\mu\text{L}$  of Dynabeads M-280 Tosylactivated beads are washed twice in 0.1 M Na-phosphate buffer (pH 7.4) for 10 min. The tubes containing washed beads are placed on a magnet ( 6-tube magnetic separation rack, Invitrogen Inc.) for 1 min, and the supernatant is removed. The washed beads are resuspended in 100  $\mu\text{L}$  of 0.1 M Na-phosphate buffer (pH 7.4) and 100  $\mu\text{L}$  of 3 M ammonium sulfate (pH 7.4). The ability to capture and isolate target bacteria from a bacterial cell suspension is examined in

two different immobilization modes for receptor binding proteins: random coating and oriented immobilization. Figure 6.1 shows the schematic of various events during immobilization of RBPs and capture of *C. jejuni* cells on magnetic particles. For random un-oriented immobilization, 100  $\mu\text{L}$  of GST-Gp48 RBPs is added to the suspension containing pre-washed beads and the mixture is incubated overnight on an orbital shaker at 1000 rpm. The tube containing RBP-coated magnetic beads is placed on a magnet and the supernatant is removed. The RBP coated magnetic beads are washed four times in PBS-BSA buffer (PBS (pH 7.4) containing 0.1% (w/v) BSA) to block any uncoated surface. The BSA blocked beads are resuspended in 1 ml of PBS buffer (pH 7.4) and stored at 4  $^{\circ}\text{C}$  (Figure 6.1, top panel).

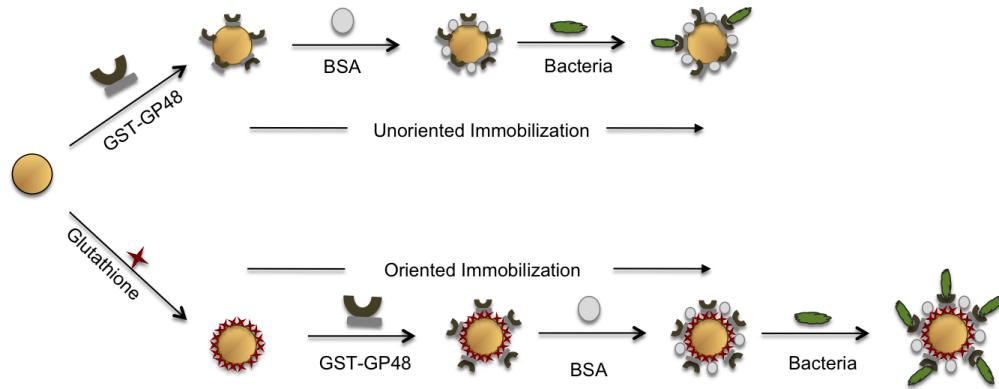


Figure 6.1: Diagram of steps involved in surface immobilization of GST-Gp48 proteins on magnetic beads.(A) Direct un-oriented immobilization (B) Oriented immobilization based on GSH SAM [189]-Reproduced by permission of The Royal Society of Chemistry.

For oriented immobilization, the washed beads are incubated in 100  $\mu\text{L}$  of 1 mg per ml solution of glutathione in PBS, and incubated overnight on an orbital shaker at 1000 rpm to form a self-assembled monolayer of glutathione (GSH SAM)). The GSH SAM beads are washed in PBS once and then placed on a magnet and the supernatant is removed. The GSH-SAM beads are incubated in 40  $\mu\text{g}$  of GST-Gp48 RBPs in PBS for 1 h on an orbital shaker at 1000 rpm. The RBP derivatized magnetic beads are washed four times in PBS-BSA buffer to block free surface. The BSA blocked beads are resuspended in 1 ml of PBS buffer (pH 7.4) and stored at 4  $^{\circ}\text{C}$  until used for bacterial capture (Figure 6.1, bottom panel).

### 6.2.6 Capture and Separation of Bacterial Cells

The desired amount of RBP-derivatized beads (10  $\mu\text{L}$  to 300  $\mu\text{L}$  of RBP-coated beads ( $3.3 \times 10^6$  to  $10^8$  beads)) are exposed to the sample containing host or non-host bacteria for 1 h. The absolute number of beads is indicated based on the correlation between weight (mg) of beads and the number of beads as provided by the manufacturer [9, 8]. The tubes containing bacteria-bead clusters are placed on a magnet and the supernatant is removed. The bacteria-bead clusters are washed in PBS twice to remove loosely bound bacteria. After magnetic separation, bacteria-bound beads are resuspended in 100  $\mu\text{L}$  of PBS and stored in 4  $^\circ\text{C}$ .

Bacterial capture is assessed using fluorescent imaging. To that end, bacteria suspended in PBS are stained with 1  $\mu\text{g}/\text{ml}$  concentration of SYTO 12 green fluorescent dye for 5 min. The stained bacteria are washed twice in PBS prior to exposure to RBP-derivatized beads. An Olympus IX81 microscope (Tokyo, Japan) equipped with a FITC filter and a Roper Scientific Cool-Snaps HQ CCD camera (Duluth, GA, USA) is used to record the fluorescence images of the captured bacteria.

## 6.3 Results and Discussion

### 6.3.1 Analysis of Bacterial Capture on Immobilized GST-GP48 and Derivatives

The protein-immobilized substrates were exposed to host or nonhost bacteria for 20 min on an orbital shaker at 1000 rpm. The substrates were subsequently washed with 0.05% PBS Tween-20 for 5 min followed by 2 similar washes in PBS for 5 min each. The substrates were incubated in a 2% solution of glutaraldehyde in water for 1 h to fix the captured bacteria on the surface. The fixed substrates were washed twice with water for 5 min followed by sequential incubation in serial dilutions of ethanol (i.e. 60, 70, 80, 90 and 100%) 5 min each. Finally, the substrates were blow dried with clean  $\text{N}_2$  and imaged using the Hitachi S-4800 scanning electron microscope (SEM). The bacterial capture density was determined from the SEM images using the cell counter plugin of ImageJ software (NIH, USA). The standard deviation in capture density was obtained from counting 8 images for each experiment.

The GSH SAM based immobilization technique uses the GST tag of the GST-GP48 proteins and therefore provides an oriented way of immobilization of proteins on the surface. In the first set of experiments, the purified GST-GP48 full length, N-GP48, C-GP48, NC-GP48, CC-GP48, 3C-GP48, and 4C-GP48 derivatives were immobilized onto the gold surfaces as described in section 6.2.3. The TSP functionalized substrates were exposed to  $10^9$  cfu ml<sup>-1</sup> of *Campylobacter jejuni* NCTC 11168 cells suspension in PBS for 30 min.

Figure 6.2 shows the scanning electron micrographs of the resulting surfaces. The *C. jejuni* cells were captured on full length GST-GP48, C-GP48 and CC-GP48 immobilized substrates. However, there was no binding on N-GP48 or NC-GP48 immobilized substrates indicating that the host binding domain are localized on the C-terminal of GP48. The results of these experiments also suggests that the host binding site was lost when the protein was further truncated to 3C-GP48 and 4C-GP48 as no capture of bacteria was observed on the 3C-Gp48 and 4C-GP48 immobilized substrates.

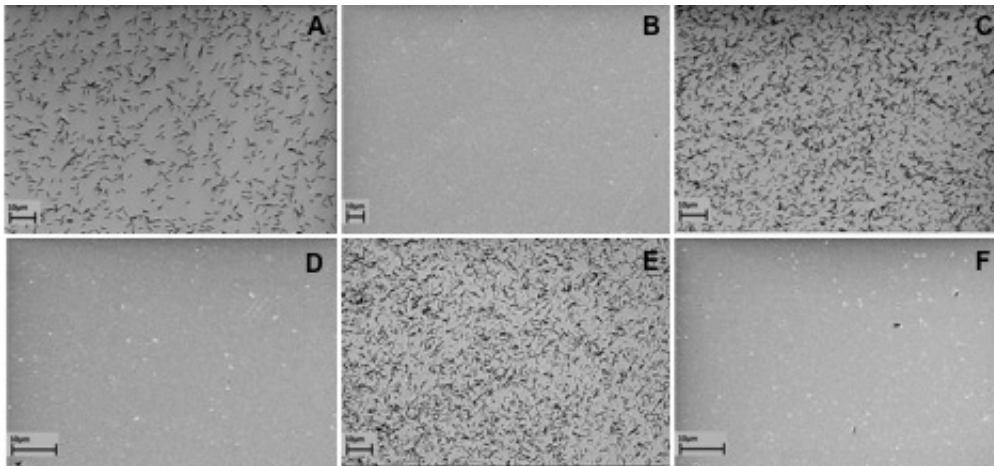


Figure 6.2: Scanning electron microscopy images of *C. jejuni* cells captured by the immobilized Gp48 and its derivatives. (A) GST-fused Gp48, (B) truncated N-Gp48, (C) C-Gp48, (D) NC-Gp48, (E) CC-Gp48, 3C-Gp48 (not shown) and (F) 4C-Gp48 parts were immobilized onto gold-coated surfaces and binding of *C. jejuni* NCTC11168 was studied. The results showed that the host binding domains of Gp48 are localized in the C-terminal quarter (CC-Gp48) as in addition to wild type Gp48. *C. jejuni* cells were captured by C-Gp48, CC-Gp48 only [110].

We analyzed the SEM images and compared the capture efficiency for GST-GP48 full length, C-GP48 and CC-GP48 proteins. Table 6.3 summarizes the capture

density for each protein derivatives upon exposure to  $10^9$  cfu ml<sup>-1</sup> *C. jejuni* cells. As expected, the smaller proteins provide better bacterial capture efficiency.

Table 6.3: Capture density for different protein derivatives

Protein	Capture Density [bacteria/100 $\mu$ m <sup>2</sup> ]
GST-GP48	12.04 $\pm$ 0.92
C-GP48	26.98 $\pm$ 1.4
CC-GP48	39 $\pm$ 1.7

Finally, the selectivity of recognition and capture was confirmed by using different controls. GST-GP48 immobilized gold surfaces were exposed to  $10^9$  cfu ml<sup>-1</sup> concentrations of *Salmonella*, *Ecoli*, and *Campylobacter fetus* as negative controls in addition to *Campylobacter jejuni* as a positive control. Figure 6.3 shows insignificant capture of bacteria for negative control experiments. This confirms that the recognition of the GP48 protein is specific towards its host.

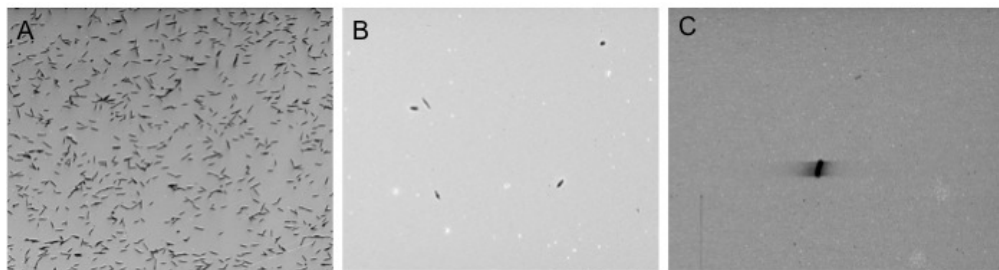


Figure 6.3: Scanning electron microscopy images of different bacteria captured by the immobilized GST-Gp48, (A) *Campylobacter jejuni*, (B) *Campylobacter fetus*, and (C) *Ecoli*. Bacterial recognition and capture is specific to *Campylobacter jejuni*.

### 6.3.2 Bacterial Capture on RBP-derivatized Magnetic Beads

Two types of magnetic beads, Dynabeads M-270 Epoxy and Dynabeads M-280 Tosyl-activated beads were immobilized with GST-Gp48 in two different immobilization modes, namely: un-oriented immobilization and oriented immobilization. In the case of un-oriented immobilization, any free amine groups (-NH<sub>2</sub>) of the GST-Gp48 fusion protein react with the functionalized groups on magnetic particles, which results in random orientation of protein on the surface (Figure 6.1, top panel). The bottom panel on Figure 6.1 illustrates the process for oriented immobilization of

RBPs. A self-assembled monolayer of reduced glutathione (GSH) is initially formed on magnetic particles. The GST tag of the GST-Gp48 protein has natural binding affinity towards GSH and thus provides a definite orientation of the protein on the surface with receptor binding proteins available for capture of bacteria.

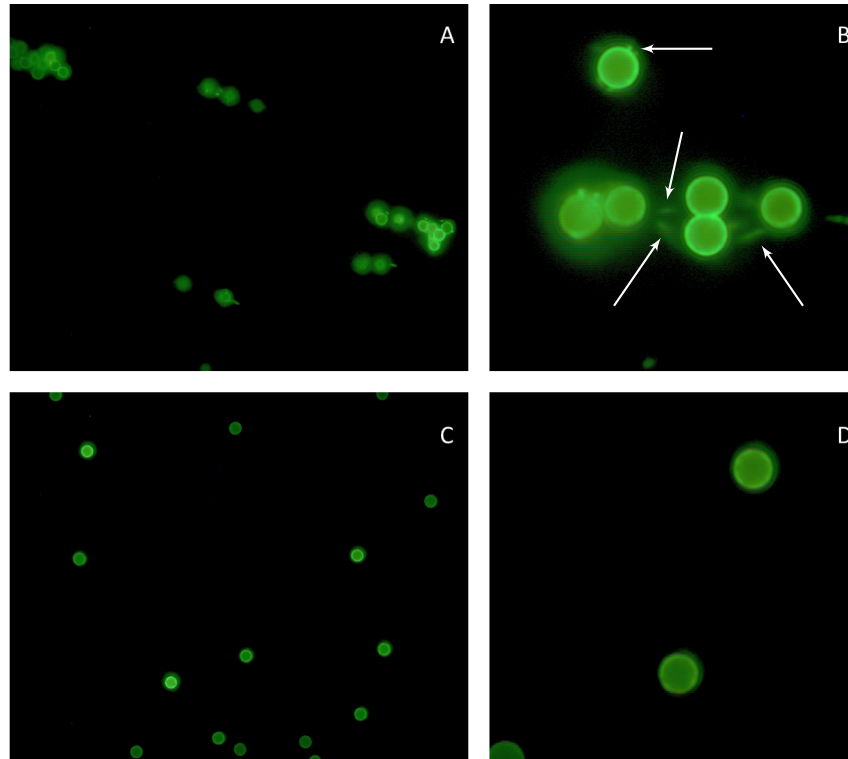


Figure 6.4: Fluorescent images of bacterial capture by GST-Gp48 derivatized Tosylactivated beads (A) Capture of *C. jejuni* on GST-Gp48 derivatized Tosylactivated beads, (B) zoomed in view; (C) No capture of *Salmonella* as negative control on GST-Gp48 derivatized Tosylactivated beads, (D) zoomed in view. The Tosylactivated magnetic beads were also clearly seen on fluorescent images due to their auto-fluorescence properties. The captured bacteria are seen as a fluorescent dot attached to magnetic beads. For the sake of clarity, the bacteria are pointed at with arrows. In all experiments,  $10^8$  RBP-derivatized beads were exposed to  $10^4$  cfu/mL of bacteria. The images on the left column were captured at 100x magnification. The captured images were zoomed in further to visualize the bacteria capture as shown on the right column. [189].

In total  $10^8$  RBP-derivatized magnetic beads were exposed to *C. jejuni* suspension containing  $10^4$  cfu/ml cells for 1h. Fluorescent imaging of the beads exposed to *C. jejuni* followed by bacterial cell staining with CYTO 12 green dye confirmed that both types of beads, i.e. Tosylactivated (Figure 6.4a,b) and Epoxy (Figure 6.5e,f) beads coated with GST-Gp48 captured *C. jejuni* cells. The slight aggregation of

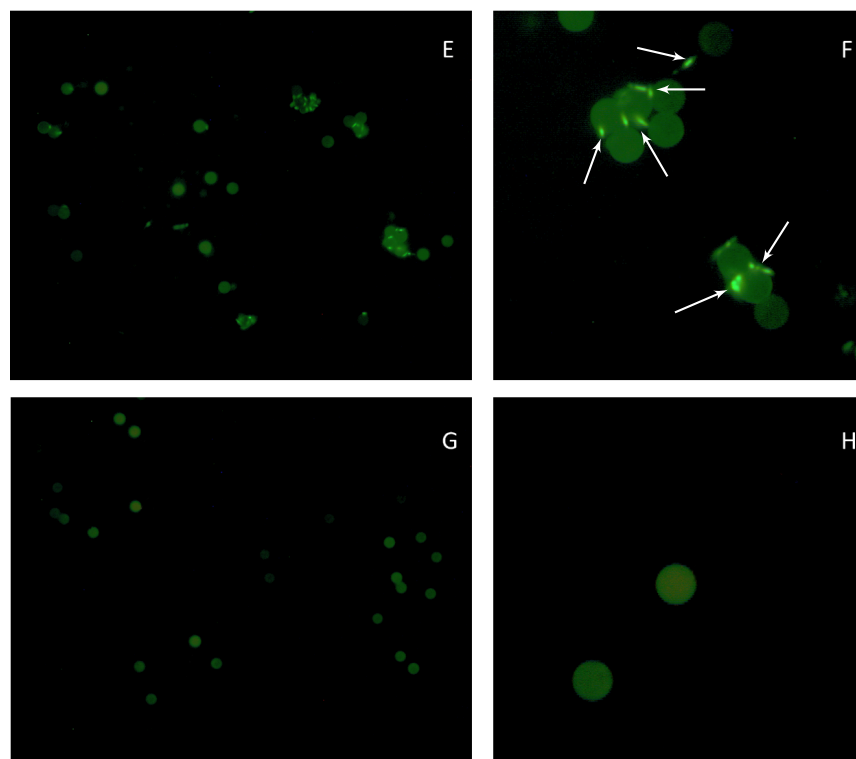


Figure 6.5: Fluorescent images of bacterial capture by GST-Gp48 derivatized Epoxy beads. The captured bacteria are seen as a fluorescent dot attached to magnetic beads. (E) Capture of *C. jejuni* on GST-Gp48 derivatized Epoxy beads and (F) zoomed in view. (G) No capture of *Salmonella* as negative control on GST-Gp48 derivatized Epoxy beads and (H) zoomed in view. The Epoxy beads do not show significant auto-fluorescence, thus can hardly be seen on the fluorescent images. The small fluorescent dots correspond to the captured bacteria. For the sake of clarity, the bacteria are pointed at with arrows. In all experiments,  $10^8$  RBP-derivatized beads were exposed to  $10^4$  cfu/mL of bacteria. The images on the left column were captured at 100x magnification. The captured images were zoomed in further to visualize the bacteria capture as shown on the right column [189].

beads occurred as a result of cross-linking of bacteria, as a single bacterium can potentially bind to more than one bead simultaneously. The specificity of capture was confirmed using *Salmonella Typhimurium* as negative control in which no bacteria were captured on GST-Gp48 derivatized beads (Figure 6.4c,d and Figure 6.5g,h). Results suggest that GST-Gp48 derivatized beads specifically and selectively capture *C. jejuni* cells and can be used as a reliable pre-concentration method for extraction of *C. jejuni* from food samples.

## 6.4 Conclusion

In this chapter, we explored methods for surface immobilization of phage receptor binding proteins onto gold surfaces as well as magnetic particles. We also studied the receptor binding domain of the respective receptor binding proteins, and produced shorter derivatives of these proteins to achieve better yields. The efficiency of bacterial capture was assessed for the host bacteria, i.e. *C. jejuni*. The specificity of capture was confirmed using negative controls, *C. fetus*, *E. coli* and *Salmonella*, where no significant number of bacteria were captured on the surface. Three negative controls gives a certain amount of confidence that the specificity is retained. More work could be done across a larger library of bacteria, or screening against the carbohydrates of pathogens.

## Chapter 7

# Phage RBP-based Microresonator Array for Detection of Bacteria

### 7.1 Introduction

Micromechanical resonators have been proposed as promising platforms for high-throughput and label-free diagnosis of multiple biomarkers as they are extremely sensitive, scalable and conducive to integration into large arrays. These devices operate by monitoring the resonance frequency shift, attributed to the mass of the adsorbed target analyte. Biospecificity is usually achieved by immobilizing the devices with target-specific bioreceptors. Cantilevers are the most widely investigated micromechanical resonators and have been used to detect various food-borne pathogenic bacteria [264, 157, 281, 82, 42, 172, 74] with mass sensitivities down to the single cell level [107]. Although scaling down the dimensions of cantilevers improves its mass sensitivity, it also reduces the effective area for capture of bacteria. This limitation can be overcome with integration of a large number of cantilevers into compact arrays. Nonetheless, efforts have so far mostly been limited to individual cantilever designs. There is thus a need for the design of compact arrays that

---

<sup>1</sup>All work in this chapter was performed by S. Poshtiban except the fabrication of the microresonator arrays. The microresonator arrays were designed and fabricated at Micalyne Inc. The technical support on these devices were provided by Glen Fitzpatrick

<sup>2</sup>A version of this chapter has been published by S. Poshtiban *et al.* [190].

optimizes the effective capture area.

The capture of a target analyte onto the cantilever surface reduces the resonance frequency due to the added mass. However, some counteractive phenomena may influence the frequency shift of a cantilever after capture of target analyte. For instance, it has been known that the added mass shifts resonance to lower frequencies, and adsorption-induced surface stress shifts resonance to higher frequencies [106, 196]. Therefore, the application of micromechanical resonators for detection of bacteria requires a good understanding about the effects of these opposing factors for the specific target of interest.

We developed an innovative ultra-compact micromechanical resonator array that leverages phage TSPs as bioreceptors. This platform offers several features that overcome the limitations of previous designs. The structural design of each resonating beam is optimized to realize wide beams with a large surface area without compromising the high natural frequency and mass sensitivity. In addition, each beam is attached to an electrode and therefore is individually addressable for electrostatic actuation. One thousands of these beams are integrated into a compact array on a small area ( $\approx 13.5 \text{ mm}^2$ ) with a micron wide gap between two adjacent beams. The dense arrangement of individual beams on these arrays further increases the effective area for the capture of bacteria. This layout also makes this resonator array suitable for integration with an automated microfluidic sample delivery system in an encapsulated microfluidic channel [123].

We used three-dimensional finite element analysis (FEA) to evaluate the performance of these resonators for the capture of bacteria. We modeled the bacteria on these devices and studied the effect of mass and stiffness of bacteria on the resonance response. FEA simulations show that the frequency shift is mainly dominated by mass loading effects; and adsorption of such kind of soft massive objects does not change the flexural rigidity of these devices significantly. Simulations also show a linear relationship between the frequency shift and the added mass of randomly distributed bacteria. This is in a good agreement with theoretical expectations for frequency changes due to addition of uniformly distributed mass. Our analysis of the experimental results further confirms this correlation. The number of captured bacteria is calculated from the experimentally observed frequency shift with more

than 88% accuracy.

We studied the potential application of these resonators for specific detection of bacteria. For this purpose, we immobilized the Gp48 TSPs of NCTC12673 phage on these resonators, and we exposed the functionalized devices to *Campylobacter jejuni* (*C. jejuni*) cells. In a typical dip-and-dry experiment,  $N = 225 \pm 13$  bacteria were captured on a single resonator beam which resulted in  $\Delta f = -1.47 \pm 0.43$  KHz frequency shift, measured in a vacuum. Calculations suggests that this frequency shift corresponds to the unit mass of a single bacterium around  $m_b = 159$  fg which is well within the expected range for dry *C. jejuni* cell. Our analysis did not show any significant change to the quality factor after the immobilization and capture of bacteria. The specificity of detection was confirmed using *E. coli* as a negative control where negligible number of bacteria was captured on the devices, and therefore no frequency shift was occurred. To the best of our knowledge, this is the first realization of TSP-derivitized microresonator arrays for the specific detection of pathogenic bacteria.

## 7.2 Device Structure and Fabrication

Figure 7.1a shows a typical microresonator array chip which is composed of 1000 individually addressable deformable elements in a small area (i.e.  $300 \mu\text{m} \times 41$  mm). Individual deformable elements are separated by a micron wide gap. Figure 7.1b illustrates the schematic of cross sectional view of two adjacent beams; each single beam is mounted on a pedestal and is composed of two resonating wings extending laterally from the pedestal. The  $Si_3N_4$  beams are coated with a Cr/Au film stack to provide an electrode for electrostatic actuation. The SEM micrograph of a section of an array is shown in Figure 7.1c.

These devices were designed and realized at Micralyne Inc. The first step in the fabrication process is the growth of thermal oxide layer followed by sputtering thin film of Au layer to form the first electrode. In the second step, three successive layers were deposited by PECVD starting with a standard  $Si_3N_4$  layer as an insulating layer, followed by an amorphous silicon layer as a sacrificial layer, and a low stress silicon nitride film. The Cr/Au layers were formed by sputtering. All of the films

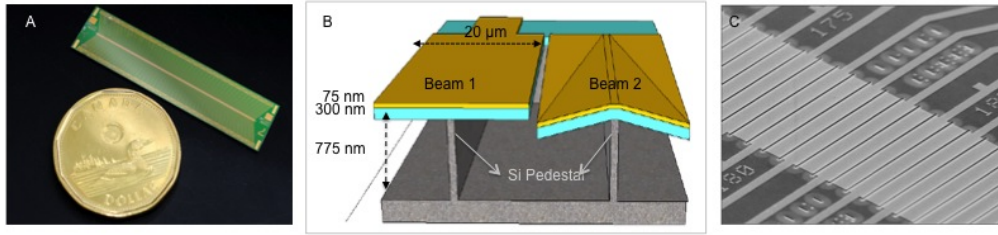


Figure 7.1: Microresonator array chip. (A) Ultra-compact resonators array composed of 1000 beams over a small area. (B) Schematic of two adjacent resonating beams (cross sectional view) - each beam is mounted on a pedestal in the center along its longitudinal axis, thus composed of two resonating wings that flex about the long axis, and (C) SEM micrograph of an array [190].

except metals were sequentially deposited one after another in the same PECVD tool without patterning. The low stress silicon nitride layer was achieved by a secondary ion bombardment of the substrate during deposition. This reduced the tensile stress in the silicon nitride layer to roughly 200 MPa. The silicon nitride film was lithographically patterned into a grid of deformable elements in the form of elongated beams. The etch started from the sidewall exposed by RIE, so the propagation was quite linear and predictable. Ending the etch was determined by a separate etch monitor structure which indicated to submicron accuracy what the central spine dimension was [3], [1].

## 7.3 Finite Element Modeling

### 7.3.1 Finite Element Model Verification

#### Unloaded Resonator Model

We studied the resonance behaviors of these microresonator using finite element modeling (FEM) methods. Simulations were performed using COMSOL 4.2a (COMSOL Group, Burlington, MA) in 3D solid, stress-strain mode using its structural mechanics module. A single resonating wing of an Au-coated beam was modeled with dimensions of  $20 \mu\text{m}$  long in the  $y$ -direction and  $300 \mu\text{m}$  wide in the  $x$ -direction. The inherent symmetry of the structure with respect to the longitudinal axis was considered in the geometry composition, and only one resonating wing of a beam was modeled in order to reduce the computational complexity (Figure

7.2a). For this purpose, the symmetric plane was considered in the center of the support pedestal, perpendicular to the substrate. The support pedestal was modeled with a  $1\ \mu\text{m} \times 300\ \mu\text{m}$  fixed boundary beneath the  $\text{Si}_3\text{N}_4$  layer along the x-axis. The shorter edges of  $\text{Si}_3\text{N}_4$  layer were constrained on both extremities along the longer edge.

Table 7.1 summarizes the material properties used in these simulations. We constructed approximately 40,000 prism mesh elements using swept meshing techniques. The convergence was studied to ensure that the relative error in the eigenfrequency analysis is less than 0.1%. Simulations were conducted in a vacuum neglecting the fluid-structure interactions. Initial stress and external force were set to zero for the purpose of undamped resonant frequency simulations.

Table 7.1: Material properties

Material	E [GHz]	$\rho$ [Kg/cm <sup>3</sup> ]	$\nu$
$\text{Si}_3\text{N}_4$	160	3100	0.23
Cr	279	7150	0.21
Au	70	19300	0.44

The validity and accuracy of the simplified model (i.e. single wing) was confirmed by comparing the unloaded resonance frequencies to the resonance frequencies of two more complicated models, one including both wings (Figure 7.2b), and another one including both wings and the pedestal (Figure 7.2c). Results show negligible difference between various models as shown in Table 7.2

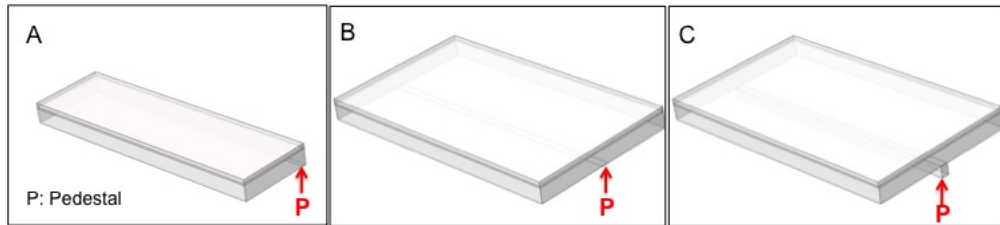


Figure 7.2: Unloaded resonator model, (A) simplified model, (B) model including both wings, (C) model including both wings and the pedestal

Table 7.2: Simulated frequency

Simulated Frequency [MHz]	Simplified Model	Model with two wings	Model with two wings plus pedestal
$f_0$	1.102	1.098	1.0952
$f_1$	1.14	1.143	1.148
$f_2$	1.102	1.2	1.218

### Loaded Resonator Model Verification

In this study, we employ FEM to analyze the resonance response of these microresonator to the capture of bacteria. To verify the accuracy of our approach, we first applied our FEM method to a doubly clamped SiCN cantilever resonators with experimentally known response to the added mass. These resonators were fabricated using nanoimprint lithography with width ranging from 120 to 300 nm, thicknesses of 40 and 70 nm, and a length of 14  $\mu\text{m}$  resulting in average resonant frequencies of  $16.6 \pm 2$  MHz, and  $21.7 \pm 0.3$  MHz, respectively. Figure 7.3 shows the SEM image of a resonator element. These devices were successfully employed as elements of arrays for the detection of straptividin after coating with biotin yielding downward frequency shifts ranging from 100 to 300 KHz, corresponding to capture densities of roughly 1 to 5 molecules per 100  $\text{nm}^2$ .

We modelled the doubly clamped beam with a rectangular box with dimensions of 14  $\mu\text{m}$  long and 300 nm wide, and thicknesses of 40 and 70 nm constrained at both extremities along the long axis. The material properties employed were a density  $\rho = 2200 \text{ kg m}^{-3}$  and a Youngs modulus of  $E = 108 \text{ GPa}$ , as per experimentally measured values reported in Ref. [83] for this material. The intrinsic tensile stress was defined along the longer axis in the linear elastic material model as an initial stress.

We approximately constructed 2780 tetrahedral mesh elements using physics-controlled meshing technique such that there was denser mesh distribution at the vicinities of the clamped edges and the centre of the beam. The eigenfrequency analysis for prestressed structure was performed in two steps. The first step was stationary analysis to solve for the effect of the initial stress and preload on the stiff-

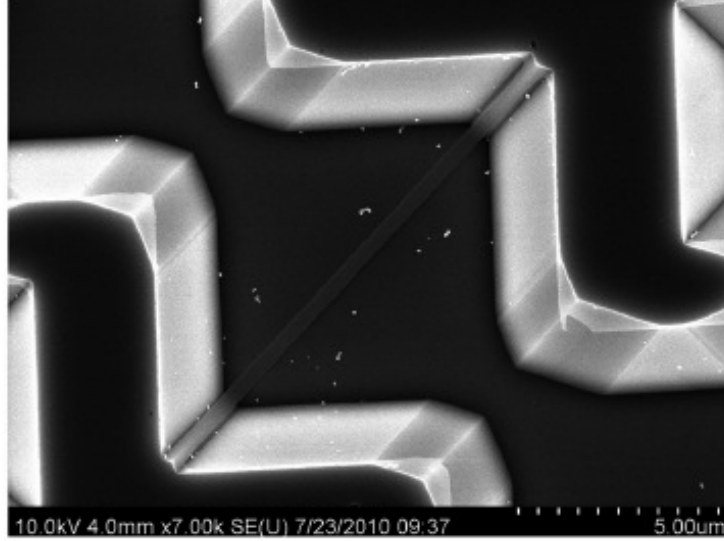


Figure 7.3: Scanning electron micrograph of a resonator element fabricated by imprint lithography. This single device was used for validation of our FEA method for analysis of frequency response to bacterial detection [109].

ness matrix of the resonator. The frequency response of the resonator was computed in the next study step using eigenfrequency analysis. The geometric nonlinearity was taken into account to ensure the prestress contribution to the equations.

The fundamental resonant frequency of a doubly clamped beam of rectangular cross-section under a tensile stress  $\sigma$ , vibrating in the vertical direction (perpendicular to the width of the beam), is given by:

$$f_0 = \frac{22.373}{4\pi} \sqrt{\frac{Et^2}{3\rho L^4} + \frac{4\sigma}{22.373\rho L^2}} \quad (7.1)$$

where  $L$ ,  $t$ ,  $E$ , and  $\rho$  are the length, thickness, Youngs modulus and density, respectively. A systematic study of single clamped and double-clamped resonators fabricated in this material was reported in Ref. [83]. Double-clamped resonators showed a  $L^{-0.999}$  dependence of  $f_0$ , suggesting that the devices indeed operate in this high-stress limit and thus dominated by the second term of equation 7.1. A finite element analysis of the resonant frequency of  $L = 14 \mu\text{m}$  long, and  $t = 40 \text{ nm}$  and  $t = 70\text{-nm}$ -thick beams as function of tensile stress  $\sigma$  is presented in Figure 7.4. FEM results were in agreement with experimental measurements confirming that the relationship between stress and frequency is linear above the values of 400 MPa, thus devices are nominated by the second term of equation 7.1 above this stress

value.

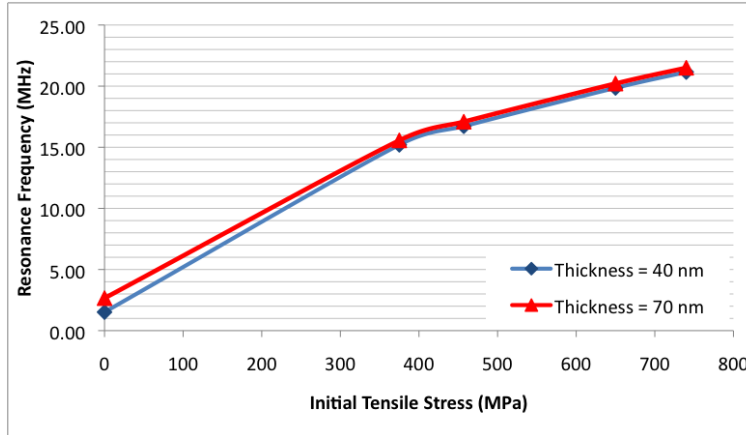


Figure 7.4: Finite element analysis of the resonant frequency measurements of  $L = 14 \mu\text{m}$  long double-clamped beam, with thicknesses  $t = 40 \text{ nm}$  and  $t = 70 \text{ nm}$ , under increasing value of tensile stress  $\sigma$ . The relationship becomes linear at stress values above the  $\sigma = 400 \text{ MPa}$  range [109].

We next simulated the effect of an accrued mass uniformly distributed on the resonator surface using the added mass feature on the top boundary of the beam to model the gravimetric effect of the captured streptavidin monolayer. The eigenfrequencies were computed through the aforementioned two-step analysis. The frequency shifts were calculated with respect to the eigenfrequency of the unloaded resonator. Such FEA analysis was then employed to extract the accrued mass inferred from experimentally observed frequency shifts.

The calculation of the accrued streptavidin mass has been performed through both application of Equation 3.30 as well as through the related FEA data point reported in Figure 7.5. Both Equation 3.30 and FEA report values of  $\Delta m$  agreeing within 0.5% for all experiments. This assessment neglects the possibility of any upwards shifts that could be related to surface stress effects, which are expected to be small compared with those net values. The specific capture of streptavidin resulted in an additional added mass of  $3.5 \pm 1.5 \text{ fg}$ . We can use the estimated mass density of streptavidin which is approximately  $60,000 \text{ g/mol}$  to determine an approximate surface density of 1 streptavidin molecule per  $100 \text{ nm}^2$ .

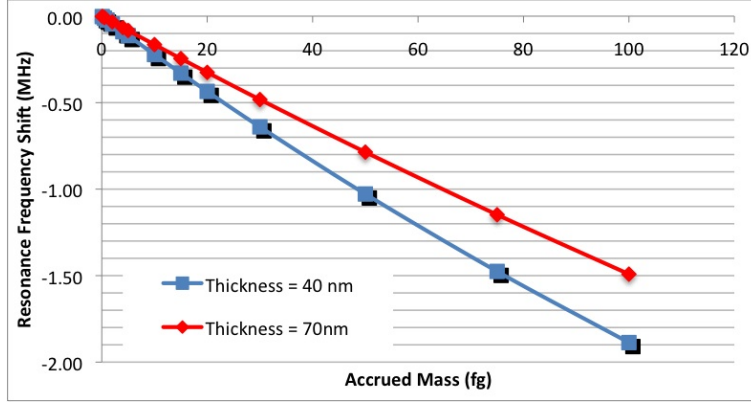


Figure 7.5: Finite element analysis of the resonant frequency shift induced by an evenly distributed accrued mass  $\Delta m$  [109].

### 7.3.2 Bacterial Detection Frequency Analysis

The frequency shift of a cantilever-based mass sensor is attributed to the added mass using equation 3.30 for the added masses with uniform distribution. However, it has been demonstrated that the position of the discrete mass significantly affects the magnitude and sign of frequency shift in the case of singly-clamped cantilevers [58]. Ramos *et al.* observed a significant positive frequency shift because of changes in flexural rigidity when bacteria were absorbed near the clamped edge [196]. We performed FEA to understand how such kind of phenomena play a role in the context of our microresonator platform for detection of bacteria.

In the first set of simulations, we studied the frequency response of these microresonator beams as a function of position of bacteria with respect to the free edge. To this end, we modelled a roll composed of several discrete bacteria at different distances from the free edge along the length of the beam. Each bacterium was modelled with a brick of the dimension of  $4 \mu\text{m} \times 0.4 \mu\text{m} \times 0.4 \mu\text{m}$  to represent a typical *Campylobacter jejuni* cell, which is the target pathogen in our study. Each bacterium was separated from the next one with  $0.5 \mu\text{m}$  gap to ensure the entire added object does not appear as a large continuous block. Figure 7.6a shows an example of the model geometry; in which bacteria roll is located at the free edge. Fine triangular mesh elements were constructed at the contact surface between each bacterium and the surface of resonator. The rest of the model geometry was meshed as described previously. As described previously, simulation of frequency response

consisted of two steps. Initially, the static analysis was conducted to obtain the flexural rigidity matrix of the resonator that reflects the impact from adsorption of bacteria. The resonance response was then computed using eigenfrequency analysis. The geometric nonlinearity function was activated to ensure eigenfrequency analysis accounts for the contribution of the stiffness of bacteria in equations.

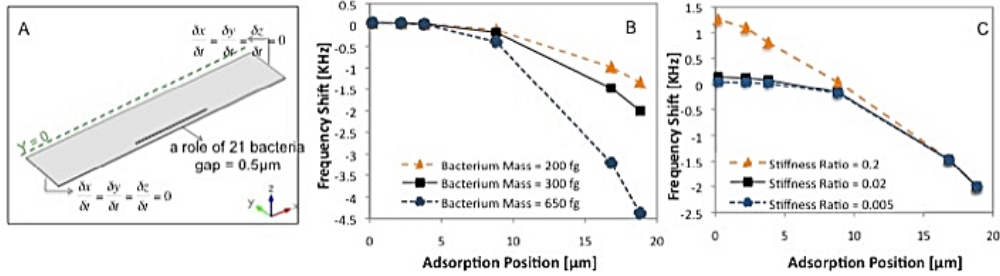


Figure 7.6: The effect of mass and stiffness of bacteria on resonance response, (A) FEA model geometry, a single resonating wing; the dashed green line corresponds to the symmetric plane considered in the center of a pedestal on  $xz$ -plane. The beam is constrained on both short edges along the  $yz$ -plane. (B) Frequency shift versus the adsorption position for different unit mass values of bacteria, the frequency has a linear relationship with mass near the free edge. (C) Frequency shift versus the adsorption position for various stiffness ratios ( $E_b/E_r$ ), capture of soft objects like bacteria does not significantly change the flexural rigidity [190].

FEA results show that the frequency shift is mainly dominated by the mass of captured bacteria. The added mass always decreases resonance frequency, with the maximum negative frequency shift for the mass added near the free edge (Figure 7.6b). Results of these simulations suggest that the capture of soft objects like bacteria does not change the flexural rigidity of resonator significantly as shown on Figure 7.6c. However, the adsorption of rigid objects may change the flexural rigidity if the stiffness ratio between the added object and the resonator exceeds a certain level ( $E_b/E_r > 0.02$ ) resulting in a distinguishable positive frequency shift (Figure 7.6c). The accepted range for the Young's modulus of dry bacteria is between  $E_b = 300$  MPa to 400 MPa according to atomic force microscopy (AFM) measurements [272], which corresponds to a small stiffness ratio (i.e.  $E_b/E_r < 0.005$ ). Thus, the adsorption of such soft massive bacterial cells has a negligible impact on the flexural rigidity of these resonators, and the frequency shift is mainly due to the mass loading effects of captured bacteria.

In the next step, we simulated the dynamic behaviour of this platform in real

experimental condition, in which bacteria are captured on the resonators surface with a random orientation. SEM imaging shows that approximately 200 bacteria are captured on a single beam in a typical experiment. We modeled 200 bacteria on resonator surface with random distribution as shown on Figure 7.7a. The Young's modulus of bacteria was set to  $E_b = 400$  MPa. We studied the frequency shift as a function of added mass by varying the unit mass of bacteria within the expected range from 90 fg to 650 fg. Simulations show that the frequency shift has a linear relationship with the mass of randomly distributed bacteria. As shown on Figure 7.7b, the simulated frequency shift is in a close agreement with the expected values, calculated using Eq. 3.30. This implies that this equation can be used with high certainty to quantify the number of captured bacteria from the experimentally measured frequency shift in real applications. Experiments support FEA results as will be discussed in greater details in the following section.

## 7.4 Experimental Methods

### 7.4.1 Resonator Frequency Measurements

Resonant frequencies are measured in a custom optical interferometer setup as shown on Figure 7.8. The resonator chip is mounted on a piezoelectric disk that is contained within a small vacuum chamber pumped down to the millitorr range. The piezoelectric element is actuated by a sinusoidal signal in a close span of resonant frequency by the tracking output of a spectrum analyzer. A He-Ne gas laser beam is guided through a beamsplitter and focused on the resonator using a microscope objective. The displacement of the resonator relative to the substrate creates a moving fringe pattern that is reflected off the beamsplitter on an ac-coupled photodetector. It is worth to note that the moving fringe patterns only occurs when the two plates are in parallel, thus the interference between light reflected from moving substrate and stationary optics does not create moving fringe pattern. The photodetector output is connected to the input of the spectrum analyzer to monitor resonance spectrum of the resonator. Laser power is kept at minimum (typically on the order of  $40 \mu\text{W}$ ) to minimize heating effects.

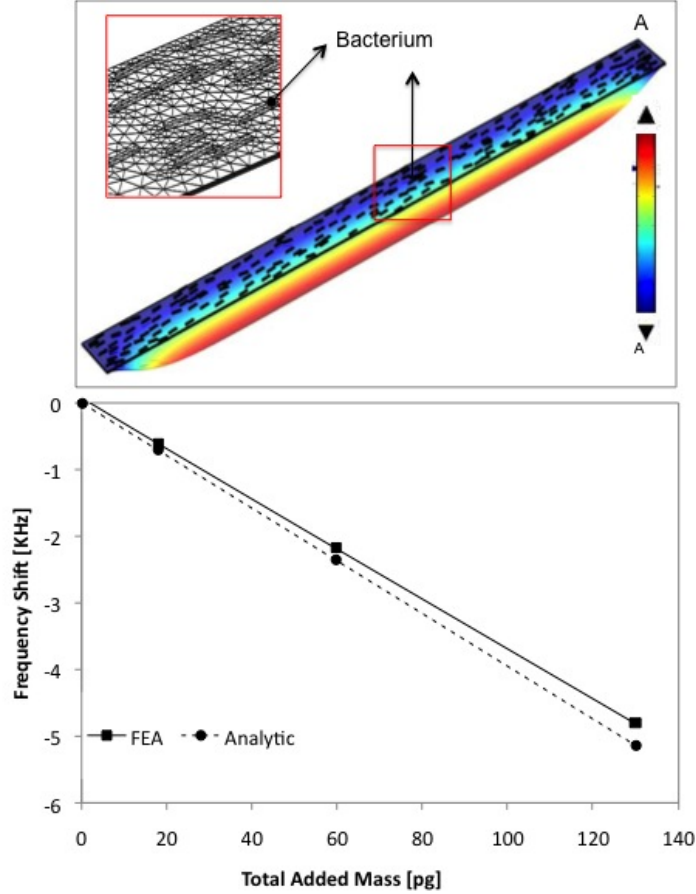


Figure 7.7: Resonance response to random capture of bacteria, (A) FEA model geometry and deformation of resonator, (B) frequency shift versus total added mass, linear relationship between frequency shift and added mass with a good agreement with analytical calculations using Eq. 3.30 [190].

#### 7.4.2 Phage RBP Immobilization onto Resonators

We tested the application of these resonators for bacterial detection by functionalizing gold-coated resonators with GST-Gp48 TSP for specific detection of *C. jejuni* cells. The devices were washed sequentially in acetone, isopropyl alcohol, ethanol, and water for 5 min each to clean the surface prior to functionalization. The clean devices were incubated in  $2 \text{ mg ml}^{-1}$  solution of glutathione in PBS for 1 h on an orbital shaker at 1000 rpm. The formation of a glutathione self-assembled monolayer (GSH-SAM) ensures oriented attachment of proteins, resulting in 3-fold improvement in bacteria capture density [20]. The GSH-SAM devices were washed twice in PBS for 5 min each to wash away the excess reagent from the surface. The functionalized devices were immersed in  $5 \mu\text{g ml}^{-1}$  solution of GST-GP48 protein in PBS for

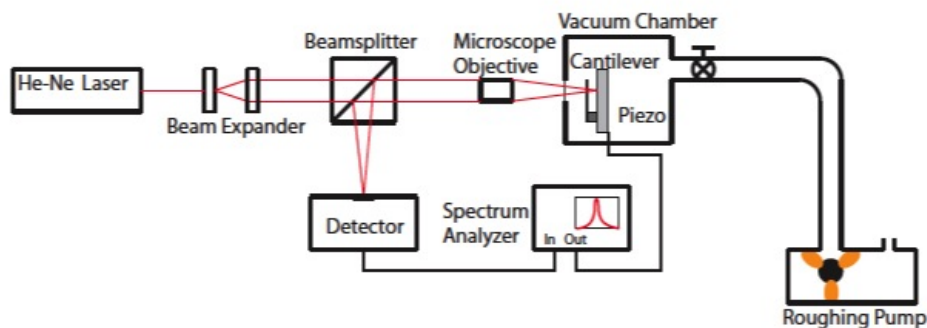


Figure 7.8: Schematic of resonance measurement interferometric setup [168].

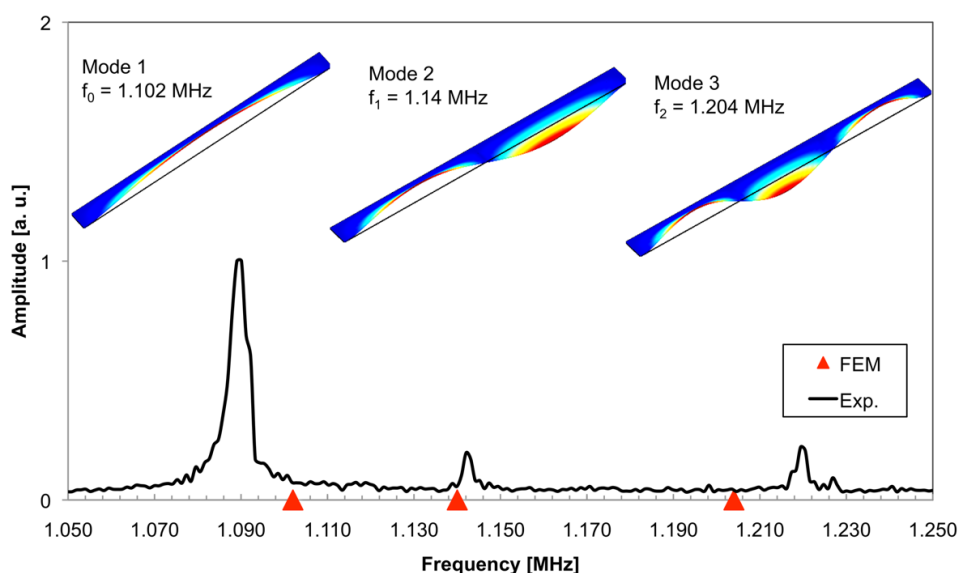


Figure 7.9: Optically measured resonance spectrum and simulated resonance modes for a typical resonator. The red triangles indicate the simulated values for eigenfrequencies [190].

1 h on an orbital shaker at 1000 rpm followed by 5 min wash in 0.05% Tween-20 PBS and two 5 min washes in PBS. The  $1 \text{ mg ml}^{-1}$  solution of bovine serum albumin (BSA) was used to block any non-specific binding. The TSP-immobilized devices were incubated in 1 ml of *C. jejuni* cell suspension in PBS with the concentration of  $10^8 \text{ cfu ml}^{-1}$  for 20 min. The devices were washed twice with PBS-Tween 20 (0.05%) followed by PBS. Then, the captured bacteria were fixed in a 2% solution of glutaraldehyde in MilliQ water for 60 min followed by serial ethanol dehydration steps (50 - 95% for 10 min each). The devices were finally dried under clean nitrogen gas and imaged using the Hitachi S-4800 scanning electron microscope (SEM).

## 7.5 Results and Discussion

### 7.5.1 Characterization of Unloaded Resonators

Figure 7.9 shows the resonance spectrum and simulated modal shapes for a typical microresonator beam. The largest displacement is observed for the first resonant mode at  $f_0 = 1.095 \pm 0.005$  MHz, with the quality factor of  $Q = 450$  in a vacuum. Finite element analysis predicts the eigenfrequencies accurately with less than 1% difference, and show that the first resonance mode is purely flexural without any torsional vibration coupling. The experimental characterization supports this behavior and indicates no vibration nonlinearity even when a large ac driving voltage is applied (Figure 7.10).

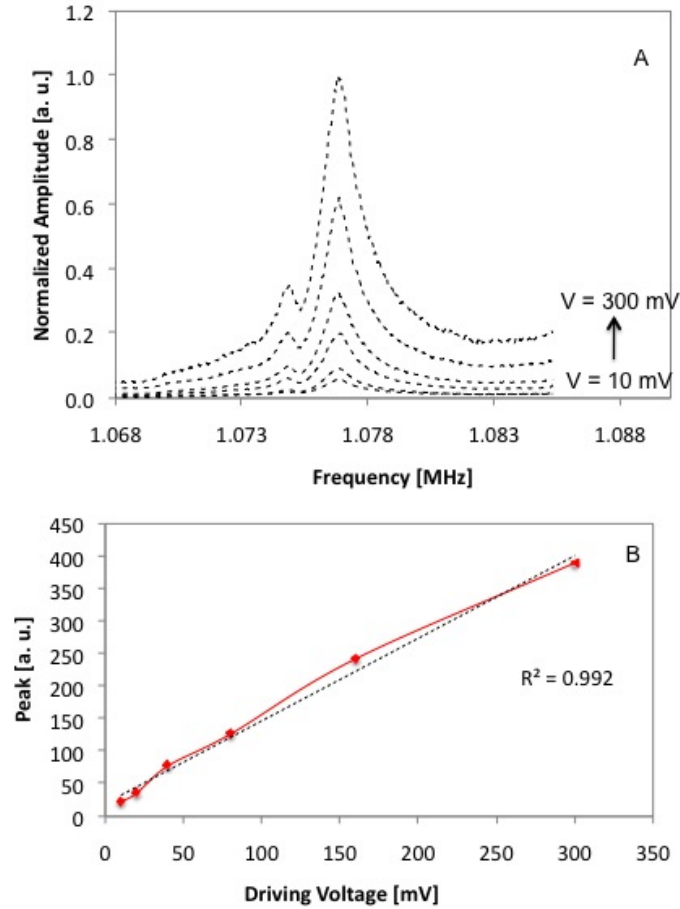


Figure 7.10: Device characterization, (A) resonance spectra for various ac driving voltage ranging from 10-300 mV, (B) vibration amplitude for various ac driving voltages; nonlinear vibration was not observed even at high ac driving voltages [190].

It is desirable to operate biosensors in fluid for most applications, however, the fluid viscosity usually affects the resonance response reducing the quality factor. Figure 7.11 shows that the quality factor and resonance frequency did not change significantly below  $p = 1.5$  Torr, suggesting that the dissipative process is not dominated with viscous damping in this range. However, the quality factor drops at pressures above  $p = 1.5$  Torr due to viscous damping. Nonetheless, the quality factor ( $Q_{air} = 80$ ) is relatively high even at atmospheric pressure. This value of quality factor is comparable to that of the previously reported cantilever sensors for bacterial detection [41, 195, 173, 281].

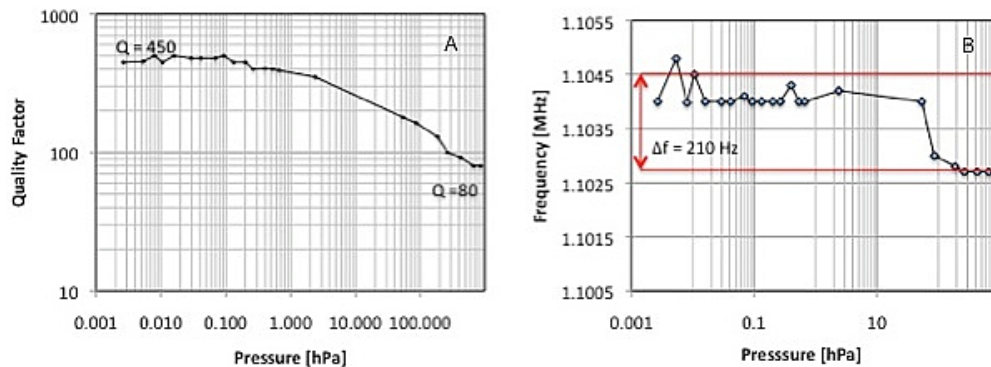


Figure 7.11: Pressure dependency analyses, (A) Quality factor *vs.* ambient pressure, (B) resonance frequency *vs.* ambient pressure [190].

We estimated the mass sensitivity of these microresonator arrays at approximately  $\sigma_m \approx 52\text{fg}$  (in vacuum) and  $\sigma_m \approx 123\text{fg}$  (in air) using Eq. 3.31. This is lower than mass of a single *C. jejuni* cell. Dry *Campylobacter jejuni* cells are usually coccoidal approximately  $4 - 6 \mu\text{m}$  in length and  $0.3 \mu\text{m} - 0.5 \mu\text{m}$  in width. Given that the mass density is around  $300 \text{kg}/\text{m}^3$ , the unit mass of a single cell is within the range of  $150 \text{fg}$  to  $200 \text{fg}$ .

### 7.5.2 Effect of Functionalization Layers on Frequency Response of Resonators

An initial set of experiments was performed to study the mass loading effect of functionalization layers (i.e. GSH SAM, TSP, BSA, and Glutaraldehyde) on resonance response prior to capture of bacteria. To that end, the microresonator beams were functionalized as explained in section 6.2.3 but without any exposure to bacteria. As

shown on Figure 7.12, resonance frequency did not change significantly after functionalization. This indicates that the frequency response to the functionalization layer is not purely due to the mass loading effects. We can explain this behavior by considering the counteractive effects of the surface stress induced after adsorption of functionalization layers. It has been reported that the formation of alkanethiol self-assembled monolayer (SAM) on flat gold surfaces induces surface stress [233]. It was also previously shown that the adsorption of chemicals on the cantilever surface changes the spring constant resulting in upward frequency shift [48]. We believe that the total frequency shift results from the equal contribution of two factors, mass and stress. In other words, the absolute value of negative frequency shift due to the mass of functionalization layers is comparable to the absolute value of the positive frequency shift due to the adsorption-induced surface stress from SAM, and therefore the net frequency shift is not measurable.

### 7.5.3 Detection and Quantification of *C. jejuni* Cells

We, then, functionalized these microresonator arrays with GST-Gp48 tail-spike proteins (TSP) and captured *Campylobacter jejuni* cells. Figure 7.13a, 7.13b shows the SEM micrograph of functionalized resonators after the capture of bacteria. The number of bacteria was counted on SEM images for every resonating beam on the array under test. The results show that an average of  $N = 225 \pm 13$  bacteria was bound to a single element with capture density of  $\approx 3.86 \pm 0.25$  bacteria/ $100\mu\text{m}^2$ . This resulted in an average negative frequency shift of  $\Delta f_0 = -1.46$  KHz. Figure 7.12a shows the resonance spectra for a beam at a zero mass load with a peak at  $f_0 = 1.091$  MHz and after the capture of bacteria with a peak at  $f_L = 1.0895$  MHz. According to Eq.1 this frequency shift suggests that the total added mass is  $\delta m \approx 36$  pg, which corresponds to a single bacterium unit mass of  $m_b \approx 159$  fg. Corresponding FEA using this value of mass also indicates a similar resonance frequency shift. This value is well within the expected range because a typical dry *C. jejuni* cell weighs approximately 150 fg -200 fg. These results imply that the number of added bacteria can be quantified from experimentally observed frequency shift with high certainty provided that the bacteria are randomly distributed on the resonators.

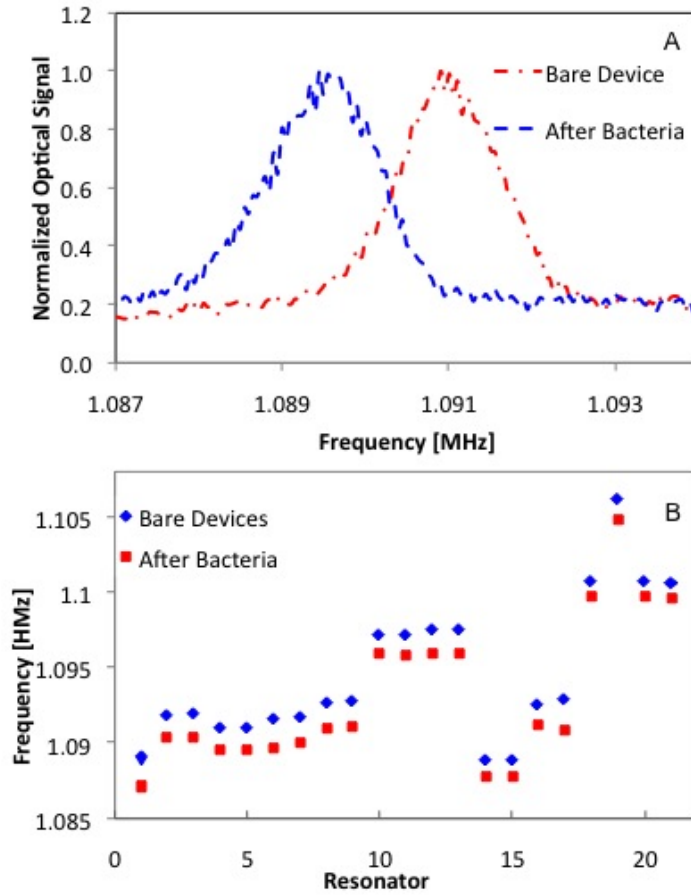


Figure 7.12: Resonant frequency measurements for (-) unloaded resonator, (—) after functionalization [190].

#### 7.5.4 Capture Specificity

In the final set of experiments, we studied the specificity of detection to *C. jejuni*. With that goal, the GST-GP48 immobilized microresonator were exposed to *E. coli*. The TSP functionalized resonators show minimal affinity to *E. coli* cells as indicated by negligible shift in resonance frequency and further confirmed by SEM imaging.

#### 7.5.5 Practical Limitations

We faced several challenges during the course of these experiments. The major impediments to the application of this platform is the transportation of bacteria onto the surface of device. So far, experiments have been performed in the "dip and dry" format which is not automated and therefore is a significant barrier for field

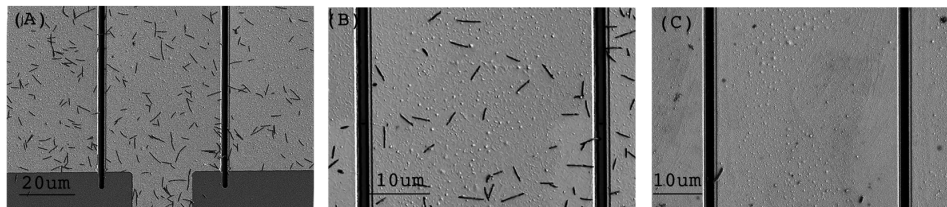


Figure 7.13: Bacterial capture on a microresonator array, (A) SEM image shows the capture of *C. jejuni* bacteria on GST-GP48 TSP-functionalized resonators, no bacteria were captured on  $\text{Si}_3\text{N}_4$  regions confirming the selectivity of immobilization to gold. (B) Zoomed in SEM image of a section of a beam, the capture density is  $\approx 3.86 \pm 0.25$  bacteria/ $100\mu\text{m}^2$ . (C) Specificity of detection, SEM image shows negligible capture of *E. coli* cells on a TSP-functionalized resonating beam [190].

applications. In addition, it is desired to operate the biosensor in liquid environment in most biosensing applications. However, the quality of resonance decreases significantly due to viscous damping resulting in low sensitivity. Moreover, it is challenging to control the landing point of bacteria on the surface of resonators. Figure 7.14 shows several bacterial capture artifacts such as bacteria bridging between two adjacent resonators (Figure 7.14a,b) and bacteria wedging underneath a resonator (Figure 7.14c,d). In any case, these artifacts changes the resonance behaviour of resonators leading to unpredictable frequency shift after capture of bacteria. Integrating these microresonator array with an automated sample delivery microfluidic device may circumvent this limitation [123].

## 7.6 Conclusion

We present an innovative ultra-compact micromechanical resonator array that leverages phage TSPs as bioreceptors. This platform offers several features that overcome the limitations of previous designs. The structural design of each resonating beam is optimized to realize wide beams with a large surface area without compromising the high natural frequency and mass sensitivity. In addition, each beam is attached to an electrode and therefore is individually addressable for electrostatic actuation. One thousands of these beams are integrated into a compact array on a small area ( $\approx 13.5 \text{ mm}^2$ ) with a micron wide gap between two adjacent beams. The dense arrangement of individual beams on these arrays further increases the effective area for the capture of bacteria. This layout also makes this resonator array suitable for

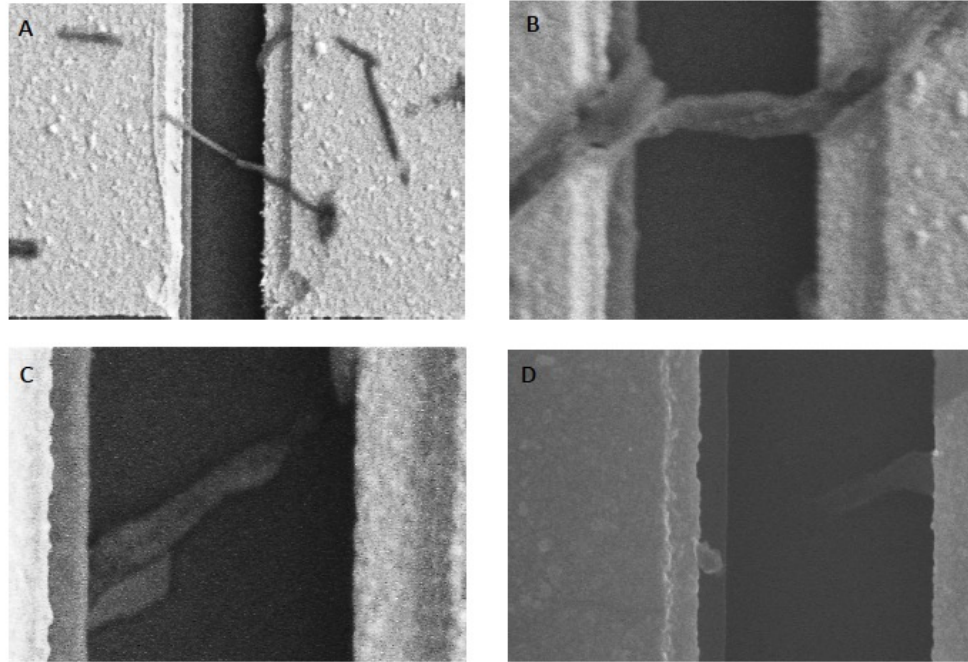


Figure 7.14: SEM images showing bacterial capture artifacts on a microresonator array, (A, B) bacteria bridging between two adjacent resonator beams. (C, D) bacteria wedging underneath the resonator beam.

integration with an automated microfluidic sample delivery system in an encapsulated microfluidic channel [123]. We used three-dimensional FEA to evaluate the performance of these resonators for the capture of bacteria. We modeled the bacteria on these devices and studied the effect of mass and stiffness of bacteria on the resonance response. FEA simulations show that the frequency shift is mainly dominated by mass loading effects; and adsorption of such kind of soft massive objects does not change the flexural rigidity of these devices significantly. Simulations also show a linear relationship between the frequency shift and the added mass of randomly distributed bacteria. This is in a good agreement with theoretical expectations for frequency changes due to addition of uniformly distributed mass. Our analysis of the experimental results further confirms this correlation. The number of captured bacteria is calculated from the experimentally observed frequency shift with more than 88% accuracy. We studied the potential application of these resonators for specific detection of bacteria. For this purpose, we immobilized the Gp48 TSPs of NCTC12673 phage on these resonators, and we exposed the functionalized devices to *Campylobacter jejuni* (*C. jejuni*) cells. In a typical dip-and-dry experiment, N

=  $225 \pm 13$  bacteria were captured on a single resonator beam which resulted in  $\Delta f = -1.47 \pm 0.43$  KHz frequency shift, measured in a vacuum. Calculations suggests that this frequency shift corresponds to the unit mass of a single bacterium around  $m_b = 159$  fg which is well within the expected range for dry *C. jejuni* cell [38]. Our analysis did not show any significant change to the quality factor after the immobilization and capture of bacteria. The specificity of detection was confirmed using *E. coli* as a negative control where negligible number of bacteria was captured on the devices, and therefore no frequency shift was occurred. To the best of our knowledge, this is the first realization of TSP-derivitized microresonator arrays for the specific detection of pathogenic bacteria.

As a future direction, each resonating beam can be actuated individually with electrostatic actuation for capacitive detection. Furthermore, control beams will be considered to quantify specificity. In this case, the control beams will be treated with all steps of immobilization except exposure to the target specific TSPs. The difference between frequency shift for TSP immobilized beams and control beams will be used as a measure for capture of bacteria.

## Chapter 8

# Phage RBP-derivatized Magnetic Pre-Enrichment Coupled with PCR

### 8.1 Introduction

Identification of pathogenic contaminations in food samples is critical for prevention of food born outbreaks. Although cooking process or pasteurization kills any potential bacteria that are present in food, the contamination of food products is still a major problem both in developed as well as third world countries. The food styles have changed in recent years and more processed and ready to eat food are available nowadays. In developing countries, the consumption of unpasteurized dairy products is still very common. More importantly, in addition to direct bacterial contaminations, the enterotoxins of bacteria can also cause foodborne diseases even after killing bacteria. Therefore, there is still great interest to develop rapid and accurate technologies for detection of contaminations in food samples.

Polymerase chain reaction (PCR) based detection methods offer major advantages in terms of speed, specificity, and sensitivity. However, direct application of PCR in food samples is problematic due to the inhibitory effects of the residual food components on PCR enzymatic activity [203]. Another major impediment to

---

<sup>1</sup>A version of this chapter has been published by S. Poshtiban *et al* [189]-Reproduced by permission of The Royal Society of Chemistry.

the application of PCR for real-time detection of foodborne pathogens is the low infectious dose ( $\approx 10 - 1000$  bacterial cells) [211]. Such a low number of pathogens may be hard to detect by PCR, especially in the presence of natural inhibitors of DNA polymerase present in food matrixes. Various DNA extraction kits have been developed for extraction and purification of bacterial DNA prior to amplification; however, their efficiency is significantly compromised in crude food samples. Therefore, there is a need for a sample preparation step prior to detection which can circumvent these methodological hurdles by selectively isolating and subsequently concentrating the target bacteria from complex food samples.

In this chapter, we employ the proposed phage RBP-derivatized magnetic pre-enrichment method in conjunction with PCR for analysis of artificially contaminated food samples. Previous studies reported successful detection of  $10^2$  cfu/ml of *C. jejuni* cells and  $10^3$  cfu/ml of *Salmonella* in buffered samples with phage TSP immobilized SPR sensors [219, 220]. We demonstrate the ability of this pre-enrichment method to isolate, purify and pre-concentrate bacteria from food suspensions, resulting in elimination of PCR inhibition by matrix-related refractory components. We artificially spiked various food samples including skim milk, milk with 2% fat and chicken broth with known concentration of *C. jejuni* bacteria. Recovery rates, assessed by real-time PCR, were greater than 80% for the samples spiked with as low as 100 cfu/ml of *C. jejuni* cells. The specificity of capture was confirmed using *Salmonella Typhimurium* as a negative control where no bacteria were captured on the RBP-derivatized magnetic beads. The combination of RBP-based magnetic separation and real-time PCR improved PCR sensitivity and allowed the detection of *C. jejuni* cells in milk and chicken broth samples without a time consuming culture-based pre-enrichment. The total sample preparation and analysis time in the proposed RBP-based method coupled with real-time PCR was less than 3h.

## 8.2 Experimental Methods

### 8.2.1 Primer and Probe Design

Primers and TaqMan probe (Applied Biosystems) were designed using Primer Express 3.0 software to amplify a fragment of gene *lpxA* of *C. jejuni* bacteria. The list

of primers and probes used for real-time PCR is given in Table 8.1.

Table 8.1: List of primers and probes; the TaqMan probe was labeled with a 6-FAM reported at the 5' end and a MGB quencher at 3' end

Assay Type	Primer of Probe	Nucleotide Sequence 5'-3'
Conventional PCR (Product Size = 288 bp)	Forward	CTCCTTTAGCTGTACCTGAATTTATCGTT
	Reverse	GTGCGGTGATTGAAGAGGGTG
Realtime PCR (Product size = 70 bp)	Forward	GGCGGGCTTACACCTATTCA
	Reverse	AGTGCACTTGCTCCTGCTATCA
	MGB Probe	6FAM-AATTTGTCAAAGTAGGTGAGGGT

### 8.2.2 Conventional PCR Assay

Reactions for conventional PCR were done in 25  $\mu$ L PCR mixtures containing 1U *Taq* DNA polymerase, 200 ng BSA, 200  $\mu$ L dNTPS, 2mM MgCl<sub>2</sub>, 1x Invitrogen *Taq* PCR buffer, 500 nM each primer, 1 $\mu$ L of cell dilutions. The thermal cycle protocol was started with a pre-denaturation for 4 min at 94°C followed by 35 cycles of denaturation for 10 sec at 94°C, annealing for 20 sec at 55°C and extension for 20 sec at 72°C. PCR products were loaded in 2% agarose gel stained with ethidium bromide and electrophorased at 90V for 30 min. Gel was visualized under UV light using a transilluminator apparatus and camera.

### 8.2.3 TaqMan Real Time PCR Assay

The real-time PCR reactions were performed on an ABI 7500 Fast (Applied Biosystems) in a 10  $\mu$ L PCR mixture containing 1x Taqman Universal PCR Mastermix (Applied Biosystems), 900 nM of each primer, 250 nM TaqMan Probe (Life Technologies, Inc.), PCR grade nuclease-free water and 1  $\mu$ L of template. The thermal cycling profile consisted of 2 min at 50 °C, 10 min 95 °C, followed by 40 cycles of 15 sec denaturation at 92 °C and 1 min annealing/extension at 60 °C.

### 8.2.4 Primer and Probe Concentration Optimization

A series of experiments were performed to determine the optimal primer concentrations. To that end, a 10  $\mu$ L PCR reaction mix was prepared to run three replicates of each of the nine conditions as shown in Table 8.2. The thermal cycling condition

was similar to the condition described previously. At the end of the run, the minimum forward and reverse primer concentration were chosen that yield the minimum Ct value.

Table 8.2: PCR reaction mix for primer optimization

<b>Reverse Primer (nM)</b>	<b>Forward Primer (nM)</b>		
	<b>50</b>	<b>300</b>	<b>900</b>
<b>50</b>	50/50	300/50	900/50
<b>300</b>	50/300	300/300	900/300
<b>900</b>	50/900	300/900	900/900

Similarly, the optimal probe concentration was determined through a series of experiments using various probe concentrations as shown on Table 8.3. The optimal primer concentrations determined in previous experiment were used in this experiment to find the optimal probe concentration.

Table 8.3: PCR reaction mix for probe optimization

Probe Concentration (nM)	50	100	150	200	250	500

### 8.2.5 DNA Extraction from Bacterial Cells

The commercially available DNA extraction kit (QIAamp DNA Mini Kit, Qiagen) was used to extract and purify DNA from *C. jejuni* culture. The extracted DNA was treated with RNase A (Qiagen) to obtain RNA-free DNA. DNA concentration was determined using the NanoDrop ND 1000 spectrophotometer (NanoDrop Technologies Inc., Wilmington, DE, USA). Original concentration of DNA was adjusted to 50 ng/ml for sensitivity testing. Details about this method of DNA extraction is provided in Appendix A.3.

### 8.2.6 Creating Standard Curve with Genomic DNA for PCR Sensitivity Analysis

The standard curves were created with purified genomic DNA of culture of *C. jejuni* NCTC 11168 to study the sensitivity of primer-probe set for PCR assay. The stan-

standard curve was created using purified genomic DNA of *Campylobacter jejuni* at the range of  $28 \times 10^6$  to 28 copies. The genome size of *Campylobacter jejuni* subsp. *C. jejuni* NCTC 11168 (ATCC 700819) is estimated at 1.64 Mb [10]. The mass of the *C. jejuni* DNA per genome is calculated at 1.797 fg using the Equation 8.1:

$$m = (n)(1.096e^{-21}) \frac{g}{bp} \quad (8.1)$$

in which  $n$  is the genome size (bp) and  $m$  is the mass. Dividing the mass of the genome by the copy number of gene *lpxA* per haploid (i.e. one), we calculate the mass per copy number of the gene of interest. Next, we calculated the mass of gDNA containing the copy #s of interest, from 280,000 to 28 copies as summarized in Table 8.3. The final concentrations are calculated by dividing the needed DNA mass for desired copy # by the volume to be pipetted into each PCR reaction mix, which is  $1 \mu\text{L}$  in this work (Table 8.3).

Table 8.4: Mass of DNA (fg) and final concentration of DNA vs Copy #

Copy #	Mass of DNA per genome	Mass of gDNA (fg)	volume per reaction	Final Concentration (fg/ $\mu\text{L}$ )
280,000	$\times 1.797 \text{ fg}$	503,160	$\div 1 \mu\text{L}$	503,160
28,000		50,316		50,316
2,800		5,031		5,031
280		503		503
28		50		50

The Equation 8.2 is used to prepare the serial dilutions of the gDNA.

$$C_1.V_1 = C_2.V_2; \quad (8.2)$$

in which  $C_1$  is the stock concentration of *C. jejuni* gDNA,  $V_1$  is the volume needed to be pipetted for each dilution,  $C_2$  is the desired final concentration of gDNA per dilution, and  $V_2$  is the desired final volume of each dilution.

### 8.2.7 Preparation of Artificially Contaminated Food Samples

Chicken broth stock (Campbell) and fresh partly skimmed milk with 2% fat (Dairyland) were purchased from local grocery stores. Skim milk was made using skim milk powder (Difco). Food samples were mixed with 1 ml of appropriate dilutions

of *C. jejuni* to obtain the contamination rate of  $10^2$  to  $10^5$  cfu/ml. Artificially contaminated samples were used immediately and 1 ml of each sample was exposed to the desired amount of RBP functionalized beads. Following bacterial capture, the bead-bacteria clusters were separated from background using a magnet and the supernatant was removed. The clean bead-bacteria clusters were resuspended in 100  $\mu$ L of PBS and used in real-time PCR assays.

### 8.2.8 Coupling RBP-based Magnetic Pre-enrichment with qPCR

Total bacterial DNA of *C. jejuni* cells was extracted using a previously reported method [160, 247] which involves heating up each sample to 95 °C for 10 min. The standard curve was constructed by isolating DNA from 10-fold serial dilution of a suspension of pure *C. jejuni* cells suspended in PBS. Ten-fold serial dilutions of *C. jejuni* cells in the range of  $10$ - $10^6$  cfu/reaction were amplified in duplicates by real-time PCR. The Ct values were plotted as a function of the logarithm of known spiked *C. jejuni* cells to obtain the standard curve.

### 8.2.9 Calculation of Recovery Rate (RR) (%) and Statistical Analysis

The bacterial capture efficiency of RBP-derivatized beads was assessed by enumerating the number of captured cells using real-time PCR and subsequently calculating the recovery rate [269]. The cell number per PCR reaction for unknown samples was obtained by comparing the Ct value with a standard curve generated during the same run of PCR. The cell number per PCR reaction was multiplied by 100 to calculate the cell number per 100  $\mu$ L of unknown sample, as 1  $\mu$ L out of 100  $\mu$ L of pre-concentrated sample was used in each PCR reaction. The recovery rate (RR) was calculated using the following equation:

$$RR(\%) = 100 \times \frac{C_c}{C_0}; \quad (8.3)$$

where  $C_0$  is the initial number of cells spiked in the sample and  $C_c$  is the number of cells captured to the RBP beads.

## 8.3 Results and Discussion

### 8.3.1 Sensitivity and Linear Range of *C. jejuni* qPCR Assay

The sensitivity of primer-probe set for PCR assay was determined using the standard curves created with purified genomic DNA of culture of *C. jejuni* NCTC 11168. The standard curve spanned six orders of magnitude ranging from  $2.8 \times 10^1$  to  $2.8 \times 10^6$  genome copies per reaction and showed linearity over the entire quantification range with the slope equal to -3.49 and the R<sup>2</sup> value equal to 0.99. The efficiency of the real-time PCR assay was 93.43% with the limit of detection of 28 genome copies/PCR reaction. Figure 8.1 shows the dynamic range and sensitivity of *C. jejuni* purified DNA real-time PCR assay.

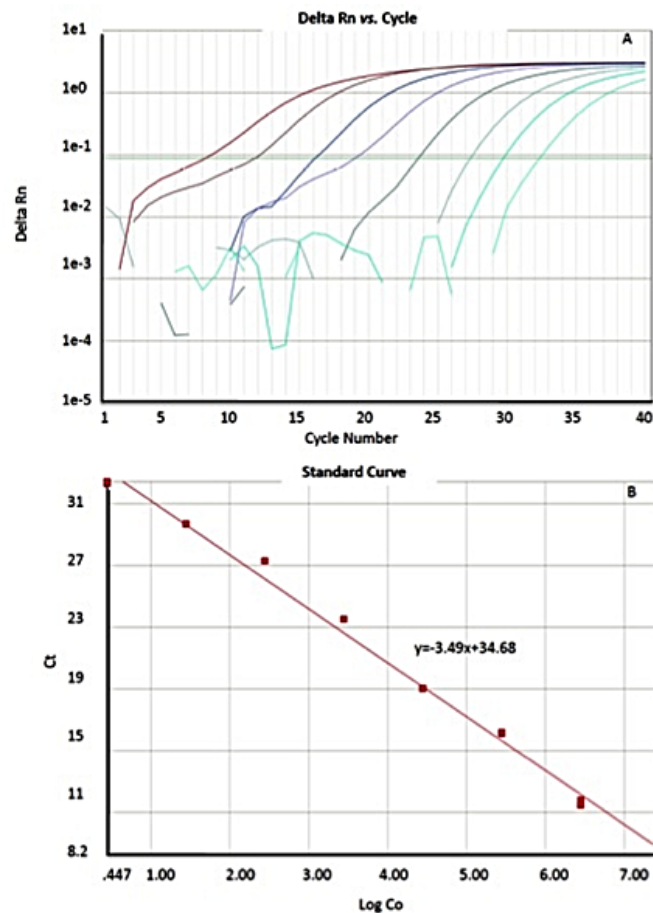


Figure 8.1: Dynamic range and sensitivity of *C. jejuni* real-time PCR assay. Standard curve for 10-fold dilution series of *C. jejuni* purified genomic DNA from  $2.8 \times 10^1$  to  $2.8 \times 10^6$  genome copies per PCR reaction. Each dot represents the results of triplicate amplification of each dilution. The slope of the regression curve is -3.66 and the coefficient of determination is  $R^2 = 0.99$  [189].

### 8.3.2 DNA Extraction from Bacteria Captured on RBP-Derivatized Magnetic Beads

Initially, we attempted to extract DNA of *C. jejuni* captured on RBP-derivatized magnetic beads using QIAamp DNA Mini Kit, Qiagen. To that end, we applied the bacteria-bead samples after magnetic separation to the QIAamp extraction and purification procedure. We quantified the extracted DNA copy number using Realtime PCR. However, comparing the efficiency of the extraction protocol for bead-bacteria samples with the clean samples of bacteria suspended in buffer with similar quantities indicated the failure of this method for bead-bacteria clusters. Results show that the DNA copy number is around zero regardless of the number of cells per sample for bead-bacteria samples. We believe this is due to the fact that beads clog the filter on the purification column and thus prevents DNA from binding to the filter membrane resulting in the failure of the entire procedure.

### 8.3.3 Capture Efficiency and Recovery Rate of RBP-Derivatized Beads

A series of experiments were carried out to study the effect of various parameters on capture efficiency and recovery rate of *C. jejuni* cells using RBP-coated magnetic beads. Skimmed milk was chosen as the food matrix in all characterization experiments. The results showed that the oriented immobilization based on GSH SAM improved the capture efficiency compared to the direct un-oriented immobilization for both types of magnetic beads (i.e. Epoxy and Tosylactivated beads) (Figure 8.2a). Both type of beads captured and recovered *C. jejuni* cells with the same level of efficiency when immobilized with receptor binding proteins in oriented fashion.

RBP-functionalized beads were able to separate and pre-concentrate more than 85% of *C. jejuni* cells from samples spiked with  $10^2$  cfu/ml. A gradual decrease in capture efficiency was observed by increasing the cell concentrations due to limiting bead binding surface capacity (Figure 8.2b). A similar trend was observed for other food samples such as milk with 2% fat and chicken broth. Table 8.5 compares the recovery rate of RBP-based magnetic separation method for isolation of *C. jejuni* cells from various food samples at different cell concentrations using  $10^8$  RBP-

immobilized beads in all experiments.

Figure 8.2c shows that increasing the number of beads improves the binding surface area and thus increases the recovery rate at higher cell concentrations. It is noteworthy that the high recovery rate is particularly important at low cell concentration to improve upon the minimum detectable level of cells by PCR. As will be discussed later, the relatively higher capture efficiency at lower cell concentrations does result in a net improvement of detection threshold of the overall assay for the matrix studied here.

Table 8.5: Efficiency of RBP magnetic separation method for the recovery of *C. jejuni* from different food samples. All experiments were performed with  $10^8$  RBP-derivatized Tosylactivated beads [189].

Cell Number [cfu/ml]	Recovery Rate %		
	Skim Milk	Milk with 2% fat	Chicken Broth
100000	15.08 ± 1.05	10.20 ± 1.2	19.42 ± 2.3
10000	36.21 ± 4.45	14.45 ± 2.21	36.53 ± 4.32
1000	54.73 ± 3.22	30.21 ± 4.53	67.81 ± 8.3
100	85.31 ± 5.1	49.9 ± 3.4	89.21 ± 6.2

### 8.3.4 Analysis of Artificially Spiked Food Samples Using RBP-based Pre-enrichment Method and qPCR

We integrated RBP magnetic separation with TaqMan PCR to reduce PCR inhibition of food compounds and to obtain a highly sensitive and specific semi-real-time assay for direct analysis of food samples. To that end, RBP-functionalized beads were used to isolate *C. jejuni* cells from different artificially contaminated food samples including skimmed milk, 2% partially skimmed milk, and chicken broth. The total genomic DNA was extracted from *C. jejuni* cells captured on beads by boiling without the need for more extensive DNA extractions and used as template for real-time PCR. The standard curve was created as described earlier to correlate the Ct value to the cell number. The standard curve showed a linear relationship ( $y = -4.65x + 37.92$ ,  $R^2 = 0.99$ ) with dynamic range of six orders of magnitude (Figure 8.3). The reaction efficiency was comparable to previous reports when boiling was used to extract DNA from whole cells [160]. Boiling, employed as a DNA extraction

method for the sake of simplicity, was considered suitable, as the sensitivity was not compromised.

The RBP-based magnetic separation method coupled with real-time PCR is able to specifically detect *C. jejuni* within 3 h at levels of  $10^2$  cfu/ml in all kinds of samples. This is two folds increase in detection sensitivity as a similar real-time PCR assay without any RBP magnetic separation failed to reliably quantify the number of cells for samples with less than  $10^4$  cfu/ml due to inhibitory effects of milk components. Figure 6a shows the Ct value versus different cell concentrations for various samples including clean sample (i.e. cells spiked in PBS buffer), milk with 2% fat, skim milk, and chicken broth. The Ct value increased for all kind of food samples compared to the clean samples suggesting the inhibition of PCR by matrix-related refractory factors. Milk with 2% fat and skim milk inhibited PCR more drastically, and caused complete failure of PCR at cell concentrations lower than  $10^4$  cfu/ml, which can be seen with the absence of data points at these concentrations (i.e.  $\leq 10^4$  cfu/ml) on Figure 8.4a. Figure 8.4b, 8.4c and 8.4d compare the Ct values vs. cell concentrations for different spiked samples without any treatment and after isolation and pre-enrichment of cells with RBP-derivatized magnetic beads.

The presence of data points at all concentration of spiked cells after pre-enrichment suggests that the RBP-based magnetic separation reduces the matrix-related inhibitory effects and allows the amplification of small number of cells, which was otherwise inhibited. It is noteworthy that this pre-enrichment method does significantly improve the Ct values at higher cell concentrations given the relatively low recovery rate accomplished at these higher concentrations (righthand data points of Fig 8.4c). This being said, overall capture efficiency improves at low cell concentration, resulting in an improvement of overall detection threshold. Indeed, as indicated by the lefthand data points of Fig 8.4c), no amplification was observed whatsoever at  $10^3$  cfu/ml and below without inclusion of this RCP-mediated pre-enrichment step. Therefore, the ability of this short pre-enrichment technique to selectively isolate and purify *C. jejuni* cells from food suspensions and improve limit of detection of qPCR assay in this specific matrix represents a proof-of-concept of the potential of phage

## 8.4 Conclusion

Real time PCR is a rapid, sensitive and specific method for quantitative analysis. However, reliability and sensitivity of this technology for food analysis is compromised due to the presence of inhibitory factors in food components. We demonstrated the potential of using an RBP-derivatized magnetic separation method as an upstream sample preparation step for real-time PCR detection of *C. jejuni* cells in skim milk, milk with 2% fat, and chicken broth. The RBP-based magnetic separation method was able to recover more than 80% of *C. jejuni* cells and in combination with real-time PCR was able to detect *C. jejuni* cells at levels of  $10^2$  cfu/ml in less than 3h. Use of *Salmonella Typhimurium* as a negative control confirmed that GST-Gp48 derivatized beads did not capture any non-specific bacteria. This method can be generalized to other food samples as well as other pathogens by using the target specific phage proteins.

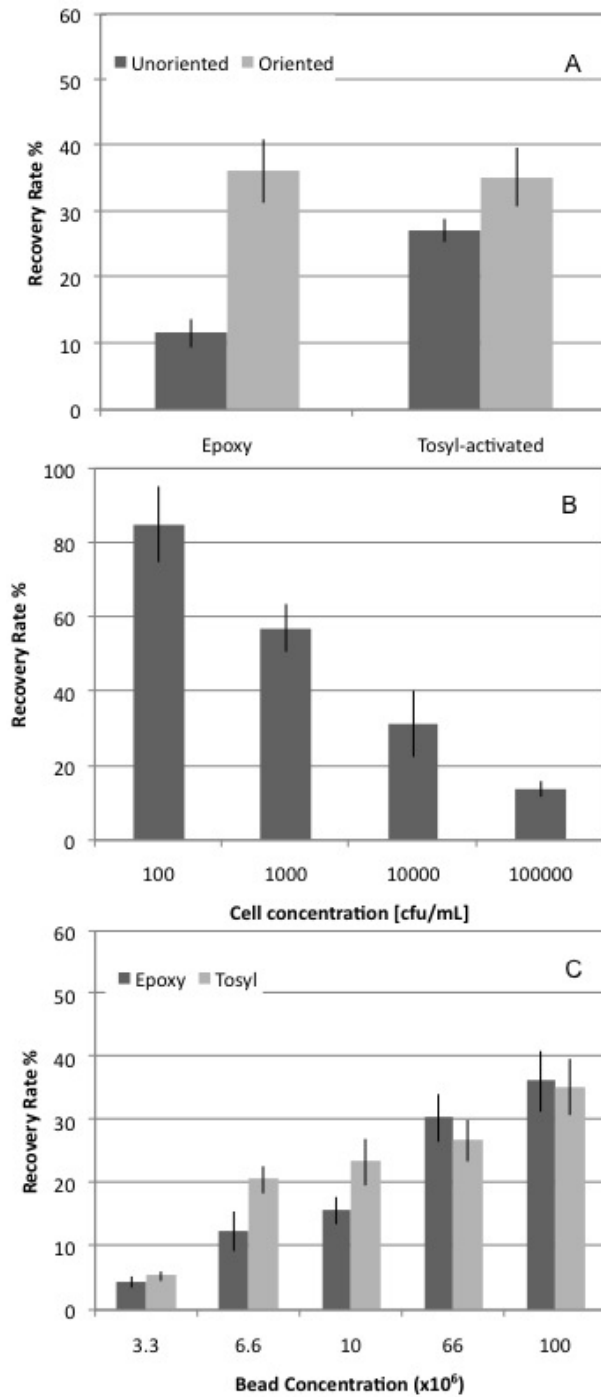


Figure 8.2: Capture efficiency of GST-Gp48 magnetic beads. (A) GSH SAM based oriented immobilization versus direct unoriented immobilization (with  $10^4$  cells,  $10^8$  beads) (B) different cell concentrations (with  $10^8$  Tosylactivated beads) (C) different concentrations of RBP-derivatized Tosylactivated beads per 1 ml assay volume containing  $10^4$  cells [189].

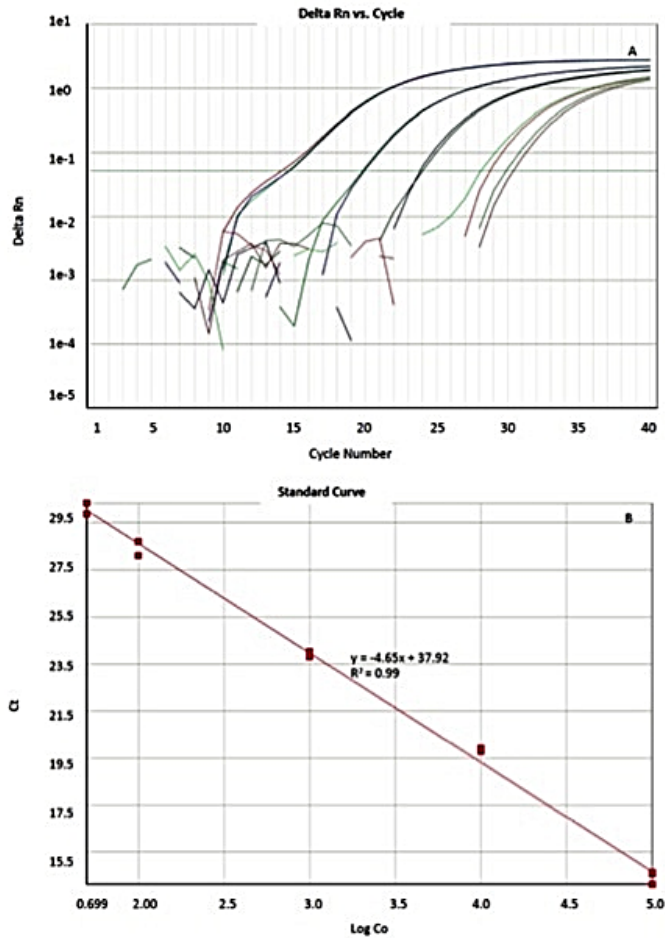


Figure 8.3: Standard curve of *C. jejuni* PCR assay. (A) Detection of 10-fold serial dilution of *C. jejuni* in PBS by the real-time TaqMan assay performed in duplicates from  $10^1$  to  $10^5$  cfu per PCR reaction. The fluorescent signal (Delta Rn) is plotted versus the cycle numbers. (B) Standard curve produced from correlation of the threshold cycle values (Ct) with the log10 of the concentration of *C. jejuni* cells in each dilution (Log C0) [189].

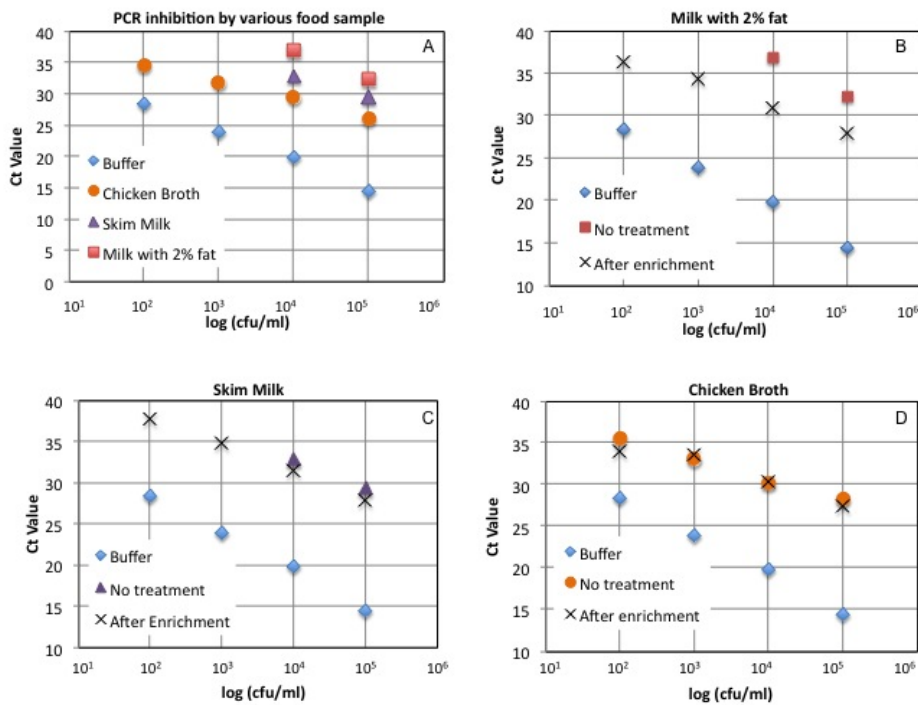


Figure 8.4: PCR on artificially contaminated food samples with/without RBP magnetic enrichment. (A) Threshold cycle value (Ct) versus *C. jejuni* cell concentration spiked in buffer, milk with 2% fat, skim milk, and chicken broth. Milk inhibits PCR resulting in higher Ct values compared to reference samples (i.e. cells spiked in buffer) at concentrations higher than 10<sup>4</sup> cfu/ml, and causes complete failure of PCR amplification at lower concentrations. Chicken broth also inhibits PCR, but has less refractory effects compared to milk. (B, C) Isolation and enrichment of *C. jejuni* cells from milk with RBP-based magnetic separation improves PCR efficiency. (D) Chicken broth has less inhibitory effect on PCR. Less significant improvement was observed after RBP-based magnetic separation [189].

## Chapter 9

# Thermal Management of a PCR Lab-on-a-Chip Device

### 9.1 Introduction

Lab-on-a-chip (LOC) devices, capable of integrating several laboratory functions in a single chip, have been the centre of attention from research community in recent years. Microfluidic devices were initially used in the development of inkjet printheads, but now they are central components of multiplex systems for various applications ranging from chemical analysis to genetic analysis and point-of-care diagnosis. We are interested in microfluidic devices capable of performing polymerase chain reaction (PCR) with the ultimate goal to integrate PCR with our TSP-based magnetic separation method onto a single chip. Polymerase chain reaction (PCR) is a powerful technique in molecular biology which amplifies small quantities of DNA to detectable levels. Typically, PCR process consists of 30-40 cycles, with each cycle consisting of three temperature steps: denaturation (92°C - 96°C), annealing (45°C - 65°C), and extension (68°C - 74°C). Thermal management is critical in adapting polymerase chain reaction into nano-scale and micro-scale lab-on-a-chip devices. The DNA amplification process throughout PCR requires precise and localized temperature control to achieve an efficient amplification. The comprehensive studies emphasize on the importance of more than  $\pm 1^\circ\text{C}$  temperature precision and

---

<sup>1</sup>All work in this chapter was performed by S. Poshtiban except for Microfluidic chip system model presented in Sec. 9.2.2. The system model was developed by R. Banaei Khosroushahi

rapid transition time for optimal amplification efficiency. Rapid thermal cycling of the reaction chamber in DNA amplification not only improves the required amplification time by an order of magnitude, but it is also important to ensure stability of biological reagents during amplification and specificity of the amplified product. Large overshoots and undershoots during transitions are undesired as they may deteriorate the replicating enzyme activity resulting in less than optimal magnitude of amplification or amplification of unspecific products. Therefore, there is a need for design and implementation of a temperature controller which provides rapid but smooth transitions between different temperature stages during PCR.

Accurate temperature control requires the measurement of the temperature inside the miniaturized reaction chamber, which is usually in the order of a few microlitres. The fundamental challenge however is the temperature measurement without perturbation. Any sensing device in direct contact with such a small volume will change the dynamics of the system affecting the DNA cycling. Moreover, implanting a sensor inside the reaction chamber increases the risk of contamination which can be detrimental to the success of DNA amplification. Therefore, it is highly desirable to estimate the temperature inside the reaction chamber based on an outside measurement in close proximity of the chamber. The dynamics of the system between the sensor and the reaction chamber must be considered when designing the temperature controller.

The PCR microfluidic chip used in this study is composed of three layers, glass-PDMS-glass; the PCR reaction chamber is etched in the top glass layer, and a thin film resistor element is patterned in the bottom layer which acts as both heater and sensor providing the only temperature measurement for the entire system. Therefore, the chamber temperature is estimated based on the heater temperature, and the heater temperature is used for thermal management of the PCR subsystem. We designed a robust observer-based state feedback controller using heater temperature as a feedback signal. Since the reaction chamber system does not respond to the temperature transients as fast as the heater system due to the physical distance between the heater and the chamber system, we optimized the feedforward trajectory for the heater temperature so that the chamber temperature follows the thermal profile as desired for a PCR reaction. We used thermochromic liquid crystal to qualitatively verify the accuracy of the temperature in the PCR reaction chamber.

## 9.2 PCR Microchip

### 9.2.1 Microfluidic Chip Structure

The PCR microfluidic chip used in this study was developed by researchers in the Applied Miniaturization Lab (AML) at the University of Alberta. Figure 9.1 shows the picture of the PCR microchip. The microchip is designed into a three layer glass/PDMS/glass structure as shown in Figure 9.2, in which the top and bottom glass layers are called flow layer and control layer, respectively. The fluidic channel and PCR reaction chamber are etched on the top glass later, and the round thin film resistive element is patterned on the bottom glass layer. The square metal plates are the contact pads. The thin film resistive element acts simultaneously as a temperature actuator and a sensor, and it provides the only information about temperature.

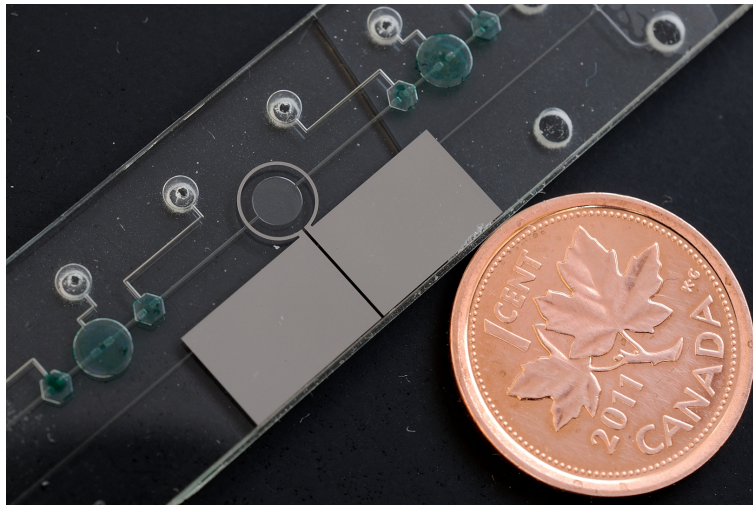


Figure 9.1: PCR microfluidic chip [21].

This design of heater simplifies fabrication and makes integration feasible by eliminating the need for the second resistive element and its accompanying electronic and instrumentation. Nevertheless, this design creates a distance between temperature sensor and PCR reaction chamber which implies two main challenges for the design of temperature controller. First, the reaction chamber temperature is predicted based on the measurements of heater temperature due to the lack of direct measurements on the chamber temperature. In addition, the chamber temperature follows the dynamics of temperature transitions with slower rate compared to the

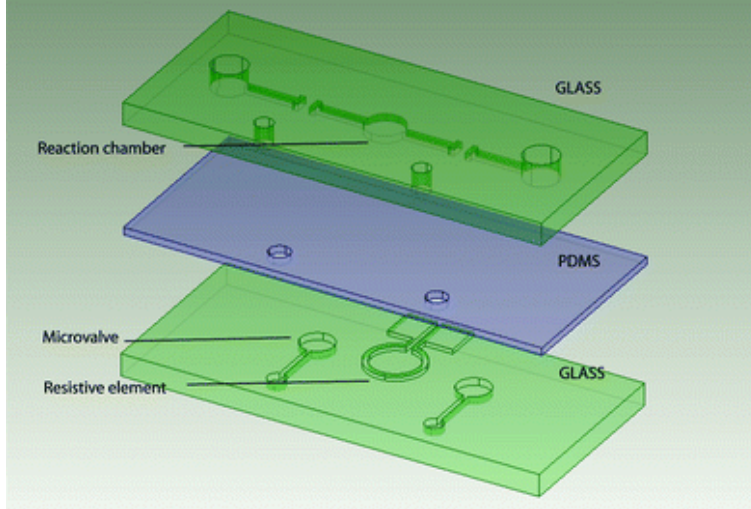


Figure 9.2: PCR microchip architecture [96].

heater temperature.

### 9.2.2 Microfluidic Chip System Model

The thermal cycler on this LOC device, consisting of a reaction chamber and heater element, can be modelled with a serial configuration of two subsystems, heater and chamber subsystems as shown on Figure 9.3. The heater temperature is controlled based on the input current and the chamber temperature is predicted based on heater temperature. The static and dynamic behaviour of the heater and chamber subsystem are identified by FEM analysis using Comsol Multiphysics [20].

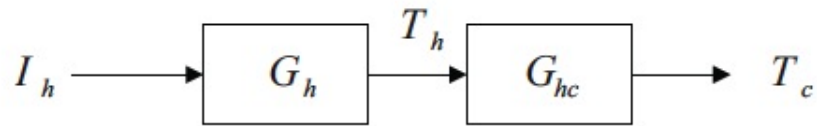


Figure 9.3: System level model of PCR lab-on-a-chip device.

#### Heater Subsystem Model

Figure 9.4 shows the block diagram of the heater subsystem. The heater subsystem is composed of a nonlinear stationary part and a minimum phase second order dynamic linear part with a stable zero as given by Equation 9.1.

$$T_h(s) = G_h(s) \cdot \mathcal{L}[f(I_h(t), T_{hs}(t))] \quad (9.1)$$

where

$$G_h(s) = \frac{2.3235(s + 0.2352)}{(s + 4.2655)(s + 0.1281)} \quad (9.2)$$

and

$$\begin{aligned} f(I_h, T_{hs}) = & 34.1326 \sinh(22.3182 I_h - 0.7540) \\ & + 0.0215 \sinh(5.6896 I_h + 0.4.1996)(T_{hs} - 22) \\ & + 22.4371 \end{aligned} \quad (9.3)$$

where  $T_h$  is the heater temperature,  $I_h$  is the heater current and  $T_{hs}$  is the heatsink temperature.

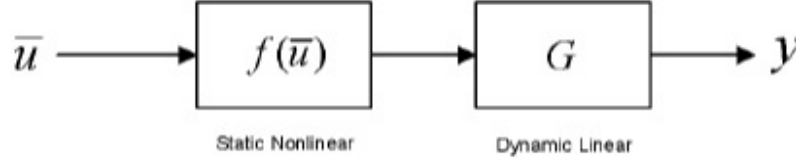


Figure 9.4: Heater subsystem, consisting of a static nonlinear subsystem followed by a linear dynamic part.

The dynamic part of the heater subsystem can be easily converted to a state-space model as shown in Figure 9.5:

$$A_h = \begin{bmatrix} 0.1281 & 0.3273 \\ 0 & -4.2655 \end{bmatrix} \quad B_h = \begin{bmatrix} 0 \\ 2 \end{bmatrix}$$

$$C_h = \begin{bmatrix} 0.3802 & 1.1618 \end{bmatrix} \quad D_h = 0$$

It is noteworthy that this state-space model does not represent the linearized heater system. The linearization of the nonlinear input function will change the value of input matrix  $B_h$ .

### Chamber Subsystem Model

The model of chamber subsystem is identified with a static part and a dynamic part as shown in Figure 9.6 and given by Equation 9.4, in which the static part is

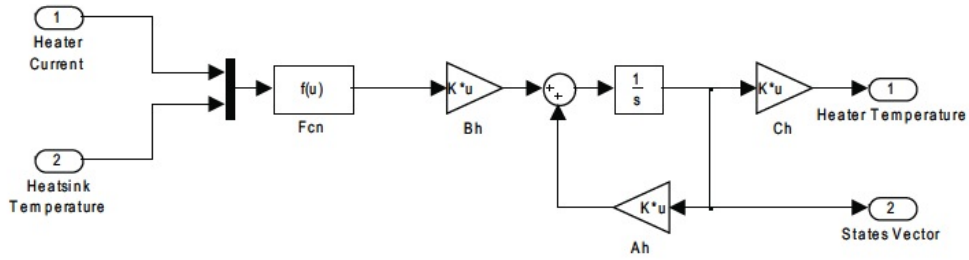


Figure 9.5: State-space representation of heater subsystem.

inherently linear.

$$T_c(s) = G_{hc}(s) \cdot \mathcal{L}[g(T_h(t), T_{hs}(t))] \quad (9.4)$$

where

$$G_{hc}(s) = \frac{-0.0902(s - 3.0314)}{(s + 0.2024)(s + 1.3514)} \quad (9.5)$$

and

$$g(T_h, T_{hs}) = 0.4704T_h + 0.5294T_{hs} - 0.0249 \quad (9.6)$$

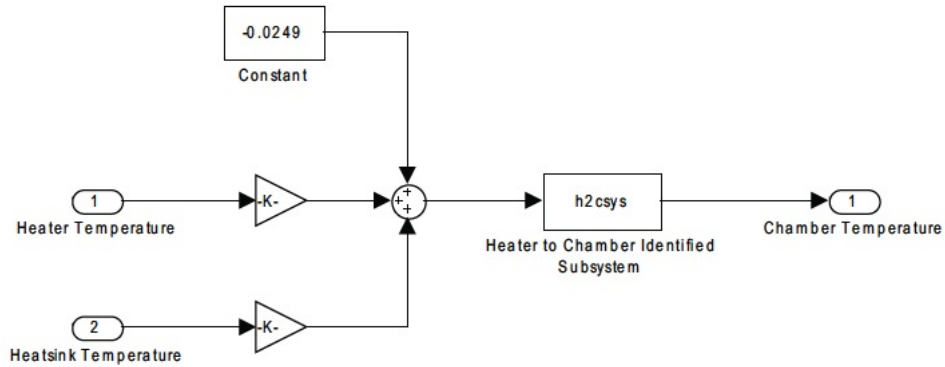


Figure 9.6: Model of chamber subsystem.

### 9.2.3 Model Linearization

The first step towards linearization of the nonlinear heater model is to find an appropriate operating point. Given that chamber temperature varies roughly from 55°C to 95 °C during PCR, the middle point of the operating range (i.e. 75°C) is chosen

Table 9.1: System parameters at the operating point

Parameter	Value	Unit
$T_{hs0}$	22	$^{\circ}\text{C}$
$T_c0$	75	$^{\circ}\text{C}$
$T_h0$	134.5412	$^{\circ}\text{C}$
$I_h0$	0.1191	A
$X_0$	$\begin{bmatrix} 161.1614 \\ 63.0834 \end{bmatrix}$	N/A

as an operating point. This chamber temperature approximately corresponds to  $134.5412^{\circ}\text{C}$  at heater. We assume the heatsink temperature is equal to the ambient temperature at  $22^{\circ}\text{C}$ . We solve Equation 9.3 to find  $I_h$  by substituting the operating point values. The state values at the operating point is calculated using the following equation:

$$X_0 = -A_h^{-1}B_hT_{h0} = \begin{bmatrix} 161.1614 \\ 63.0834 \end{bmatrix} \quad (9.7)$$

where  $A_h$  and  $B_h$  are the state and input matrixes of the dynamic part of heater subsystems. Table 9.1 lists the values for system parameters at the operating point:

Using these parameters, we linearize the function  $f(I_h, T_{hs})$  of the heater subsystem using the Taylor series expansion of first order:

$$f(I_h, T_{hs}) = f(I_{h0}, T_{hs0}) + \frac{\partial f}{\partial I_h} \Big|_{(I_{h0}, T_{hs0})} (I_h - I_{h0}) + \frac{\partial f}{\partial T_{hs}} \Big|_{(I_{h0}, T_{hs0})} (T_{hs} - T_{hs0}) + H.O.T. \quad (9.8)$$

Neglecting the H.O.T. (Higher Order Terms), we use the linear approximation instead of the nonlinear function in our controller design. Given that the DC-gain of dynamic part is equal to unity, we conclude that  $f(I_{hs}, T_{hs}) \approx T_{h0}$ . So, the Equation 9.8 can be re-written as:

$$f(I_h, T_{hs}) \approx T_{h0} + B_{h1}(I_h - I_{h0}) + B_{h2}(T_{hs} - T_{hs0}) \quad (9.9)$$

Figure 9.7 shows the block diagram of the linearized model for the heater subsystem. It is noteworthy that the input matrix for heater current input is  $B_{hs}B_h$ .

It is worth to note that the input signal, reference signal and output signal needs to be shifted properly before implementation of the liner controller on nonlinear

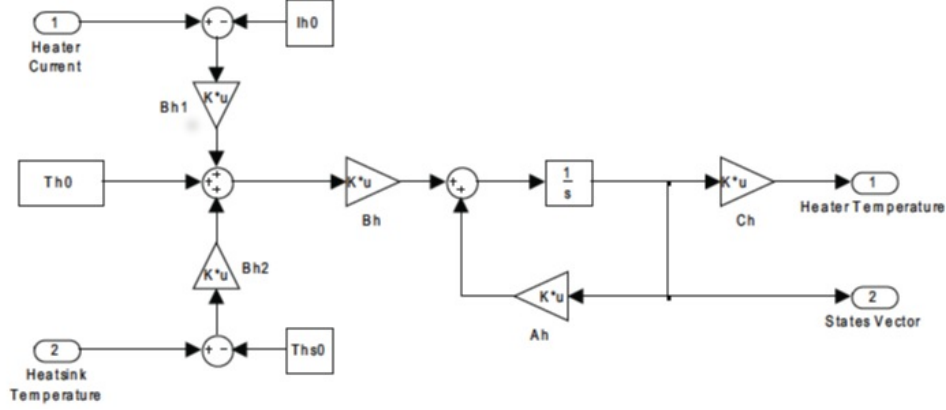


Figure 9.7: Linearized model of heater subsystem.

system. To shift the linearized model from operating point to the zero equilibrium point, we define the new input, output, and state vector as follows:

$$\tilde{X} = X - X_0 \quad (9.10)$$

$$\tilde{I}_h = I_h - I_{h0} \quad (9.11)$$

$$\tilde{T}_{hs} = T_{hs} - T_{hs0} \quad (9.12)$$

$$\tilde{T}_h = T_h - T_{h0} \quad (9.13)$$

and we re-write the system equation as follows:

$$\dot{\tilde{X}} = A_h \tilde{X} + B_{h1} B_h (\tilde{I}_h - I_{h0}) + B_{h2} B_h (\tilde{T}_{hs} - T_{hs0}) \quad (9.14)$$

$$\tilde{T}_h = C_h \tilde{X} - T_{h0} \quad (9.15)$$

### 9.3 Thermal Calibration of PCR Microfluidic Chip

The major challenge for thermal management of microfluidic chip is the lack of direct measurements of the reaction chamber temperature. Thermochromic liquid crystals are used to verify the temperature accuracy in the reaction chamber. Thermochromic liquid crystals (TLC) are compact and effective materials for monitoring temperature at the microscale by displaying different colors at different temperatures. The TLC suspension has milky white color at room temperature. The color of TLC changes successively into red, green and blue as heated. The color of TLC

returns to milky white when the temperature rises above the color change range. The spectra of TLC color are analyzed to study the chamber temperature. There are several parameters that may influence thermochromic liquid crystal measurements, including: light disturbances, illumination intensity, and film thickness. Therefore, it is necessary to provide a consistent surface preparation techniques and experimental setup to ensure repeatable performance and reliable results of TLCs.

## 9.4 Controller Design

### 9.4.1 Observability and Controllability

The controllability of system has been verified by checking the rank of the controllability matrix. Although the input matrix for the heater current is  $B_{h1}B_h$ , the controllability matrix is calculated for  $[A_h, B_h]$ . Since introducing a new gain does not change the controllability of a system, we calculated the controllability matrix as follows:

$$C = \begin{bmatrix} B_h & A_h \cdot B_h \end{bmatrix} \quad (9.16)$$

$$\rho(C) = \rho\left(\begin{pmatrix} 0 & 1711.8139 \\ 5230.724 & -22311.6534 \end{pmatrix}\right) = 2. \quad (9.17)$$

The observability of the system has also been confirmed by calculating the observability matrix as follows:

$$O = \begin{bmatrix} C_h \\ C \cdot A_h \end{bmatrix} \quad (9.18)$$

$$\rho(O) = \rho\left(\begin{pmatrix} 0.3802 & 1.1618 \\ -0.0487 & -4.831 \end{pmatrix}\right) = 2. \quad (9.19)$$

### 9.4.2 Eigenvalue Selection

The desired closed loop system eigenvalues have been selected based on performance criteria. The maximum overshoot and the settling times were chosen to be less than 10%, and less than 2 seconds, respectively. The eigenvalues were select by calculating Equation 9.20

$$M_p = exp\left(\frac{-\zeta\pi}{\sqrt{1-\zeta^2}}\right) \quad (9.20)$$

and Equation 9.21

$$t_s = \frac{4}{\omega_n\zeta}. \quad (9.21)$$

The values of  $\zeta$  and  $\omega_n$  are calculated by considering the aforementioned performance criteria. The poles are given by  $-\sigma \pm j\omega_d$ , where  $\sigma = \zeta\omega_n$  and  $\omega_d = \omega_n\sqrt{1-\zeta^2}$ . In our system, the desired eigenvalues are located at  $\lambda_1 = -2 + 2.6667j$  and  $\lambda_2 = -2 - 2.6667j$ . The observer eigenvalues are chosen to be 6 times faster than the eigenvalues of the closed loop system.

### 9.4.3 State Feedback Controller on Linearized Model

The pole placement method was used to design the state feedback controller by placing the closed loop eigenvalues in the pre-determined place in s-plane. Considering the state space model of the linearized model as:

$$\dot{x} = A_h x + B u \quad (9.22)$$

$$y = C_h x \quad (9.23)$$

where  $B = B_{h1}B_h$ , the state feedback controller was designed such that the closed loop system has the following state space model:

$$\dot{x} = (A_h - Bk)x + B u \quad (9.24)$$

$$y = C_h x \quad (9.25)$$

where  $k = [K_1 \& K_2]$ .

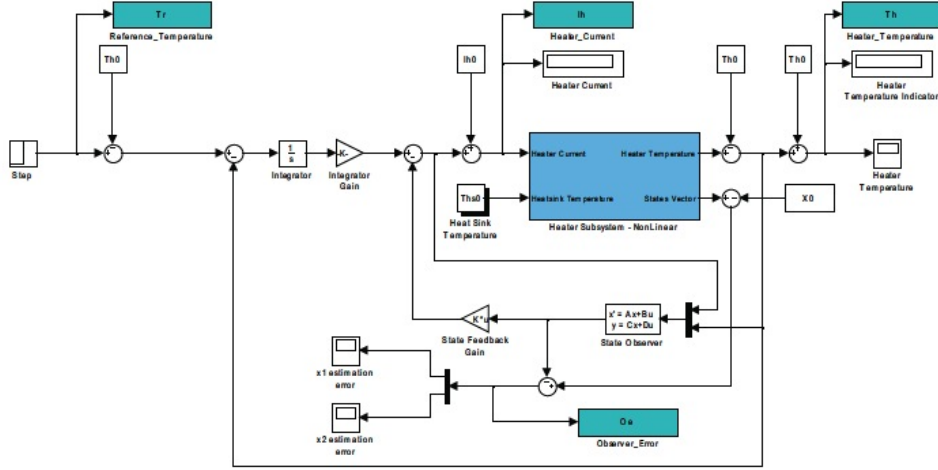


Figure 9.8: Block diagram of controller design on linearized model.

A dynamic compensator and an output feedback was employed based on the internal model principle to reject any disturbances. To that end, an integrator with the gain  $-K_i$  was inserted as a compensator to perfectly track the step signal with zero tracking error at steady state. The block diagram of the robust trajectory tracking controller designed for linearized model is shown in Figure 9.8. In this system, the main source of disturbance is the variations in heatsink temperature. Denoting any disturbance to the system with  $w$ , the state feedback equation can be modified as:

$$\dot{x} = (A_h - Bk)x + Bu + Bw \quad (9.26)$$

$$y = C_h x \quad (9.27)$$

Now, lets denote the output of integrator with  $x_i$ . Then, the system has augmented state vector  $[x \& X_i]'$ . The input to the system is:

$$R = T_r - T_{h0} \quad (9.28)$$

and the output of the system is :

$$Y = T_h - T_{h0} \quad (9.29)$$

Therefore,

$$\dot{X}_i = R - Y = R - C_h x \quad (9.30)$$

$$u = \begin{bmatrix} K & K_i \end{bmatrix} \begin{bmatrix} X \\ X_i \end{bmatrix} \quad (9.31)$$

Substituting this in Equation 9.26, it will yield into:

$$\begin{bmatrix} \dot{X} \\ \dot{X}_i \end{bmatrix} = \begin{bmatrix} A + BK & BK_i \\ -C & 0 \end{bmatrix} \begin{bmatrix} X \\ X_i \end{bmatrix} \begin{bmatrix} 0 \\ 1 \end{bmatrix} R + \begin{bmatrix} B \\ 0 \end{bmatrix} w \quad (9.32)$$

$$Y = \begin{bmatrix} C & 0 \end{bmatrix} \begin{bmatrix} X \\ X_i \end{bmatrix} \quad (9.33)$$

Since  $(A_h, B_h)$  is controllable and the  $H_h(s) = C_h(SI - A_h)^{-1}B$  has no zero at  $s = 0$ , the eigenvalues of the new matrix A in Equation 9.32 can be arbitrarily assigned by selecting the feedback gain  $[KK_i]$ . We designed the feedback gain by using the eigenvalues at  $\lambda_1 = -2 + 2.6667j$ ,  $\lambda_2 = 2 + 2.6667j$ , and  $\lambda_3 = -8$ , and calculated the gain of closed loop system as:

$$K_f = \begin{pmatrix} -0.1965 & 0.0015 & -0.0622 \end{pmatrix} \quad (9.34)$$

We also designed a state observer so that the output of system generated an estimate of the internal states. The eigenvalues of the observer are chosen 6 times faster than the eigenvalues of the closed loop system. The observer equation is given as:

$$\dot{\hat{X}} = (A_h - LC_h)\hat{X} + B_{h1}B_h\tilde{I}_h + L\tilde{I}_h \quad (9.35)$$

and the estimation error is calculated as the error between the actual state and the estimated state using the following equation:

$$e(t) = X(t) - \hat{X}(t). \quad (9.36)$$

### 9.4.4 Feedforward Compensator

The heater subsystem has a zero at  $s = -0.2352$ , therefore, a feedforward compensator was designed to cancel the effect of zero. The compensator is designed as a first order system with a pole at  $s = -0.2352$  and a unit DC gain. The block diagram of the controller with compensator is shown in Figure 9.9.

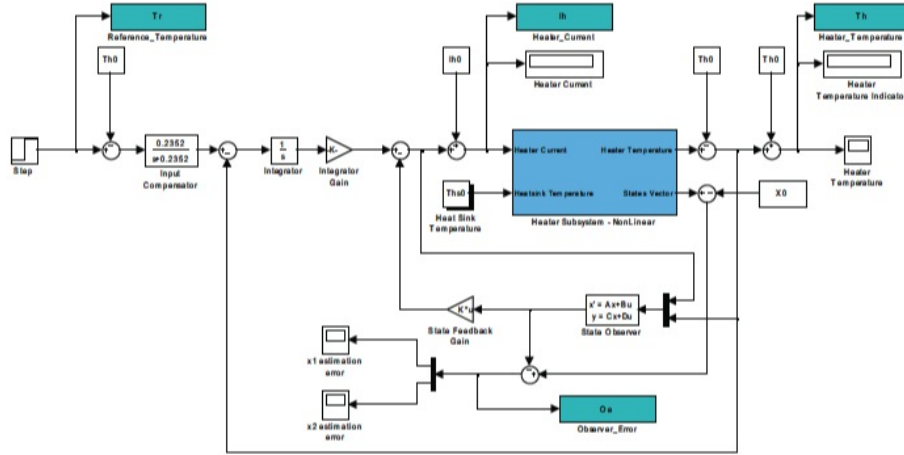


Figure 9.9: Block Diagram of controller design with feedforward compensator on linearized model.

### 9.4.5 Inverse Nonlinear Function for Nonlinear System

The state feedback controller described earlier was designed for linearized model of microchip device. Although this controller would provide the desired performance at the linearized operating points, it is expected to observe undesired performance at set points other than the linearized operating point. To overcome the effect of nonlinearity on the performance of the controller, the inverse of nonlinear function is applied in the forward path. The nonlinear function, given in Equation 9.3, has two inputs, heater current  $I_h$  and heatsink temperature  $T_{h,s}$ . Given that variations in heatsink temperature is small and the coefficient of this term is also small compared to the other terms in nonlinear heater function, the dominant source of nonlinearity is the heater current. Therefore, for the sake of simplicity, the heatsink temperature is assumed constant, and the reverse function is calculated as :



timing for the bandwidth of overshoots/undershoots are optimized considering the time constant of chamber subsystem.

## 9.5 Results and Discussion

### 9.5.1 Performance of Controller

The performance criteria for PCR microchip governs that the steady state heater temperature is regulated at 34°C, and the heater current does not exceed 500 mA. Figure 9.11a and Figure 9.11b show the tracking output of the closed loop system and the heater current for the linearized model after implementation of the controller without feedforward compensator, respectively. As seen on these graphs, the overshoot in heater temperature is more than 4 times and the transient current exceed the maximum overshoot limit reaching 800 mA. Another interesting outcome of this simulation is the large undershoot when the controller tries to track a temperature lower than its initial temperature. To be able to see this effect on the results, we deliberately dismissed the absolute function on the heater model. Therefore the negative currents can produce negative temperatures in this simulation. This performance is definitely not desirable.

So far, all the simulations were performed on the linearized model of the PCR microchip. Next, we applied the designed controller with feedforward compensator on the actual model of the microchip with includes the nonlinear part of the heater subsystem. The reference signal was set as a step function with two set points consisting of 20 s at lower than operating point at 70°C followed by 30s at the operating point (i.e. 134°C). Results show that the controller can track the trajectory as desired for the linearization operating point (i.e. 134°C). However, the undershoot increases at lower set point (Figure 9.12a, Figure 9.12b) and the observer error also increases significantly (Figure 9.12c).

The undesired overshoot is due to the presence of a zero at  $s = -0.2352$  in real heater subsystem. However, we assumed the system is a second order system consisting of two poles without any zero. A feedforward compensator was designed to cancel the effect of zero. Figure 9.13a and Figure 9.13b show the tracking output of system and the heater current after implementation of the feedforward compensator.

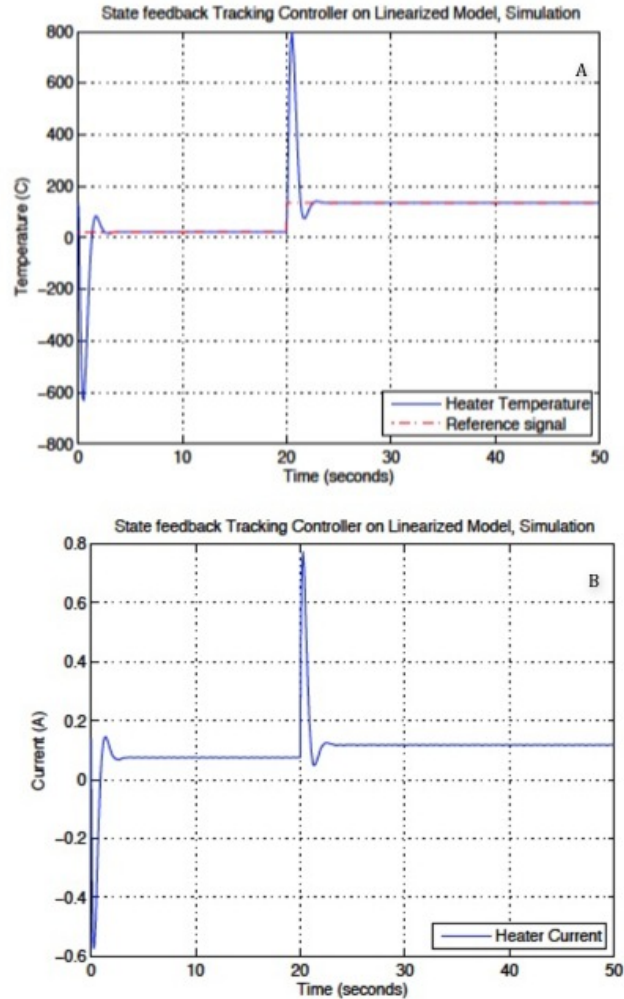


Figure 9.11: Controller performance on linearized model, (A)reference tracking results, (B) heater current.

These results show that the overshoot in the tracking output is within the acceptable range and the maximum heater current is controlled below 160 mA. Figure 9.13 C shows that the observer error is near zero suggesting that the observer can estimate the states accurately. In this simulation the ambient temperature is considered  $0^{\circ}\text{C}$  resulting in a positive current in tracking  $22^{\circ}\text{C}$ .

To overcome the effect of nonlinearity on the performance of the controller, the inverse of nonlinear function is applied in the forward path. As a result, the closed loop system can track the trajectory successfully with overshoot and undershoots within 10% of the setpoints at any temperatures shown in Figure 9.14a. Figure 9.14b shows that the maximum heater current is also limited to 140 mA which is

significantly lower than the maximum allowed range (500 mA). The observer can also estimate the states accurately for any set point with the maximum error of 0.05 (Figure 9.14c).

### 9.5.2 Discretization and Implementation

The temperature control system is a sampled-data system, thus the designed controller was discretized by ZOH with the sampling rate of 10 ms before implementation. When the sampled-data system is simulated in Matlab, a slight decrease in robustness was observed due to the sampling. Therefore, the performance criteria are modified slightly for slower response to reduce the stress on the controller. In addition, an antiwindup algorithm is obtained for the implementation on the real system to ensure that the control parameters do not exceed the given threshold. The implementation results with and without trajectory optimization module is shown in Figure 9.15. The chamber temperature profile is simulated with FEM analysis using the heater temperature profile which is recorded during the experimental thermal cycling. Using this controller, the total transition time is less than 40s and PCR amplification with 30 cycles can be performed in less than 20 min.

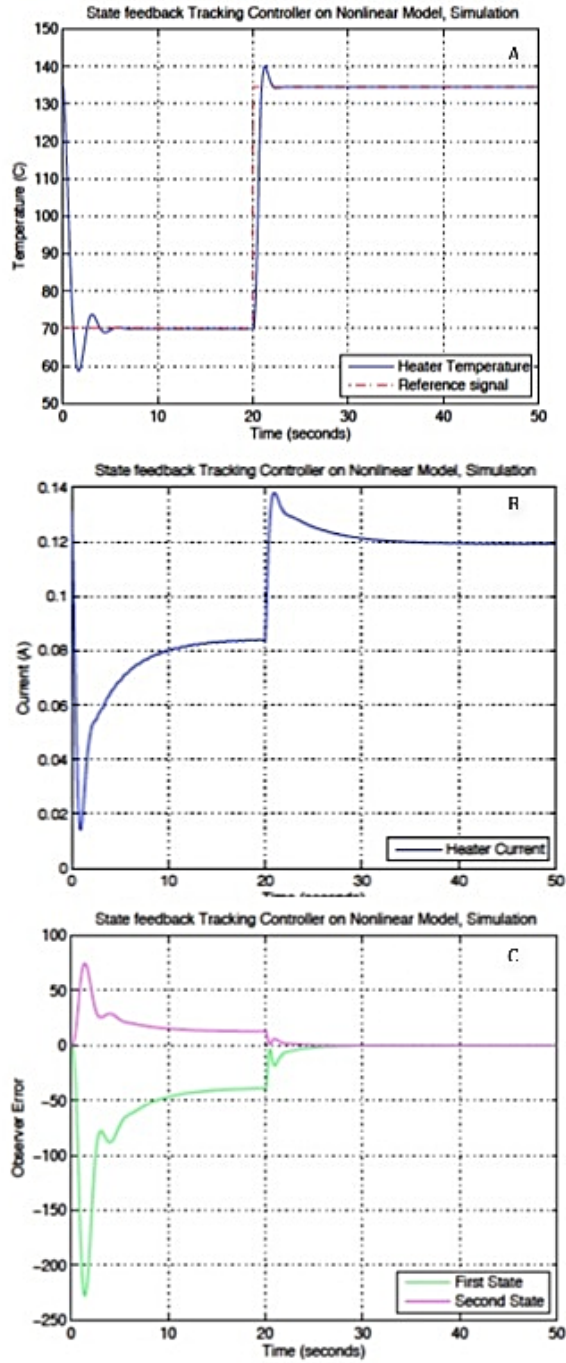


Figure 9.12: Performance of controller with feedforward compensator on heater model with the nonlinearity, (A)reference tracking, (B) heater current, (C) observer error.

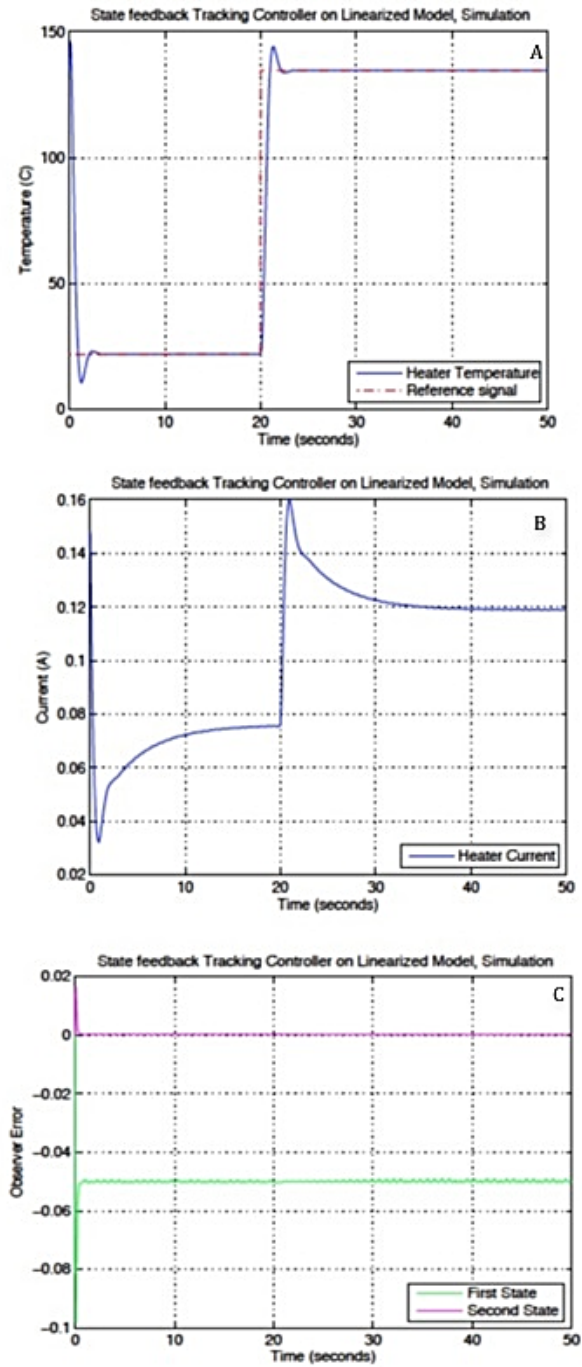


Figure 9.13: Performance of controller with feedforward compensator on the linearized model, (A) reference tracking, (B) heater current, (C) observer error.

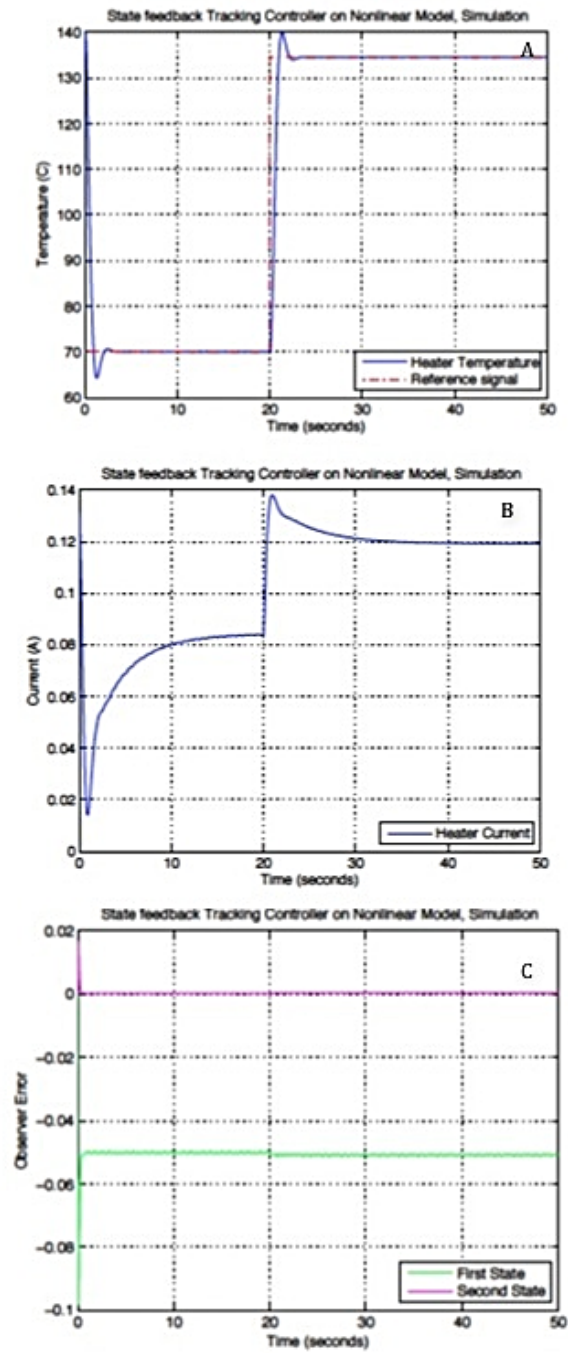


Figure 9.14: Performance of controller with nonlinear inverse function and feedforward compensator on heater model with the nonlinearity, (A)reference tracking, (B) heater current, (C) observer error.

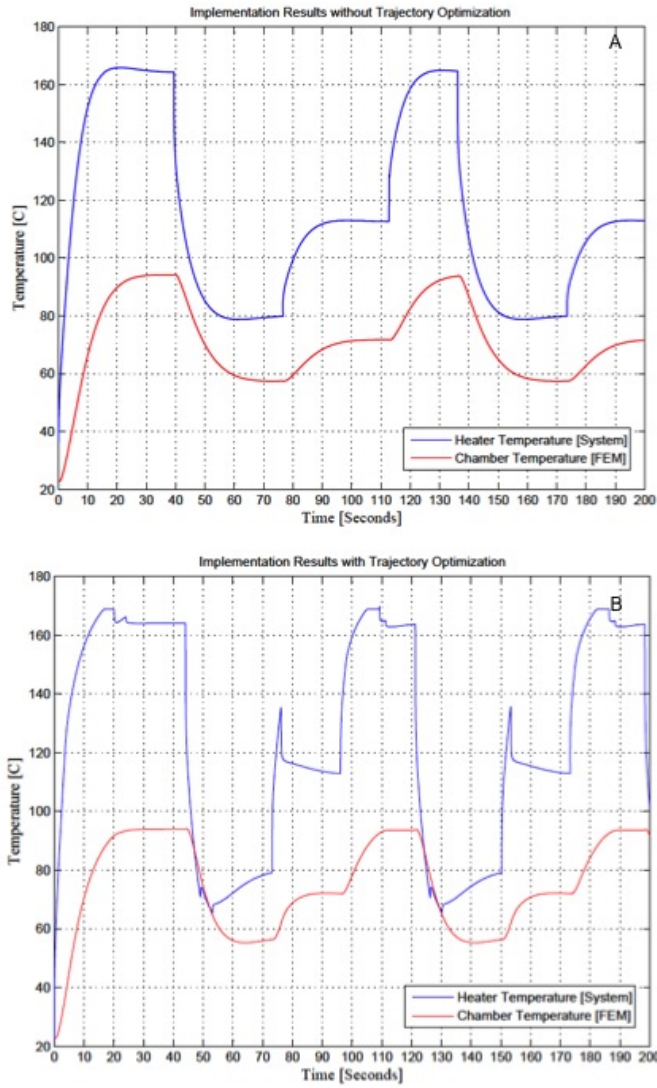


Figure 9.15: Performance of controller, (A) without trajectory optimization, (B) with trajectory optimization.

## Chapter 10

# Summary and Conclusions

### 10.1 Thesis Contribution

The work presented in this dissertation describes new phage RBP-derivatized technologies for detection of foodborne pathogenic bacteria. Despite many preventive strategies, foodborne outbreaks are still major health, financial and social concern. And the ability to directly analyze bacterial contaminations in food samples in industrial firms in realtime is the key to prevent such outbreaks. The nature of this project needed a collaborative effort to identify target specific phage, isolate and purify the appropriate phage tail spike protein, develop phage RBP immobilization protocols for functionalization of gold surfaces and magnetic particles, develop RBP-based microresonator arrays, and develop RBP-based magnetic pre-enrichment method. Hence, The key collaborator's name base been mentioned alongside each contribution (listed below), where applicable.

Contributions:

- Assessed various detection technologies to identify barriers (such as cost, stability, sensitivity, and specificity) that limit their applicability for direct analysis of food samples. The core theme of this thesis is that the sensitive diagnosis tools such as PCR exists, however, their widespread application is limited due to the matrix-related refractory factors. On the other hand, biosensors are proposed as newer detection platforms with potential advantages such as compact layout, high sensitivity and amenity for integration with other functionalities

for high throughput analysis. However, they generally lack the specificity of recognition. Although antibodies are suggested as target-specific bioreceptors, they have very short shelf time due to instabilities as a result of variations in environmental factors. We aimed to develop a microresonator-based biosensor. We propose phage RBPs as biorecognition elements to obtain specificity for detection of target bacteria. In addition, we use phage RBPs to develop a magnetic pre-enrichment method as an upstream sample preparation to overcome the limitations of PCR for detection of bacterial contaminations in food produces. We have also looked into integration of the proposed RBP-based sample pre-enrichment step with PCR on a single microfluidic chip. As a work progress, we studied the thermal management problem of microfluidic PCR chip.

- In collaboration with Dr. Szymanski's group at Biology Department at the University of Alberta, we identified phage NCTC12673 and its putative receptor binding protein, GP48, as specific element for recognition of the host bacteria *C. jejuni*. Gp48 phage RBP was isolated and purified genetically to be used for future applications.
- Developed surface functionalization methods for immobilization of phage receptor binding proteins (GP48) onto solid surfaces (i.e. magnetic particles and gold surfaces) for specific recognition and capture of bacterial cells (*C. jejuni* in this case). The capture efficiencies were assessed by microscopy techniques. The specificity of recognition was confirmed using other bacteria types as negative controls.
- In collaboration with Dr. Afzal Muhamad Javed in Dr. Szymanski's group, the host binding domain in the GP48 RBPs were localized. The capability and efficiency of various derivative of GP48 was analyzed thoroughly.
- Fully characterized a set of microresonator array for detection of pathogenic bacteria through extensive finite element modelling (FEM) analysis as well as experimental measurement. Enhanced microresonator arrays were selected for this study which were originally designed and fabricated at Micralyne Inc. for

other applications.

- Developed a phage RBP-derivatized microresonator array biosensors for detection of pathogenic bacteria. The proposed platform have been successfully employed for detection of *C. jejuni* cells.
- Developed a phage RBP-based magnetic pre-enrichment method for isolation, purification and pre-concentration of bacteria from food samples. Artificially contaminated food samples such as milk and chicken broth have been studied. The RBP-based magnetic separation method was used as an upstream sample preparation step to remove the refractory components of food samples and enhance the sensitivity of PCR for analysis of food samples.
- We looked into integration of the phage RBP-based magnetic pre-enrichment method with PCR on a single microfluidic chip. We studied a microfluidic chip that was designed and realized at the Applied Miniaturization Laboratory at the University of Alberta. This chip integrates magnetic separation module, PCR and capillary electrophoresis, thus is ideal for our proposed application. Precise and accurate temperature management in PCR reaction chamber is critical for successful DNA amplification. We designed a robust observer based state feedback controller to manage temperature in the reaction chamber.

## 10.2 Future Directions

The work presented in this dissertations opens the door for additional research into the development of phage RBP-based bacterial detection technologies. In particular, three new extensions could apply to advance the work presented in previous chapters. We have done some preliminary assessment on feasibility of the suggested extensions.

### 10.2.1 Integration of RBP-based Magnetic Separation with PCR on a Lab-on-a-Chip Device

The ultimate goal for development of advanced bacterial detection technologies is to realize in-field testing for food samples. Initial work with PCR assays coupled with RBP-based magnetic separation method in Chapter 8 showed the potential of this

technology for isolation, purification and pre-concentration of cells from complex food matrixes. The proposed method can evolve into point-of-care (POC) detection scheme by integration of the proposed sample preparation method, PCR/real time PCR, and DNA measurement method within a LOC device.

Developments in microfluidic technology enabled handling and control of fluid manipulations such as transportation, separation, and mixing in micro scale. Therefore, it paved the way for realization of lab-on-a-chip (LOC) devices that integrate various chemical and biological assays on a single chip. Microfluidic lab-on-a-chip devices offer many advantages in terms of rapid detection, cost-effectiveness, portability, and amenability for multiplexing and high-throughput analysis that make them favourable for POC applications. Integrating PCR onto microfluidic devices reduces the size of amplification reaction chamber to  $\mu\text{L}$  and  $\text{nL}$  and increases the surface to volume ratio, thus yields lower thermal capacities and a higher heat transfer rates leading to faster amplification ( 5-10 minutes) compared to the conventional PCR systems (30 min - 2h). Capillary gel electrophoresis and fluorescence detection are the most common techniques for measurement of amplified DNA products that have been integrated within microfluidic devices. Further efforts have been expanded so far as to integration of sample preparation modules along with detection methods. The common approaches for separation of cells, bacteria, viruses from clinical samples are hydrodynamic forces [102, 206, 261, 265, 270, 271], microfiltration [52, 213, 243, 256], acoustic forces [133, 262], dielectrophoretic (DEP) forces [23, 24, 70], and magnetic separators [258, 200]. Miniaturization and integration of sample preparation, amplification and detection reduces the required sample volume and processing time and paves the way for realization of POC instruments for on-site analysis of food samples.

### **10.2.2 Automated Sample Delivery System for Microresonator Array**

The proposed microresonator array in Chapter 7 offers large surface area for capture of bacteria and high mass sensitivity with threshold for detection of a single bacterial cell over the entire array. Immobilization with phage RBPs provides the specificity of recognition which is critical for development of biosensors. We have experimentally

demonstrated their successful application as bacterial detection sensor. However, the initial experiments so far has been performed in "dip and dry" format, requiring large quantity of analyte in addition to being a barrier for automated realtime analysis. Therefore, the transportation and landing of bacteria on the surface is still a practical challenge. We believe integration of this platform within a flow-through microfluidic channel may circumvent this limitation by providing an automated sample delivery setup similar to the approach proposed by [123]

# Appendix A

## Protocol for Bacteria DNA Extraction

*This appendix chapter supplements the data presented in Chapter 8.*

This protocol has been developed based on the instruction provided in QIAamp DNA Mini Kit manual (Qiagen) and has been used successfully for DNA extraction from gram-negative bacteria such as *C. jejuni* and *Salmonella* using QIAamp DNA Mini Kit (Qiagen).

### A.1 Equipments and Reagents

The following equipments are required for this protocol:

- Microcentrifuge
- vortexer
- Water bath
- Heating block
- QIAamp mini spin columns (Qiagen)
- Collection tubes (Qiagen)
- 1.5 ml microcentrifuge tubes

- Pipet tips with aerosol barrier

Reagents necessary for this protocols are listed below:

- Phosphate buffered saline (PBS)
- Ethanol (96-100%)
- Buffer AL (Qiagen)
- Buffer ATL (Qiagen)
- Buffer AW1 (Qiagen)
- Buffer AW2 (Qiagen)
- Buffer AE (Qiagen)
- Proteinase K (Qiagen)
- RNase A (100mg/ml) (Qiagen)

## A.2 Notes and Precautions

- All samples are equilibrated to room temperature before starting.
- The heating block is warmed up to 70 °C.
- The water bath is heated up to 56 °C
- All centrifugation steps are performed at room temperature.
- The sample needs to be applied to the spin column carefully without wetting the rim of the column.

## A.3 Protocol

Figure A.1 shows the procedure involved in the DNA extraction using QIAamp DNA Mini Kit. The technical details are provided in the following:

1. Pipet 1 ml of sample containing bacteria into 1.5 ml micro centrifuge tube, and centrifuge for 5 min at 7500 rpm to form a pallet. Remove the supernatant.

2. Add Buffer ATL to the pallet to the final concentration of 180  $\mu$ l.
3. Add 20  $\mu$ l proteinase K to the tube, vortex, and incubate at 56 ° for 3h to completely lyse the cells. Cortex 2-3 times per hour during incubation.
4. Add 4  $\mu$ L RNase A (100 mg/ml), vortex for 15s to mix, and incubate for 2 min at room temperature.
5. Briefly centrifuge tubes to remove drops from the lid.
6. Add 200  $\mu$ l Buffer AL, vortex for 15s, and incubate at 70 ° for 10 min.
7. Add 200  $\mu$ l ethanol (96-100% to the sample, and pulse vortex to mix. Centrifuge briefly to remove drops from inside the lid.
8. Apply the sample carefully to the QIAamp Mini spin column placed on 2 ml collection tube without wetting the rim. Centrifuge at 8,000 rpm for 1 min.
9. Place the spin column on a clean 2 ml collection tube, and discard the previous collection tube containing the filtrate.
10. Add 500  $\mu$ l Buffer AW1 to the spin column. Incubate for 5 min at room temperature. Centrifuge at 8,000 rpm for 1 min.
11. Place the spin column on a clean 2 ml collection tube, and discard the previous collection tube containing the filtrate.
12. Add 500  $\mu$ l Buffer AW2 to the spin column. Incubate for 5 min at room temperature. Centrifuge at full speed (14,000rpm) for 3 min.
13. Place the spin column on a clean 2 ml collection tube, and discard the previous collection tube containing the filtrate.
14. Repeat step 12 and step 13.
15. Centrifuge at full speed (14,000rpm) for 1 min.
16. Place the spin column on a clean 1.5 ml microcentrifuge tube, and discard the collection tube containing the filtrate.

17. Add 50  $\mu$ l Buffer AE to spin column. Incubate for 5 min. Centrifuge at 8,000 rpm for 1 min.
18. Repeat step 17.
19. Aliquote Extracted DNA to the desired amount and store them at -20 °C.

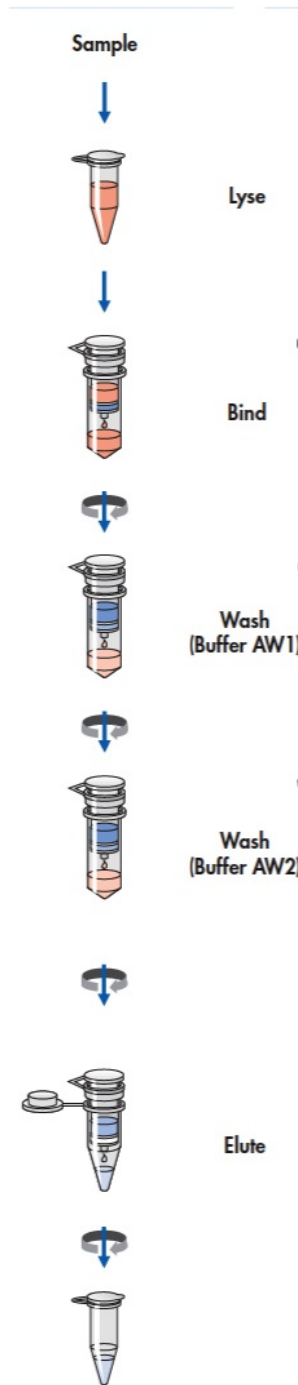


Figure A.1: Spin column procedure for DNA extraction [193].

# Bibliography

- [1] US 5,311,360. *United States Patent*, 1994.
- [2] Advances in biosensors for detection of pathogens in food and water. *Enzyme and Microbial Technology*, 32(1):3–13, 2003.
- [3] US 6,661,561 B2. *United States Patent*, 2003.
- [4] Antibody-based sensors: principles, problems and potential for detection of pathogens and associated toxins. *Sensors*, 9(6):4407–4445, 2009.
- [5] Applied Biosystems 7300/7500/7500 fast Real-time PCR System, Absolute Quantification using Standard Curve. Technical report, Applied Biosystems, 2010.
- [6] Applied Biosystems 7500/7500 fast Real-time PCR System, Standard Curve Experiment. Technical report, Applied Biosystems, 2010.
- [7] CDC estimate of foodborne illness in the united states. Technical report, Centers for Disease Control and Prevention, 2011.
- [8] Dynabeads® M-270 Epoxy. Technical report, invitrogen by Life Technologies, 2013.
- [9] Dynabeads® M-280 Tosylactivated. Technical report, invitrogen by Life Technologies, 2013.
- [10] *Campylobacter jejuni* subsp. *jejuni* NCTC 11168 = ATCC 700819, August 2013.

- [11] I. Abdel-Hamid, D. Ivnitiski, P. Atanasov, and E. Wilkins. Flow-through immunofiltration assay system for rapid detection of *E. coli* O157: H7. *Biosensors and Bioelectronics*, 14(3):309–316, 1999.
- [12] K. AbuRabeah, A. Ashkenazi, D. Atias, L. Amir, and R. Marks. Highly sensitive amperometric immunosensor for the detection of *Escherichia coli*. *Biosensors and Bioelectronics*, 24(12):3461–3466, 2009.
- [13] C. Aldus, A. Van Amerongen, R. Ariens, M. Peck, J. Wichers, and G. Wyatt. Principles of some novel rapid dipstick methods for detection and characterization of verotoxigenic *Escherichia coli*. *Journal of Applied Microbiology*, 95(2):380–389, 2003.
- [14] G. Amagliani, E. Omiccioli, A. Campo, I. Bruce, G. Brandi, and M. Magnani. Development of a magnetic capture hybridization-PCR assay for *Listeria monocytogenes* direct detection in milk samples. *Journal of Applied Microbiology*, 100(2):375–383, 2006.
- [15] H. Anany, W. Chen, R. Pelton, and M. W. Griffiths. Biocontrol of *Listeria monocytogenes* and *Escherichia coli* O157:H7 in meat by using phages immobilized on modified cellulose membranes. *Applied and Environmental Microbiology*, (77):6379–6387, 2011.
- [16] S. Artault, J. Blind, J. Delaval, Y. Dureuil, and N. Gaillard. Detecting *Listeria monocytogenes* in food. *International Food Hygiene*, 12(3):23, 2001.
- [17] S. K. Arya, A. Singh, R. Naidoo, P. Wu, M. T. McDermott, and S. Evoy. Chemically immobilized T4-bacteriophage for specific *Escherichia coli* detection using surface plasmon resonance. *Analyst*, 136(3):486–492, 2011.
- [18] H. Ayçiçek, H. Aydoğan, A. Küçükkaaslan, M. Baysallar, and A. C. Başustaoğlu. Assessment of the bacterial contamination on hands of hospital food handlers. *Food Control*, 15(4):253–259, 2004.
- [19] S. Balasubramanian, B. Sorokulova, V. J. Vodyanoy, and A. L. Simonian. Lytic phage as a specific and selective probe for detection of *Staphylococcus*

- aureus* - a surface plasmon resonance spectroscopic study. *Biosensors and Bioelectronics*, 2007.
- [20] R. Banaei Khosroushahi. Identifiacion of LOC system based on FEM Analysis, Private Communication. August 2008.
- [21] R. Banaei Khosroushahi. *PDE backstepping boundary observer design with application to thermal management of PCR process in Lab-on-a-Chip device*. PhD thesis, University of Alberta, Edmonton, Alberta, September 2013.
- [22] S. Barbirz, M. Becker, A. Freiberg, and R. Seckler. Phage Tailspike Proteins with  $\beta$ -Solenoid Fold as Thermostable Carbohydrate Binding Materials. *Macromoleculuar bioscience*, 9(2):169–173, 2009.
- [23] I. Barbulovic-Nad, X. Xuan, J. S. Lee, and D. Li. DC-dielectrophoretic separation of microparticles using an oil droplet obstacle. *Lab on a Chip*, 6(2):274–279, 2006.
- [24] L. M. Barrett, A. J. Skulan, A. K. Singh, E. B. Cummings, and G. J. Fiechtner. Dielectrophoretic manipulation of particles and cells using insulating ridges in faceted prism microchannels. *Analytical Chemistry*, 77(21):6798–6804, 2005.
- [25] P. Belgrader, W. Benett, D. Hadley, J. Richards, P. Stratton, R. Mariella Jr, and F. Milanovich. PCR detection of bacteria in seven minutes. *Science(Washington)*, 284(5413):449–450, 1999.
- [26] A. Bennett, F. Davids, S. Vlahodimou, J. Banks, and R. Betts. The use of bacteriophage-based systems for the separation and concentration of *Salmonella*. *Journal of Applied Microbiology*, 83(2):259–265, 1997.
- [27] A. Bennett, D. Greenwood, C. Tennant, J. Banks, and R. Betts. Rapid and definitive detection of *Salmonella* in foods by PCR. *Letters in Applied Microbiology*, 26(6):437–441, 1998.
- [28] A. R. Bennett, F. G. C. Davids, S. Vlahodimou, J. G. Banks, and R. P. Betts. The use of bacteriophage-based systems for the separation and concentration of *Salmonella*. *Journal of Applied Microbiology*, 83:259–265, 1997.

- [29] E. Berkenpas, P. Millard, and M. Pereira da Cunha. Detection of *Escherichia coli* O157: H7 with langasite pure shear horizontal surface acoustic wave sensors. *Biosensors and Bioelectronics*, 21(12):2255–2262, 2006.
- [30] E. L. Best, E. J. Powell, C. Swift, K. A. Grant, and J. A. Frost. Applicability of a rapid duplex real-time PCR assay for speciation of *Campylobacter jejuni* and *Campylobacter coli* directly from culture plates. *FEMS Microbiology Letters*, 229(2):237–241, 2003.
- [31] M. Birce and M. W. Griffiths. Combination of immunomagnetic separation with real-time PCR for rapid detection of *Salmonella* in milk, ground beef, and alfalfa sprouts. *Journal of Food Protection*®, 68(3):557–561, 2005.
- [32] R. M. Blasco, M. F. Sanders, and D. J. Squirrell. Specific assays for bacteria using phage mediated release of adenylate kinase. *Journal of Applied Microbiology*, 84:661–666, 1998.
- [33] G. Bonner and A. M. Klibanov. Structural stability of DNA in nonaqueous solvents. *Biotechnology and Bioengineering*, 68(3):339–344, 2000.
- [34] J. Boratynski, D. Syper, B. Weber-Dabrowska, M. Lusiak-Szelachowska, G. Pozniak, and A. Gorski. Preparation of endotoxin-free bacteriophages. *Cellular and Molecular Biology Letters*, 9:253–259, 2004.
- [35] B. Borck, H. Stryhn, A. Ersbøll, and K. Pedersen. Thermophilic *Campylobacter* spp. in turkey samples: evaluation of two automated enzyme immunoassays and conventional microbiological techniques. *Journal of Applied Microbiology*, 92(3):574–582, 2002.
- [36] J. L. Brooks, B. Mirhabibollahi, and R. Kroll. Experimental enzyme-linked amperometric immunosensors for the detection of *Salmonellas* in foods. *Journal of Applied Microbiology*, 73(3):189–196, 1992.
- [37] K. Brorson, H. Shen, S. Lute, J. S. Perez, and D. D. Frey. Characterization and purification of bacteriophages using chromatofocusing. *Journal of CHROMATOGRAPHY A*, 1207:110–121, 2008.

- [38] T. P. Burg, M. Godin, S. M. Knudsen, W. Shen, G. Carlson, J. S. Foster, K. Babcock, and S. R. Manalis. Weighing of biomolecules, single cells and single nanoparticles in fluid. *Nature*, 446(7139):1066–1069, 2007.
- [39] R. Cademartiri, H. Anany, I. Gross, R. Bhayani, M. Griffiths, and M. A. Brook. Immobilization of bacteriophages on modified silica particles. *Biomaterials*, 31:1904–1910, 2010.
- [40] H. Y. Cai, P. Bell-Rogers, L. Parker, and J. F. Prescott. Development of a real-time PCR for detection of mycoplasma bovis in bovine milk and lung samples. *Journal of Veterinary Diagnostic Investigation*, 17(6):537–545, 2005.
- [41] G. A. Campbell and R. Mutharasan. Detection of pathogen *Escherichia coli* O157: H7 using self-excited PZT-glass microcantilevers. *Biosensors and Bioelectronics*, 21(3):462–473, 2005.
- [42] G. A. Campbell and R. Mutharasan. A method of measuring *Escherichia coli* O157:H7 at 1 Cell/mL in 1 liter sample using antibody functionalized piezoelectric-excited millimeter-sized cantilever sensor. *Environmental Science and Technology*, 41:1688–1674, 2007.
- [43] S. Casjens and I. Molineux. Short noncontractile tail machines: adsorption and DNA delivery by podoviruses. In *Viral Molecular Machines*, pages 143–179. Springer, 2012.
- [44] CBCnews. Bad beef lawsuit against XL foods expands.
- [45] P. Chapman and R. Ashton. An evaluation of rapid methods for detecting *Escherichia coli* O157 on beef carcasses. *International Journal of Food Microbiology*, 87(3):279–285, 2003.
- [46] Y. Che, Y. Li, and M. Slavik. Detection of *Campylobacter jejuni* in poultry samples using an enzyme-linked immunoassay coupled with an enzyme electrode. *Biosensors and Bioelectronics*, 16(9):791–797, 2001.
- [47] C. Chen and R. A. Durst. Simultaneous detection of *Escherichia coli* O157: H7, *Salmonella spp.* and *Listeria monocytogenes* with an array-based im-

- munosorbent assay using universal protein G-liposomal nanovesicles. *Talanta*, 69(1):232–238, 2006.
- [48] G. Y. Chen, T. Thundat, E. A. Wachter, and R. J. Warmack. Adsorption-induced surface stress and its effects on resonance frequency of microcantilevers. *Journal of Applied Physics*, 77(8):3618–3622, 1995.
- [49] Y. Chen and S. J. Knabel. Multiplex PCR for simultaneous detection of bacteria of the genus *Listeria*, *Listeria monocytogenes*, and major serotypes and epidemic clones of *L. monocytogenes*. *Applied and Environmental Microbiology*, 73(19):6299–6304, 2007.
- [50] Z. Chen, M. Mauk, J. Wang, W. Abrams, P. Corstjens, R. Niedbala, D. Malamud, and H. Bau. A microfluidic system for saliva-based detection of infectious diseases. *Annals of the New York Academy of Sciences*, 1098(1):429–436, 2007.
- [51] K. Cheong, D. Yi, J. Lee, J. Park, M. Kim, J. Edel, and C. Ko. Gold nanoparticles for one step dna extraction and real-time PCR of pathogens in a single chamber. *Lab on a Chip*, 8(5):810–813, 2008.
- [52] S. Choi, S. Song, C. Choi, and J.-K. Park. Continuous blood cell separation by hydrophoretic filtration. *Lab on a Chip*, 7(11):1532–1538, 2007.
- [53] M. Chopin, A. Chopin, and E. Bidnenko. Phage abortive infection in lactococci: Variations on a theme. *Current Opinion in Microbiology.*, 8:473–479, 2005.
- [54] L. Crocia, E. Delibatoa, G. Volpeb, and G. Palleschic. A rapid electrochemical ELISA for the detection of *salmonella* in meat sample. *Analytical Letters*, 34(15):2597–2607, 2001.
- [55] M. A. Cullison and L. Jaykus. Magnetized carbonyl iron and insoluble zirconium hydroxide mixture facilitates bacterial concentration and separation from non-fat dry milk. *Journal of Food Protection*, 65(11):1806, 2002.
- [56] B. E. de Ávila, M. Pedrero, S. Campuzano, V. Escamilla-Gómez, and J. M. Pingarrón. Sensitive and rapid amperometric magnetoimmunosensor for the

- determination of *Staphylococcus aureus*. *Analytical and Bioanalytical Chemistry*, 403(4):917–925, 2012.
- [57] E. de Boer and R. R. Beumer. Methodology for detection and typing of food-borne microorganisms. *International Journal of Food Microbiology*, 50(1):119–130, 1999.
- [58] S. Dohn, R. Sandberg, W. Svendsen, and A. Boisen. Enhanced functionality of cantilever based mass sensors using higher modes. *Applied Physics Letters*, 86:233501, 2005.
- [59] H. Dwivedi and L. Jaykus. Detection of pathogens in foods: the current state-of-the-art and future directions. *Critical Reviews in Microbiology*, 37(1):40–63, 2011.
- [60] C. J. Easley, J. M. Karlinsey, J. M. Bienvenue, L. A. Legendre, M. G. Roper, S. H. Feldman, M. A. Hughes, E. L. Hewlett, T. J. Merkel, J. P. Ferrance, et al. A fully integrated microfluidic genetic analysis system with sample-in-answer-out capability. *Proceedings of the National Academy of Sciences*, 103(51):19272–19277, 2006.
- [61] R. Edgar, M. McKinstry, J. Hwang, A. B. Oppenheim, R. A. Fekete, G. Giulian, C. Merrill, K. Nagashima, and S. Adhya. High-sensitivity bacterial detection using biotin-tagged phage and quantum-dot nanocomplexes. *Proceedings of the National Academy of Sciences*, 103:4841–4845, 2006.
- [62] K. Ekinci, Y. T. Yang, and M. L. Roukes. Ultimate limits to inertial mass sensing based upon nanoelectromechanical systems. *Applied Physics*, 95(5), March 2004.
- [63] S. J. Favrin, S. A. Jassim, and M. W. Griffiths. Application of a novel immunomagnetic separation–bacteriophage assay for the detection of *Salmonella enteritidis* and *Escherichia coli* O157:H7 in food. *International Journal of Food Microbiology*, 85:63–71, 2003.

- [64] C. Fermér and E. O. Engvall. Specific PCR identification and differentiation of the thermophilic *campylobacters*, *Campylobacter jejuni*, *C. coli*, *C. lari*, and *C. upsaliensis*. *Journal of Clinical Microbiology*, 37(10):3370–3373, 1999.
- [65] A. Fluit, R. Torensma, M. Visser, C. Aarsman, M. Poppelier, B. Keller, P. Klapwijk, and J. Verhoef. Detection of *Listeria monocytogenes* in cheese with the magnetic immuno-polymerase chain reaction assay. *Applied and environmental microbiology*, 59(5):1289–1293, 1993.
- [66] M. Fricker, U. Messelhäußer, U. Busch, S. Scherer, and M. Ehling-Schulz. Diagnostic real-time PCR assays for the detection of emetic bacillus cereus strains in foods and recent food-borne outbreaks. *Applied and Environmental Microbiology*, 73(6):1892–1898, 2007.
- [67] Z. Fu, S. Rogelj, and T. L. Kieft. Rapid detection of *Escherichia coli* O157:H7 by immunomagnetic separation and real-time PCR. *International Journal of Food Microbiology*, 99(1):47–57, 2005.
- [68] H. Fukushima, Y. Tsunomori, and R. Seki. Duplex real-time SYBR green PCR assays for detection of 17 species of food-or waterborne pathogens in stools. *Journal of Clinical Microbiology*, 41(11):5134–5146, 2003.
- [69] V. I. Furdui and D. J. Harrison. Immunomagnetic T cell capture from blood for PCR analysis using microfluidic systems. *Lab on a Chip*, 4(6):614–618, 2004.
- [70] P. Gascoyne, Y. Huang, R. Pethig, J. Vykoukal, and F. Becker. Dielectrophoretic separation of mammalian cells studied by computerized image analysis. *Measurement Science and Technology*, 3(5):439, 1992.
- [71] T. Geng, B. Hahm, and A. Bhunia. Selective enrichment media affect the antibody-based detection of stress-exposed listeria monocytogenes due to differential expression of antibody-reactive antigens identified by protein sequencing. *Journal of Food Protection®*, 69(8):1879–1886, 2006.

- [72] A. Germini, A. Masola, P. Carnevali, and R. Marchelli. Simultaneous detection of *Escherichia coli* O175: H7, *Salmonella spp.*, and *Listeria monocytogenes* by multiplex PCR. *Food Control*, 20(8):733–738, 2009.
- [73] L. Gervais, M. Gel, B. Allain, M. Tolba, L. Brovko, M. Zourob, R. Mandeville, M. Griffiths, and S. Evoy. Immobilization of biotinylated bacteriophages on biosensor surfaces. *Sensors and Actuators B*, 125:615–621, 2007.
- [74] K. Y. Gfeller, N. Nugaeva, and M. Hegner. Rapid biosensor for detection of antibiotic-selective growth of *Escherichia coli*. *Applied and Environmental Microbiology*, 71:2626–2631, 2005.
- [75] E. R. Goldman, G. P. Anderson, J. L. Liu, J. B. Delehanty, L. J. Sherwood, L. E. Osborn, L. B. Cummins, and A. Hayhurst. Facile generation of heat-stable antiviral and antitoxin single domain antibodies from a semisynthetic llama library. *Analytical Chemistry*, 78(24):8245–8255, 2006.
- [76] E. R. Goldman, M. P. Pazirandeh, J. M. Mauro, K. D. King, J. C. Frey, and G. P. Anderson. Phage-displayed peptides as biosensor reagents. *Journal of Molecular Recognition*, 13(6), 2000.
- [77] L. Golshahi, K. H. Lynch, J. J. Dennis, and W. H. Finlay. In vitro lung delivery of bacteriophages KS4-M and PhiKZ using dry powder inhalers for treatment of *Burkholderia cepacia* complex and *Pseudomonas aeruginosa* infections in cystic fibrosis. *Journal of Applied Microbiology*, 110:106–117, 2011.
- [78] L. Goodridge, J. Chen, and M. Griffiths. Development and characterization of a fluorescent-bacteriophage assay for detection of *Escherichia coli* O157:E7. *Applied and Environmental Microbiology*, 65(4):1397–1404, 1999.
- [79] L. Goodridge, J. Chen, and M. Griffiths. The use of a fluorescent bacteriophage assay for detection of *Escherichia coli* O157:H7 in inoculated ground beef and raw milk. *International Journal of Food Microbiology*, 47(1-2):43–50, 1999.
- [80] A. M. Gronowski, S. Copper, D. Baorto, and P. R. Murray. Reproducibility problems with the Abbott Laboratories LCx assay for *Chlamydia trachomatis*

- and *Neisseria gonorrhoeae*. *Journal of Clinical Microbiology*, 38(6):2416–2418, 2000.
- [81] H. Gu, K. Xu, C. Xu, and B. Xu. Biofunctional magnetic nanoparticles for protein separation and pathogen detection. *Chemical Communications*, 9:941–949, 2006.
- [82] A. Gupta, D. Akin, and R. Bashir. Detection of bacterial cells and antibodies using surface micromachined thin silicon cantilever resonators. *Journal of Vacuum Science and Technology B*, 22:2785–2791, 2004.
- [83] C. Guthy, R. M. Das, B. Drobot, and S. Evoy. Resonant characteristics of ultranarrow SiCN f nanomechanical resonators. *Journal of Applied Physics*, 108:014306, 2010.
- [84] B.-K. Hahm and A. Bhunia. Effect of environmental stresses on antibody-based detection of *Escherichia coli* O157: H7, *Salmonella enterica* serotype *Enteritidis* and *Listeria monocytogenes*. *Journal of Applied Microbiology*, 100(5):1017–1027, 2006.
- [85] C. Hamers-Casterman, T. Atarhouch, S. Muyldermans, G. Robinson, C. Hammers, E. B. Songa, N. Bendahman, and R. Hammers. Naturally occurring antibodies devoid of light chains. *Nature*, 363(6428):446–448, 1993.
- [86] K.-H. Han and A. B. Frazier. Lateral-driven continuous dielectrophoretic microseparators for blood cells suspended in a highly conductive medium. *Lab on a Chip*, 8(7):1079–1086, 2008.
- [87] H. Handa, S. Gurczynski, M. P. Jackson, G. Auner, and G. Mao. Recognition of *Salmonella Typhimurium* by immobilized phage P22 monolayers. *Surface Science*, 602(7):1392–1400, 2008.
- [88] H. Handa, S. Gurczynski, M. P. Jackson, and G. Mao. Immobilization and molecular interactions between bacteriophage and lipopolysaccharide bilayers. *Langmuir*, 26(14):12095–103, 2010.

- [89] D. Harvey, C. Harrington, M. W. Heuzenroeder, and C. Murray. Lysogenic phage in *Salmonella enterica serovar heidelberg* (*Salmonella Heidelberg*): Implications for organism tracing. *FEMS Microbiol. Lett*, 108:291–295, 1993.
- [90] I. Hein, G. Flekna, M. Krassnig, and M. Wagner. Real-time PCR for the detection of *Salmonella* spp. in food: An alternative approach to a conventional PCR system suggested by the FOOD-PCR project. *Journal of Microbiological Methods*, 66(3):538–547, 2006.
- [91] I. Hein, D. Klein, A. Lehner, A. Bubert, E. Brandl, and M. Wagner. Detection and quantification of the *iap* gene of *Listeria monocytogenes* and *Listeria innocua* by a new real-time quantitative PCR assay. *Research in microbiology*, 152(1):37–46, 2001.
- [92] K. P. Hennes, C. A. Suttle, and A. M. Chan. Fluorescently labeled virus probes show that natural virus populations can control the structure of marine microbial communities. *Applied and Environmental Microbiology*, 61(10):3623–3627, 1995.
- [93] K. Hermes and A. Curtis. Direct counts of viruses in natural waters and laboratory cultures by epifluorescence microscopy. *Limnology and Oceanography*, 40(6):1050–1055, 1995.
- [94] R. Hernández, C. Vallés, A. M. Benito, W. K. Maser, F. Xavier Rius, and J. Riu. Graphene-based potentiometric biosensor for the immediate detection of living bacteria. *Biosensors and Bioelectronics*, 54:553–557, 2014.
- [95] K. A. Heyries, C. Tropini, M. VanInsberghe, C. Doolin, O. I. Petriv, A. Singhal, K. Leung, C. B. Hughesman, and C. L. Hansen. Megapixel digital pcr. *Nature methods*, 8(8):649–651, 2011.
- [96] V. N. Hoang, G. V. Kaigala, and C. J. Backhouse. Dynamic temperature measurement in microfluidic devices using thermochromic liquid crystals. *Lab on a Chip*, 8(3):484–487, 2008.
- [97] J. Homola. Surface plasmon resonance sensors for detection of chemical and biological species. *Chemical Reviews*, 108(2):462–493, 2008.

- [98] H. Hsih and H. Tsen. Combination of immunomagnetic separation and polymerase chain reaction for the simultaneous detection of *Listeria monocytogenes* and *Salmonella* spp. in food samples. *Journal of Food Protection*®, 64(11):1744–1750, 2001.
- [99] C.-F. Hsu, T.-Y. Tsai, and T.-M. Pan. Use of the duplex TaqMan PCR system for detection of shiga-like toxin-producing *Escherichia coli* O157. *Journal of Clinical Microbiology*, 43(6):2668–2673, 2005.
- [100] F. Huang, C. Liao, and G. Lee. An integrated microfluidic chip for DNA/RNA amplification, electrophoresis separation and on-line optical detection. *Electrophoresis*, 27(16):3297–3305, 2006.
- [101] J. Hudson, R. Lake, M. Savill, P. Scholes, and R. McCormick. Rapid detection of *Listeria monocytogenes* in ham samples using immunomagnetic separation followed by polymerase chain reaction. *Journal of Applied Microbiology*, 90(4):614–621, 2001.
- [102] D. Huh, H.-H. Wei, O. Kripfgans, J. B. Fowlkes, J. B. Grotberg, and S. Takayama. Gravity-driven microhydrodynamics-based cell sorter (microhycs) for rapid, inexpensive, and efficient cell separation and size-profiling. In *Microtechnologies in Medicine & Biology 2nd Annual International IEEE-EMB Special Topic Conference on*, pages 466–469. IEEE, 2002.
- [103] S. B. Humphrey, T. B. Stanton, N. S. Jensen, and R. L. Zuerner. Purification and characterization of VSH-1, a generalized transducing bacteriophage of *Serpulina hyodysenteriae*. *Journal of Bacteriology*, 179:323–329, 1997.
- [104] G. F. Ibrahim, M. J. Lyons, R. A. Walker, and G. H. Fleet. Immobilization of microorganisms for detection by solid-phase immunoassays. *Journal of Clinical Microbiology*, 22(3):361, 1985.
- [105] G. F. Ibrahim, M. J. Lyons, R. A. Walker, and G. G. H. Fleet. Rapid detection of *Salmonella* by immunoassays with titanous hydroxide as the solid phase. *Journal of Environmental Microbiology*, 50(3):670, 1985.

- [106] B. Illic, S. Krylov, K. Aubin, R. Reichenbach, and H. G. Craighead. Optical excitation of nanoelectromechanical oscillators. *Applied Physics Letters*, 86, 2005.
- [107] B. Illic, H. G. Craighead, S. Krylov, W. Senaratne, C. Ober, and P. Neuzil. Attogram detection using nanoelectromechanical oscillators. *Applied Physics*, 95(7), 2004.
- [108] C. Jacobsen and O. Rasmussen. Development and application of a new method to extract bacterial DNA from soil based on a separation of bacteria from soil with cation-exchange resin. *Applied and Environmental Microbiology*, 58(8):2458, 1992.
- [109] A. Janzen, S. Poshtiban, A. Singh, and S. Evoy. Fabrication of nanoresonator biosensing arrays using nanoimprint lithography. *Journal of Micro/Nanolithography, MEMS, and MOEMS*, 11(2):023013–1, 2012.
- [110] M. A. Javed, S. Poshtiban, D. Arutyunov, S. Evoy, and C. M. Szymanski. Bacteriophage receptor binding protein based assays for the simultaneous detection of campylobacter jejuni and campylobacter coli. *PloS one*, 8(7):e69770, 2013.
- [111] M. H. Josefsen, M. Krause, F. Hansen, and J. Hoorfar. Optimization of a 12-hour TaqMan PCR-based method for detection of *Salmonella* bacteria in meat. *Applied and environmental microbiology*, 73(9):3040–3048, 2007.
- [112] N. Jothikumar, X. Wang, and M. W. Griffiths. Real-time multiplex SYBR green I-based PCR assay for simultaneous detection of *Salmonella* serovars and *Listeria monocytogenes*. *Journal of Food Protection®*, 66(11):2141–2145, 2003.
- [113] G. Kaigala, M. Behnam, A. Bidulock, C. Bargen, R. Johnstone, D. Elliot, and C. Backhouse. A scalable and modular lab-on-a-chip genetic analysis instrument. *The Analyst*, 135:1606–1617, 2010.
- [114] G. V. Kaigala, V. N. Hoang, A. Stickel, J. Lauzon, D. Manage, L. M. Pilarski, and C. J. Backhouse. An inexpensive and portable microchip-based platform

- for integrated RT-PCR and capillary electrophoresis. *Analyst*, 133(3):331–338, 2008.
- [115] O. Kalinina, I. Lebedeva, J. Brown, and J. Silver. Nanoliter scale PCR with TaqMan detection. *Nucleic acids research*, 25(10):1999–2004, 1997.
- [116] J. F. Kennedy, S. A. Barker, and J. D. Humphreys. Microbial cells living immobilised on metal hydroxides. *Nature*, 261(5):242, 1976.
- [117] J. Khandurina, T. E. McKnight, S. C. Jacobson, L. C. Waters, R. S. Foote, and J. M. Ramsey. Integrated system for rapid PCR-based DNA analysis in microfluidic devices. *Analytical Chemistry*, 72(13):2995–3000, 2000.
- [118] S. Khare, T. A. Ficht, R. L. Santos, J. Romano, A. R. Ficht, S. Zhang, I. R. Grant, M. Libal, D. Hunter, and L. G. Adams. Rapid and sensitive detection of *Mycobacterium avium* subsp. *paratuberculosis* in bovine milk and feces by a combination of immunomagnetic bead separation-conventional PCR and real-time PCR. *Journal of Clinical Microbiology*, 42(3):1075–1081, 2004.
- [119] J. S. Kim, G. G. Lee, J. S. Park, Y. H. Jung, H. S. Kwak, S. B. Kim, Y. S. Nam, and S.-T. Kwon. A novel multiplex PCR assay for rapid and simultaneous detection of five pathogenic bacteria: *Escherichia coli* O157: H7, *Salmonella*, *Staphylococcus aureus*, *Listeria monocytogenes*, and *Vibrio parahaemolyticus*. *Journal of Food Protection*®, 70(7):1656–1662, 2007.
- [120] J. W. Kim, V. Dutta, D. Elhanafi, S. Lee, J. A. Osborne, and S. Kathariou. A novel restriction-modification system is responsible for temperature-dependent phage resistance in *Listeria monocytogenes* eci. *Applied and Environmental Microbiology*, 78:1995–2004, 2012.
- [121] P. Kinnunen, B. H. McNaughton, T. Albertson, I. Sinn, S. Mofakham, R. Elbez, D. W. Newton, A. Hunt, and R. Kopelman. Self-assembled magnetic bead biosensor for measuring bacterial growth and antimicrobial susceptibility testing. *small*, 8(16):2477–2482, 2012.
- [122] D. Klein. Quantification using real-time PCR technology: applications and limitations. *Trends in molecular medicine*, 8(6):257–260, 2002.

- [123] W. Ko. Integration of nanomechanical resonators in microfluidic systems for specific protein detection. Master's thesis, University of Alberta, 2008.
- [124] J. W. Kretzer, R. Lehmann, M. Schmelcher, M. Banz, K.-P. Kim, C. Korn, and M. J. Loessner. Use of high-affinity cell wall-binding domains of bacteriophage endolysins for immobilization and separation of bacterial cells. *Applied and Environmental Microbiology*, 73(6):1992–2000, 2007.
- [125] A. M. Kropinski, D. Arutyunov, M. Foss, A. Cunningham, W. Ding, A. Singh, A. R. Pavlov, M. Henry, S. Evoy, J. Kelly, and C. M. Szymanski. Genome and proteome of *Campylobacter jejuni* bacteriophage NCTC 12673. *Applied and Environmental Microbiology*, pages 8265–8271, December 2011.
- [126] J. Kuhn, M. Suissa, J. Wyse, I. Cohen, I. Weiser, S. Reznick, S. Lubinsky-Mink, G. Stewart, and S. Ulitzur. Detection of bacteria using foreign DNA: The development of a bacteriophage reagent for *Salmonella*. *International Journal of Food Microbiology*, 74:229–238, 2002.
- [127] E. Kutter and A. Sulakvelidze. *Bacteriophages biology and application*. CRC Press, 2005.
- [128] M. J. LaGier, L. A. Joseph, T. V. Passaretti, K. A. Musser, and N. M. Cirino. A real-time multiplexed PCR assay for rapid detection and differentiation of *Campylobacter jejuni* and *Campylobacter coli*. *Molecular and cellular probes*, 18(4):275–282, 2004.
- [129] R. S. Lakshmanan, R. Guntupalli, J. Hu, D. J. Kim, V. A. Petrenko, J. M. Barbaree, and B. A. Chin. Phage immobilized magnetoelastic sensor for the detection of *Salmonella typhimurium*. *Journal of Microbiological Methods*, 71:55–60, 2007.
- [130] R. S. Lakshmanan, R. Guntupalli, J. Hu, V. A. Petrenko, J. M. Barbaree, and B. A. Chin. Detection of *Salmonella typhimurium* in fat free milk using a phage immobilized magnetoelastic sensor. *Sensors and Actuators B*, 126:544–550, 2007.

- [131] P.-G. Lantz, B. Hahn-Hägerdal, and P. Rådström. Sample preparation methods in PCR-based detection of food pathogens. *Trends in Food Science & Technology*, 5(12):384–389, 1994.
- [132] P. G. Lantz, F. Tjerneld, E. Borch, B. Hahn-Hägerdal, and P. Rådström. Enhanced sensitivity in PCR detection of *Listeria monocytogenes* in soft cheese through use of an aqueous two-phase system as a sample preparation method. *Applied and Environmental Microbiology*, 60(3416-3418), 1994.
- [133] T. Laurell, F. Petersson, and A. Nilsson. Chip integrated strategies for acoustic separation and manipulation of cells and particles. *Chemical Society Reviews*, 36(3):492–506, 2007.
- [134] D. Lee, M. Wu, U. Ramesh, C. Lin, T. Lee, and P. Chen. A novel real-time PCR machine with a miniature spectrometer for fluorescence sensing in a micro liter volume glass capillary. *Sensors and Actuators B: Chemical*, 100(3):401–410, 2004.
- [135] H. Lee, B. Kim, K. Kim, Y. Kim, J. Kim, and M. Oh. A sensitive method to detect *Escherichia coli* based on immunomagnetic separation and real-time PCR amplification of aptamers. *Biosensors and Bioelectronics*, 24(12):3550–3555, 2009.
- [136] S. Lee, M. Onuki, H. Satoh, and T. Mino. Isolation, characterization of bacteriophages specific to microlunatus phosphovorus and their application for rapid host detection. *Letters in Applied Microbiology*, 42(259-264), 2006.
- [137] P. G. Leiman and M. M. Shneider. Contractile tail machines of bacteriophages. In *Viral Molecular Machines*, pages 93–114. Springer, 2012.
- [138] S. H. P. Leonard, J. Quinn, and R. O’Kennedy. A generic approach for the detection of whole *Listeria monocytogenes* cells in contaminated samples using surface plasmon resonanc. *Biosensors and Bioelectronics*, 19:1331–1335, 2004.
- [139] K. Leung, H. Zahn, T. Leaver, K. M. Konwar, N. W. Hanson, A. P. Pagé, C.-C. Lo, P. S. Chain, S. J. Hallam, and C. L. Hansen. A programmable droplet-based microfluidic device applied to multiparameter analysis of single

- microbes and microbial communities. *Proceedings of the National Academy of Sciences*, 109(20):7665–7670, 2012.
- [140] C. M. Leutenegger. The real-time TaqMan PCR and applications in veterinary medicine. *Vet Sci Tomorrow*, 1:1–15, 2001.
- [141] H. Li, J. R. Friend, and L. Y. Yeo. Surface acoustic wave concentration of particle and bioparticle suspensions. *Biomedical Microdevices*, 9(5):647–656, 2007.
- [142] S. Li, L. Fu, J. Barbaree, and Z.-Y. Cheng. Resonance behavior of magnetostrictive micro/milli-cantilever and its application as a biosensor. *Sensors and Actuators B: Chemical*, 137(2):692–699, 2009.
- [143] S. Li, Y. Li, H. Chen, S. Horikawa, W. Shen, A. Simonian, and B. A. Chin. Direct detection of *Salmonella typhimurium* on fresh produce using phage-based magnetoelastic biosensors. *Biosensors and Bioelectronics*, 26(4):1313–1319, 2010.
- [144] Y. Li, H. Liu, H. Lin, and S. Chen. Gold nanoparticles for microfluidics-based biosensing of PCR products by hybridization-induced fluorescence quenching. *Electrophoresis*, 26(24):4743–4750, 2005.
- [145] Y. Li, C. Zhang, and D. Xing. Fast identification of foodborne pathogenic viruses using continuous-flow reverse transcription-PCR with fluorescence detection. *Microfluidics and Nanofluidics*, 10(2):367–380, 2011.
- [146] K. Lien, W. Lin, Y. Lee, C. Wang, H. Lei, and G. Lee. Microfluidic systems integrated with a sample pretreatment device for fast nucleic-acid amplification. *Journal of Microelectromechanical Systems*, 17(2):288–301, 2008.
- [147] Y. Lin and G. Lee. Optically induced flow cytometry for continuous microparticle counting and sorting. *Biosensors and Bioelectronics*, 24(4):572–578, 2008.
- [148] P. Liu and R. A. Mathies. Integrated microfluidic systems for high-performance genetic analysis. *Trends in Biotechnology*, 27(10):572–581, 2009.

- [149] R. Liu, J. Yang, R. Lenigk, and P. Bonanno, J. and Grodzinski. Self-contained, fully integrated biochip for sample preparation, polymerase chain reaction amplification, and DNA microarray detection. *Analytical Chemistry*, 76(7):1824–1831, 2004.
- [150] Y. Liu, C. Wang, J. Wu, and G. Lee. Rapid detection of live methicillin-resistant *Staphylococcus aureus* by using an integrated microfluidic system capable of ethidium monoazide pre-treatment and molecular diagnosis. *Biomicrofluidics*, 6:034119, 2012.
- [151] M. J. Loessner, C. E. Rees, G. S. Stewart, and S. Scherer. Construction of luciferase reporter bacteriophage A511::luxAB for rapid and sensitive detection of viable *Listeria* cells. *Applied and Environmental Microbiology*, 62:1133–1140, 1996.
- [152] M. J. Loessner, M. Rudolf, and S. Scherer. Evaluation of luciferase reporter bacteriophage A511::luxAB for detection of *Listeria monocytogenes* in contaminated foods. *Applied and Environmental Microbiology*, 63:2961–2965, 1997.
- [153] L. Lucore, M. A. Cullison, and L. A. Jaykus. Immobilization with metal hydroxides as a means to concentrate foodborne bacteria for detection by cultural and molecular methods. *Applied and Environmental Microbiology*, 66(5):1769, 2000.
- [154] M. Magliulo, P. Simoni, M. Guardigli, E. Michelini, M. Luciani, R. Lelli, and A. Roda. A rapid multiplexed chemiluminescent immunoassay for the detection of *Escherichia coli* O157: H7, *Yersinia enterocolitica*, *Salmonella typhimurium*, and *Listeria monocytogenes* pathogen bacteria. *Journal of Agricultural and Food Chemistry*, 55(13):4933–4939, 2007.
- [155] B. Malorny, E. Paccassoni, P. Fach, C. Bunge, A. Martin, and R. Helmuth. Diagnostic real-time PCR for detection of *Salmonella* in food. *Applied and Environmental Microbiology*, 70(12):7046–7052, 2004.

- [156] B. Malorny, P. T. Tassios, P. Rådström, N. Cook, M. Wagner, and J. Hoorfar. Standardization of diagnostic PCR for the detection of foodborne pathogens. *International Journal of Food Microbiology*, 83(1):39–48, 2003.
- [157] J. P. McGovern, W. Y. Shih, and W. Shih. In situ detection of bacillus anthracis spores using fully submersible, self-exciting, self-sensing PMN-PT/sn piezoelectric microcantilevers. *Analyst*, 132:777–783, 2007.
- [158] M. Mejri, H. Baccar, E. Baldrich, F. D. Campo, S. Helali, T. Ktari, A. Simonian, M. Aouni, and A. Abdelghani. Impedance biosensing using phages for bacteria detection: Generation of dual signals as the clue for in-chip assay confirmation. *Biosensors and Bioelectronics*, 26(4):1261–1267, 2010.
- [159] R. Meyer, J. Luthy, and U. Candrian. Direct detection by polymerase chain reaction (PCR) of *Escherichia coli* in water and soft cheese and identification of enterotoxigenic strains. *Letters in Applied Microbiology*, 13(268), 1991.
- [160] R. Morales-Rayas, P. F. Wolffs, and M. W. Griffiths. Immunocapture and Real-Time PCR To Detect *Campylobacter* spp. *Journal of Food Protection*®, 71(12):2543–2547, 2008.
- [161] E. A. Mothershed and A. M. Whitney. Nucleic acid-based methods for the detection of bacterial pathogens: present and future considerations for the clinical laboratory. *Clinica Chimica Acta*, 363(1):206–220, 2006.
- [162] M. Mujika, S. Arana, E. Castano, M. Tijero, R. Vilares, J. Ruano-Lopez, A. Cruz, L. Sainz, and J. Berganza. Magnetoresistive immunosensor for the detection of *Escherichia coli* O157: H7 including a microfluidic network. *Biosensors and Bioelectronics*, 24(5):1253–1258, 2009.
- [163] N. Murphy, J. McLauchlin, C. Ohai, and K. Grant. Construction and evaluation of a microbiological positive process internal control for PCR-based examination of food samples for *Listeria monocytogenes* and *Salmonella enterica*. *International Journal of Food Microbiology*, 120(1):110–119, 2007.
- [164] R. Naidoo, A. Singh, S. K. Arya, B. Beadle, N. Glass, J. Tanha, C. M. Szymanski, and S. Evoy. Surface-immobilization of chromatographically purified

- bacteriophages for the optimized capture of bacteria. *Bacteriophage*, 2:15–24, 2012.
- [165] H.-M. Nam, V. Srinivasan, B. E. Gillespie, S. E. Murinda, and S. P. Oliver. Application of sybr green real-time PCR assay for specific detection of *Salmonella* spp. in dairy farm environmental samples. *International Journal of Food Microbiology*, 102(2):161–171, 2005.
- [166] V. Nanduri, I. B. Sorokulova, A. M. Samoylov, A. L. Simonian, V. A. Petrenko, and V. Vodyanoy. Phage as a molecular recognition element in biosensors immobilized by physical adsorption. *Biosensors and Bioelectronics*, 22:986–992, 2007.
- [167] C. Neiderhauser, U. Candrian, C. Hofelein, M. Jermini, H. P. B. J., and Luthy. Use of polymerase chain reaction for detection of *Listeria monocytogenes* in food. *Applied and Environmental Microbiology*, 58(5):1564, 1992.
- [168] N. Nelson-Fitzpatrick. *Novel materials for the design of cantilever transducers*. PhD thesis, University of Alberta, Edmonton, Alberta, Fall 2011.
- [169] T. Neufeld, A. Schwartz-Mittelmann, D. Biran, E. Z. Ron, and J. Rishpon. Combined phage typing and amperometric detection of released enzymatic activity for the specific identification and quantification of bacteria. *Analytical Chemistry*, 75(3):580–585, 2003.
- [170] M. A. Northrup, B. Benett, D. Hadley, P. Landre, S. Lehew, J. Richards, and P. Stratton. A miniature analytical instrument for nucleic acids based on micromachined silicon reaction chambers. *Analytical Chemistry*, 70(5):918–922, 1998.
- [171] M. A. Northrup, M. Ching, R. White, and R. Watson. DNA amplification with a microfabricated reaction chamber. In *Transducers*, volume 93, pages 924–926, 1993.
- [172] N. Nugaeva, K. Y. Gfeller, N. Backmann, H. P. Lang, M. Düggelin, and M. Hegner. Micromechanical cantilever array sensors for selective fungal im-

- mobilization and fast growth detection. *Biosensors and Bioelectronics*, 21:849–856, 2005.
- [173] N. Nugaeva, K. Y. Gfeller, N. Backmann, H. P. Lang, M. Düggelein, and M. Hegner. Micromechanical cantilever array sensors for selective fungal immobilization and fast growth detection. *Biosensors and Bioelectronics*, 21(6):849–856, 2005.
- [174] S. Nutz, K. Döll, and P. Karlovsky. Determination of the loq in real-time pcr by receiver operating characteristic curve analysis: application to qpcr assays for fusarium verticillioides and f. proliferatum. *Analytical and bioanalytical chemistry*, 401(2):717–726, 2011.
- [175] R. Oberst, M. Hays, L. Bohra, R. Phebus, C. Yamashiro, C. Paszko-Kolva, S. Flood, J. Sargeant, and J. Gillespie. PCR-based DNA amplification and presumptive detection of *Escherichia coli* O157: H7 with an internal fluorogenic probe and the 5' nuclease (TaqMan) assay. *Applied and environmental microbiology*, 64(9):3389–3396, 1998.
- [176] R. Oda, M. Strausbauch, A. Huhmer, N. Borson, S. Jurrens, J. Craighead, P. Wettstein, B. Eckloff, B. Kline, and J. Landers. Infrared-mediated thermocycling for ultrafast polymerase chain reaction amplification of dna. *Analytical Chemistry*, 70(20):4361–4368, 1998.
- [177] B. Oh, W. Lee, B. S. Chun, Y. M. Bae, W. H. Lee, and J. Choi. The fabrication of protein chip based on surface plasmon resonance for detection of pathogen. *Biosensors and Bioelectronics*, 20:1847–1850, 2005.
- [178] T. C. Oliveira, S. Barbut, and M. W. Griffiths. Detection of *Campylobacter jejuni* in naturally contaminated chicken skin by melting peak analysis of amplicons in real-time PCR. *International Journal of Food Microbiology*, 104(1):105–111, 2005.
- [179] E. Olsen, I. Sorokulova, V. Petrenko, I. Chen, J. Barbaree, and V. Vodyanoy. Affinity-selected filamentous bacteriophage as a probe for acoustic wave biode-

- tectors of *Salmonella typhimurium*. *Biosensors and Bioelectronics*, 21(8):1432–1442, 2006.
- [180] I. Palchetti and M. Mascini. Electroanalytical biosensors and their potential for food pathogen and toxin detection. *Analytical and Bioanalytical Chemistry*, 391(2):455–471, 2008.
- [181] J. Pande, M. M. Szewczyk, and A. K. Grover. Phage display: concept, innovations, applications and future. *Biotechnology Advances*, 28:849–858, 2010.
- [182] A. W. Paton and J. C. Paton. Detection and characterization of shiga toxinogenic *Escherichia coli* by using multiplex PCR assays for stx 1, stx 2, eaeA, enterohemorrhagic *E. coli* hly<sub>EHEC</sub>, rfb O111, and rfb O157. *Journal of Clinical Microbiology*, 36(2):598–602, 1998.
- [183] M. J. Payne and R. G. Kroll. Methods for the separation and concentration of bacteria from foods. *Trends in Food Science and Technology*, 2(315), 1991.
- [184] R. E. Pearson, S. Jurgensen, G. J. Sarkis, G. F. Hatfull, and W. R. Jacobs. Construction of D29 shuttle plasmids and luciferase reporter phages for detection of *Mycobacteria*. *Gene*, 183:129–136, 1996.
- [185] S. Perelle, F. Dilasser, B. Malorny, J. Grout, J. Hoorfar, and P. Fach. Comparison of PCR-ELISA and lightcycler real-time PCR assays for detecting *Salmonella* spp. in milk and meat samples. *Molecular and Cellular Probes*, 18(6):409–420, 2004.
- [186] L. Perry, P. Heard, M. Kane, H. Kim, S. Savikhin, W. Domínguez, and B. Aplegate. Application of multiplex polymerase chain reaction to the detection of pathogens in food. *Journal of Rapid Methods & Automation in Microbiology*, 15(2):176–198, 2007.
- [187] J. Pirnay, D. D. Vos, G. Verbeken, M. M. an Nina Chanishvili, M. Vaneechoutte, M. Zizi, G. Laire, R. Lavigne, I. Huys, G. V. den Mooter, A. Buckling, L. Debarbieux, F. Pouillot, J. Azeredo, E. Kutter, A. Dublanche, A. Górski, and R. Adamia. The phage therapy paradigm: Prêt-à-porter or sur-mesure? *Pharmaceutical Research*, 28:934–937, 2011.

- [188] J. Porter, C. Edwards, and R. Pickup. Rapid assessment of physiological status in *Escherichia coli* using fluorescent probes. *Journal of Applied Microbiology*, 79(4):399–408, 1995.
- [189] S. Poshtiban, M. A. Javed, D. Arutyunov, A. Singh, G. Banting, C. S. Szymanski, and S. Evoy. Phage receptor binding protein-based magnetic enrichment method as an aid for real time PCR detection of foodborne bacteria. *Analyst*, 2013.
- [190] S. Poshtiban, A. Singh, G. Fitzpatrick, and S. Evoy. Bacteriophage tail-spike protein derivitized microresonator arrays for specific detection of pathogenic bacteria. *Sensors and Actuators B: Chemical*, 2013.
- [191] H. A. Powell, C. M. Gooding, S. D. Garret, B. M. Lund, and R. A. McKee. Proteinase inhibition of the detection of *Listeria monocytogenes* in milk using the polymerase chain reaction. *Letters in Applied Microbiology*, 18:59–61, 1994.
- [192] Proceeding of the International Dairy Federation Symposium on Bacteriological Quality of Raw Milk. *Phage-Mediated detection of Staphylococcus Aureus and Escherichia coli O157: H7 using bioluminescence*, Wolfpassing, Austria, March 1996.
- [193] QIAGEN. *QIAamp DNA Mini and Blood Mini Handbook*, third edition, June 2012.
- [194] Q. Ramadan, V. Samper, D. P. Poenar, and C. Yu. An integrated microfluidic platform for magnetic microbeads separation and confinement. *Biosensors and Bioelectronics*, 21(9):1693–1702, 2006.
- [195] D. Ramos, J. Tamayo, J. Mertens, M. Calleja, L. Villanueva, and A. Zaballos. Detection of bacteria based on the thermomechanical noise of a nanomechanical resonator: origin of the response and detection limits. *Nanotechnology*, 19(3):035503, 2008.
- [196] D. Ramos, J. Tamayo, J. Mertens, M. Calleja, and A. Zaballos. Origin of the response of nanomechanical resonator to bacteria adsorption. *Journal of Applied Physics*, 100(106105), 2006.

- [197] S. Rao and F. Yap. *Mechanical Vibrations*. Pearson Education, Limited, 2005.
- [198] N. Rijpens, L. Herman, F. Vereecken, G. Jannes, J. De Smedt, and L. De Zutter. Rapid detection of stressed *Salmonella* spp. in dairy and egg products using immunomagnetic separation and PCR. *International Journal of Food Microbiology*, 46(1):37–44, 1999.
- [199] L. W. Riley, R. S. Remis, S. D. Helgerson, H. B. McGee, J. G. Wells, B. R. Davis, R. J. Hebert, E. S. Olcott, L. M. Johnson, N. T. Hargrett, P. A. Blake, and M. L. Cohen. Hemorrhagic colitis associated with a rare *Escherichia coli* serotype. *The New England Journal of Medicine*, 308(681-685), 1983.
- [200] R. Rong, J. Choi, and C. H. Ahn. An on-chip magnetic bead separator for biocell sorting. *Journal of Micromechanics and Microengineering*, 16(12):2783, 2006.
- [201] A.-C. Ronner and H. Lindmark. Quantitative detection of *Campylobacter jejuni* on fresh chicken carcasses by real-time PCR. *Journal of Food Protection*®, 70(6):1373–1378, 2007.
- [202] L. Rossen, K. Holmstrøm, J. Olsen, and O. Rasmussen. A rapid polymerase chain reaction (PCR)-based assay for the identification of *Listeria monocytogenes* in food samples. *International Journal of Food Microbiology*, 14(2):145–151, 1991.
- [203] L. Rossen, P. Nørskov, K. Holmstrøm, and O. F. Rasmussen. Inhibition of PCR by components of food samples, microbial diagnostic assays and DNA-extraction solutions. *International Journal of Microbiology*, 17:37–45, 1992.
- [204] C. A. Rowe, L. M. Tender, M. J. Feldstein, J. P. Golden, S. B. Scruggs, B. D. MacCraith, J. J. Cras, and F. S. Ligler. Array biosensor for simultaneous identification of bacterial, viral, and protein analytes. *Analytical Chemistry*, 71:3846–3852, 1999.
- [205] C. Ruana, L. Yangb, and Y. Li. Rapid detection of viable *Salmonella typhimurium* in a selective medium by monitoring oxygen consumption with electrochemical cyclic voltammetry. *2002*, 1-2(33-38), 519.

- [206] Y. Sai, M. Yamada, M. Yasuda, and M. Seki. Continuous separation of particles using a microfluidic device equipped with flow rate control valves. *Journal of CHROMATOGRAPHY A*, 1127(1):214–220, 2006.
- [207] A. D. Sails, A. J. Fox, F. J. Bolton, D. R. Wareing, and D. L. Greenway. A real-time PCR assay for the detection of *Campylobacter jejuni* in foods after enrichment culture. *Applied and environmental microbiology*, 69(3):1383–1390, 2003.
- [208] Z. Salamon and G. Tollin. Plasmon resonance spectroscopy: probing molecular interactions at surfaces and interfaces. *Spectroscopy*, 15:161–175, 2001.
- [209] S. Q. Sanders, D. H. Boothe, J. F. Frank, and J. W. Arnold. Culture and detection of *Campylobacter jejuni* within mixed microbial populations of biofilms on stainless steel. *Journal of Food Protection*®, 70(6):1379–1385, 2007.
- [210] G. J. Sarkis, W. R. Jacobs, and G. F. Hatfull. L5 luciferase reporter mycobacteriophages: A sensitive tool for the detection and assay of live *mycobacteria*. *Molecular Microbiology*, 15:1055–1067, 1995.
- [211] U. B. Schaad. Which number of infecting bacteria is of clinical relevance? *Infection*, 11(2):87–89, 1983.
- [212] P. Serwer and S. J. Hayes. Agarose gel electrophoresis of bacteriophages and related particles. I. Avoidance of binding to the gel and recognizing of particles with packaged DNA. *Electrophoresis*, 3:76–80, 1982.
- [213] P. Sethu, A. Sin, and M. Toner. Microfluidic diffusive filter for apheresis (leukapheresis). *Lab on a Chip*, 6(1):83–89, 2006.
- [214] A. Shabani, M. Zourob, B. Allain, C. A. Marquette, M. F. Lawrence, and R. Mandeville. Bacteriophage-modified microarrays for the direct impedimetric detection of bacteria. *Analytical Chemistry*, 80(24):9475–82, 2008.
- [215] W. Shen, R. S. Lakshmanan, L. C. Mathison, V. A. Petrenko, and B. A. Chin. Phage coated magnetoelastic micro-biosensors for real-time detection of *bacillus anthracis* spores. *Sensors and Actuators B: Chemical*, 137(2):501–506, 2009.

- [216] B. Shu, C. Zhang, and D. Xing. Highly sensitive identification of foodborne pathogenic *Listeria monocytogenes* using single-phase continuous-flow nested PCR microfluidics with on-line fluorescence detection. *Microfluidics and Nanofluidics*, pages 1–12.
- [217] P. C. Simpson, D. Roach, A. T. Woolley, T. Thorsen, R. Johnston, G. F. Sensabaugh, and R. A. Mathies. High-throughput genetic analysis using microfabricated 96-sample capillary array electrophoresis microplates. *Proceedings of the National Academy of Sciences*, 95(5):2256–2261, 1998.
- [218] A. Singh, D. Arutyunov, C. M. Szymanski, and S. Evoy. Bacteriophage based probes for pathogen detection. *Analyst*, 137:3405–3421, 2012.
- [219] A. Singh, D. Arutyunov, M. T. McDermott, C. M. Szymanski, and S. Evoy. Specific detection of *Campylobacter jejuni* using the bacteriophage NCTC 12673 receptor binding protein as a probe. *Analyst*, 136:4780–4786, September 2011.
- [220] A. Singh, S. K. Arya, N. Glass, P. Hanifi-Moghaddam, R. Naidoo, C. M. Szymanski, J. Tanha, and S. Evoy. Bacteriophage tailspike proteins as molecular probes for sensitive and selective bacterial detection. *Biosensors and Bioelectronics*, 26:131–138, 2010.
- [221] A. Singh, N. Glass, M. Tolba, L. Brovko, M. Griffiths, and S. Evoy. Immobilization of bacteriophages on gold surfaces for the specific capture of pathogens. *Biosensors and Bioelectronics*, 24(3645-3651), 2009.
- [222] A. Singh, S. Poshtiban, and S. Evoy. Recent advances in bacteriophage based biosensors for foodborne pathogen detection. *Sensors*, 13:1763–1786, 2013.
- [223] G. Siragusa, J. Line, and A. Schutz. Fluorescent detection of *Campylobacter* spp. on colony immunoblots. In *Abstr Gen Meet Am Soc Microbiol*, volume 101, page 577, 2001.
- [224] E. Skjerve, L. Rørvik, and O. Olsvik. Detection of *Listeria monocytogenes* in foods by immunomagnetic separation. *Applied and environmental microbiology*, 56(11):3478–3481, 1990.

- [225] M. N. Slyadnev, Y. Tanaka, M. Tokeshi, and T. Kitamori. Photothermal temperature control of a chemical reaction on a microchip using an infrared diode laser. *Analytical Chemistry*, 73(16):4037–4044, 2001.
- [226] K. Smistrup, P. T. Tang, O. Hansen, and M. F. Hansen. Microelectromagnet for magnetic manipulation in lab-on-a-chip systems. *Journal of Magnetism and Magnetic Materials*, 300(2):418–426, 2006.
- [227] G. P. Smith. Filamentous fusion phage: Novel expression vectors that display cloned antigens on the virion surface. *Science*, 228:1315–1317, 1985.
- [228] G. P. Smith and V. A. Petrenko. Phage display. *Chemical Reviews*, 97:391–410, 1997.
- [229] L. M. Stancik, D. M. Stancik, B. Schmidt, D. M. Barnhart, Y. N. Yoncheva, and J. L. Slonczewski. pH-dependent expression of periplasmic proteins and amino acid catabolism in *Escherichia coli*. *Journal of bacteriology*, 184(15):4246–4258, 2002.
- [230] K. A. Stevens and L. Jaykus. Bacterial Separation and Concentration from Complex Sample Matrices: A Review. *Critical Reviews in Microbiology*, 30(1):7–24, 2004.
- [231] Stratagene, 11011 North Torrey Pines Road, La Jolla, CA 92037 USA. *Introduction to Quantitative PCR, Methods and Application Guide*, in 70200-00/revision 84001 edition, 2004.
- [232] X. Su and Y. Li. A self-assembled monolayer-based piezoelectric immunosensor for rapid detection of *Escherichia coli* O157: H7. *Biosensors and Bioelectronics*, 19(6):563–574, 2004.
- [233] V. Tabard-Cossa, M. Godin, I. J. Burgess, T. Monga, R. B. Lennox, and P. Grutter. Microcantilever-based sensors: effect of morphology, adhesion, and cleanliness of the sensing surface on surface stress. *Analytical Chemistry*, 79:8136–8143, 2007.

- [234] M. Taha. Simultaneous approach for nonculture PCR-based identification and serogroup prediction of *Neisseria meningitidis*. *Journal of Clinical Microbiology*, 38(2):855–857, 2000.
- [235] N. S. Tawil, R. Mandeville, and M. Meunier. Surface plasmon resonance detection of *E. coli* and methicillin-resistant *S. aureus* using bacteriophages. *Biosensors and Bioelectronics*, 37(24-29), 2012.
- [236] A. D. Taylor, S. C. Q.Y., J. Homola, and S. Jiang. Comparison of *E. coli* O157:H7 preparation methods used for detection with surface plasmon resonance senso. *Sensors and Actuators B*, 107:202–208, 2005.
- [237] T. B. Taylor, E. S. Winn-Deen, E. Picozza, T. M. Woudenberg, and M. Albin. Optimization of the performance of the polymerase chain reaction in silicon-based microstructures. *Nucleic acids research*, 25(15):3164–3168, 1997.
- [238] D. S. Thomas. Electropositively charged filters for the recovery of yeasts and bacteria from beverages. *Journal of Applied Bacteriology*, 65:35, 1988.
- [239] M. Tolba, O. Minikh, L. Y. Brovko, S. Evoy, and M. W. Griffiths. Oriented immobilization of bacteriophages for biosensor applications. *Applied and Environmental Microbiology*, 76:528–535, 2010.
- [240] S. Toze. PCR and the detection of microbial pathogens in water and wastewater. *Water Research*, 33(17):3545–3556, 1999.
- [241] A. K. Trilling, H. de Ronde, L. Noteboom, A. van Houwelingen, M. Roelse, S. K. Srivastava, W. Haasnoot, M. A. Jongsma, A. Kolk, H. Zuilhof, et al. A broad set of different llama antibodies specific for a 16 kDa heat shock protein of *Mycobacterium tuberculosis*. *PloS one*, 6(10):e26754, 2011.
- [242] M. Uyttendaele, I. Van Hoorde, and J. Debevere. The use of immuno-magnetic separation (ims) as a tool in a sample preparation method for direct detection of *L. monocytogenes* in cheese. *International Journal of Food Microbiology*, 54(3):205–212, 2000.

- [243] V. VanDelinder and A. Groisman. Perfusion in microfluidic cross-flow: separation of white blood cells from whole blood and exchange of medium in a continuous flow. *Analytical Chemistry*, 79(5):2023–2030, 2007.
- [244] P. Vannuffel, J. Gigi, H. Ezzedine, B. Vandercam, M. Delmee, G. Wauters, and J.-L. Gala. Specific detection of methicillin-resistant staphylococcus species by multiplex PCR. *Journal of clinical microbiology*, 33(11):2864–2867, 1995.
- [245] M. Varshney, Y. Li, B. Srinivasan, and S. Tung. A label-free, microfluidics and interdigitated array microelectrode-based impedance biosensor in combination with nanoparticles immunoseparation for detection of *Escherichia coli* O157:H7 in food samples. *Sensors and Actuators B: Chemical*, 128(1):99–107, 2007.
- [246] T. E. Waddell and C. Poppe. Construction of mini-Tn10luxABcam/Ptac-ATS and its use for developing a bacteriophage that transduces bioluminescence to *Escherichia coli* O157:H7. *Microbiology Letters*, 182:285–289, 2000.
- [247] G. Wang, C. G. Clark, T. M. Taylor, C. Pucknell, C. Barton, L. Price, D. L. Woodward, and F. G. Rodgers. Colony multiplex PCR assay for identification and differentiation of *Campylobacter jejuni*, *C. coli*, *C. lari*, *C. upsaliensis*, and *C. fetus* subsp. *fetus*. *Journal of clinical microbiology*, 40(12):4744–4747, 2002.
- [248] H. Wang, C. Zhang, and D. Xing. Simultaneous detection of *Salmonella enterica*, *Escherichia coli* O157: H7, and *Listeria monocytogenes* using oscillatory-flow multiplex PCR. *Microchimica Acta*, 173(3-4):503–512, 2011.
- [249] L. Wang, Y. Li, and A. Mustapha. Rapid and simultaneous quantitation of *Escherichia coli* O157: H7, *Salmonella*, and *Shigella* in ground beef by multiplex real-time PCR and immunomagnetic separation. *Journal of Food Protection*®, 70(6):1366–1372, 2007.
- [250] R. F. Wang, W. W. Cao, and C. E. Cerniglia. A universal protocol for PCR detection of 13 species of foodborne pathogens in food. *Journal of Applied Microbiology*, 83(727), 1997.

- [251] W. Wang, S. Singh, D. L. Zeng, K. King, and S. Nema. Antibody structure, instability, and formulation. *Journal of Pharmaceutical Sciences*, 96(1):1–26, 2007.
- [252] S. Waseh, P. Hanifi-Moghaddam, R. Coleman, M. Masotti, S. Ryan, M. Foss, R. MacKenzie, M. Henry, C. M. Szymanski, and J. Tanha. Orally administered P22 phage tailspike protein reduces *Salmonella* colonization in chickens: Prospects of a novel therapy against bacterial infections. *PLoS One*, 5:e13904, 2010.
- [253] J. G. Wells, B. R. Davis, I. K. Wachsmuth, L. W. Riley, R. S. Remis, R. Sokolow, and G. K. Morris. Laboratory investigation of hemorrhagic colitis outbreaks associated with a rare *Escherichia coli* serotype. *Journal of Clinical Microbiology*, 18(512-520), 1983.
- [254] A. K. White, M. VanInsberghe, I. Petriv, M. Hamidi, D. Sikorski, M. A. Marra, J. Piret, S. Aparicio, and C. L. Hansen. High-throughput microfluidic single-cell rt-qpcr. *Proceedings of the National Academy of Sciences*, 108(34):13999–14004, 2011.
- [255] M. Widjojoatmodjo, A. Fluit, R. Torensma, B. Keller, and J. Verhoef. Evaluation of the magnetic immuno PCR assay for rapid detection of *Salmonella*. *European Journal of Clinical Microbiology and Infectious Diseases*, 10(11):935–938, 1991.
- [256] P. Wilding, L. J. Kricka, J. Cheng, G. Hvichia, M. A. Shoffner, and P. Fortina. Integrated cell isolation and polymerase chain reaction analysis using silicon microfilter chambers. *Analytical Biochemistry*, 257(2):95–100, 1998.
- [257] C. T. Wittwer and D. J. Garling. Rapid cycle DNA amplification: Time and Temperature Optimization. *BioTechniques*, 10(1):76–83, 1991.
- [258] T. Wong, U. Bhardwaj, J. Chen, E. McCabe, C. Ho, et al. Formation of high electromagnetic gradients through a particle-based microfluidic approach. *Journal of Micromechanics and Microengineering*, 17(7):1299, 2007.

- [259] H. Wu, X. Lin, S. Hwang, and G. Lee. A microfluidic device for separation of amniotic fluid mesenchymal stem cells utilizing louver-array structures. *Biomedical Microdevices*, 11(6):1297–1307, 2009.
- [260] Y. B. Wu and M. W. Griffiths. Influence of phage population on the phage-mediated bioluminescent adenylate kinase (ak) assay for detection of bacteria. *Letters in Applied Microbiology*, 33:311–315, 2001.
- [261] Z. Wu, A. Q. Liu, and K. Hjort. Microfluidic continuous particle/cell separation via electroosmotic-flow-tuned hydrodynamic spreading. *Journal of Micromechanics and Microengineering*, 17(10):1992, 2007.
- [262] N. Xia, T. P. Hunt, B. T. Mayers, E. Alsberg, G. M. Whitesides, R. M. Westervelt, and D. E. Ingber. Combined microfluidic-micromagnetic separation of living cells in continuous flow. *Biomedical Microdevices*, 8(4):299–308, 2006.
- [263] H. Xu, N. Roberts, F. Singleton, R. Attwell, D. Grimes, and R. Colwell. Survival and viability of nonculturable *Escherichia coli* and *Vibrio cholerae* in the estuarine and marine environment. *Microbial Ecology*, 8(4):313–323, 1982.
- [264] S. Xu and R. Mutharasan. Rapid and sensitive detection of *Giardia lamblia* using a piezoelectric cantilever biosensor in finished and source waters. *Environmental Science and Technology*, 44(5):1736–1741, February 2010.
- [265] M. Yamada, M. Nakashima, and M. Seki. Pinched flow fractionation: continuous size separation of particles utilizing a laminar flow profile in a pinched microchannel. *Analytical Chemistry*, 76(18):5465–5471, 2004.
- [266] M. Yamada and M. Seki. Hydrodynamic filtration for on-chip particle concentration and classification utilizing microfluidics. *Lab on a Chip*, 5(11):1233–1239, 2005.
- [267] C. Yang, Y. Jiang, K. Huang, C. Zhu, and Y. Yin. Application of real-time PCR for quantitative detection of *Campylobacter jejuni* in poultry, milk and environmental water. *FEMS Immunology & Medical Microbiology*, 38(3):265–271, 2003.

- [268] H. Yang, L. Qu, A. N. Wim brow, X. Jiang, and Y. Sun. Rapid detection of *Listeria monocytogenes* by nanoparticle-based immunomagnetic separation and real-time PCR. *International Journal of Food Microbiology*, 118(2):132–138, 2007.
- [269] H. Yang, L. Qu, A. N. Wim brow, X. Jiang, and Y. Sun. Rapid detection of *Listeria monocytogenes* by nanoparticle-based immunomagnetic separation and real-time PCR. *International Journal of Food Microbiology*, 118:132–138, 2007.
- [270] S. Yang, S. Hsiung, Y. Hung, C. Chang, T. Liao, and G. Lee. A cell counting/sorting system incorporated with a microfabricated flow cytometer chip. *Measurement Science and Technology*, 17(7):2001, 2006.
- [271] S. Yang, K. Lien, K. Huang, H. Lei, and G. Lee. Micro flow cytometry utilizing a magnetic bead-based immunoassay for rapid virus detection. *Biosensors and Bioelectronics*, 24(4):855–862, 2008.
- [272] X. Yao, M. Jericho, D. Pink, and T. Beveridge. Thickness and elasticity of gram-negative Murein Sacculi measured by atomic force microscopy. *Journal of Bacteriology*, 181(22):6865–6875, 1999.
- [273] P. Yim, M. Clarke, M. McKinstry, S. De Paoli Lacerda, L. Pease, M. Dobrowolskaia, H. Kang, T. Read, S. Sozhamannan, and J. Hwang. Quantitative characterization of quantum dot-labeled lambda phage for *Escherichia coli* detection. *Biotechnolog and Bioengineering*, 104(6):1059–1067, 2009.
- [274] C. S. Yixian Wang, Z.Y. and Y. Ying. Subtractive inhibition assay for the detection of *E. coli* O157:H7 using surface plasmon resonance. *Sensors*, 11:2728–2739, 2011.
- [275] D. Yoon, Y. Lee, Y. Lee, H. Cho, S. Sung, K. Oh, J. Cha, and L. G. Precise temperature control and rapid thermal cycling in a micromachined PCR chip. *Journal of Micromechanics and Microengineering*, 12:813–823, 2002.

- [276] K. Young, H. Lien, C. Lin, T. Chang, G. Lee, and S. Chen. Microchip and capillary electrophoresis for quantitative analysis of hepatitis C virus based on RT-competitive PCR. *Talanta*, 56(2):323–330, 2002.
- [277] X. Yu, M. Susa, C. Knabbe, R. D. Schmid, and T. T. Bachmann. Development and validation of a diagnostic DNA microarray to detect quinolone-resistant *Escherichia coli* among clinical isolates. *Journal of Clinical Microbiology*, 42(9):4083–4091, 2004.
- [278] G. A. Zelada-Guillén, J. Riu, A. Düzgün, and F. X. Rius. Immediate detection of living bacteria at ultralow concentrations using a carbon nanotube based potentiometric aptasensor. *Angewandte Chemie International Edition*, 48(40):7334–7337, 2009.
- [279] G. A. Zelada-Guillén, J. L. Sebastián-Avila, P. Blondeau, J. Riu, and F. X. Rius. Label-free detection of *Staphylococcus aureus* in skin using real-time potentiometric biosensors based on carbon nanotubes and aptamers. *Biosensors and Bioelectronics*, 31(1):226–232, 2012.
- [280] G. A. Zelada-Guillén, S. V. Bhosale, J. Riu, and F. X. Rius. Real-time potentiometric detection of bacteria in complex samples. *Analytical chemistry*, 82(22):9254–9260, 2010.
- [281] Q. Zhu, W. Y. Shih, and W. Shih. In situ, in-liquid, all-electrical detection of *Salmonella typhimurium* using lead titanate zirconate/gold-coated glass cantilevers at any dipping depth. *Biosensors and Bioelectronics*, 22(3132-3138), 2007.
- [282] R. Zink and M. J. Loessner. Classification of virulent and temperate bacteriophages of *Listeria* spp. on the basis of morphology and protein analysis. *Applied and Environmental Microbiology*, 58(1):296–302, 1992.